

**UNIVERSITA' DEGLI STUDI DI NAPOLI**

**FEDERICO II**

**SCUOLA POLITECNICA E DELLE SCIENZE DI BASE**

**Dipartimento di Ingegneria Chimica, dei Materiali e della  
Produzione Industriale**



**Dottorato di Ricerca in Ingegneria Chimica  
(XXVI ciclo)**

**Innovative technology for  
NO<sub>x</sub> direct decomposition**

**Scientific Committee:**

*Prof. Gennaro Russo*

*Dr. Luciana Lisi*

*Prof. Raffaele Pirone*

**PhD student:**

*Miriam Tortorelli*

**ANNO ACCADEMICO 2013/2014**

<b>Abstract</b> .....	4
<b>Chapter 1</b> .....	6
Introduction.....	6
1.1 NO <sub>x</sub> sources.....	8
1.2 NO <sub>x</sub> effects and regulation limits.....	9
1.3 NO <sub>x</sub> abatement routes .....	11
1.3.1. Selective Catalytic Reduction (SCR) .....	11
1.3.2. NO <sub>x</sub> storage/reduction (NSR).....	13
1.3.3. Non-selective catalytic reduction (NSCR).....	14
<b>Chapter 2</b> .....	15
NO direct decomposition .....	15
2.1 NO direct decomposition .....	16
2.2 NO direct decomposition on Cu-ZSM5 .....	18
2.3 Oxygen and water effect on the NO direct decomposition on Cu-ZSM5.....	19
2.4 Cu-ZSM5 .....	23
2.5 N <sub>x</sub> O <sub>y</sub> adsorbed species .....	25
<b>Thesis project</b> .....	29
<b>Chapter 3</b> .....	30
Experimental section.....	30
3.1 Catalysts preparation.....	31
3.1.1. Powder preparation.....	31
3.1.2. Structured catalyst preparation.....	31
3.2 Experimental setup.....	32
3.2.1. Experimental setup for NO adsorption/decomposition cyclic tests .....	32
3.2.1.1. Reactor for NO adsorption.....	33
3.2.1.2. Reactor for NO decomposition tests.....	34
3.2.2. Experimental setup for FTIR measurements.....	38
3.2.2.1. IR experimental setup for Cu-ZSM5 characterization.....	38
3.2.2.2. IR experimental setup for co-adsorption of NO and H <sub>2</sub> O .....	40

<b>Chapter 4</b> .....	43
Catalyst and adsorbed species characterization .....	43
4.1 Adsorption tests.....	44
4.2 Investigation of Cu-ZSM5 using IR spectroscopy of probe molecules .....	44
4.2.1. Low-temperature CO adsorption on the Cu-ZSM5.....	45
4.2.2. NO adsorption on the Cu-ZSM5 at ambient temperature .....	49
4.2.3. NO adsorption on the Cu-ZSM5 at low temperature .....	55
4.3.1. Co-adsorption of <sup>14</sup> NO and <sup>15</sup> NO .....	60
4.3.2. The oxidation state of the copper sites in the HF mononitrosyls .....	68
4.3.3. Adsorption of NO on CO-precovered sample.....	68
Conclusions.....	73
<b>Chapter 5</b> .....	74
NO adsorption' .....	74
5.1 Adsorption tests.....	75
5.1 NO adsorption after adsorption and desorption of water on LaCu-ZSM5 .....	82
5.2 IR investigation on water effect on NO adsorption .....	86
Conclusions.....	95
<b>Chapter 6</b> .....	96
NO decomposition .....	96
6.1 NO <sub>x</sub> adsorption/decomposition.....	97
6.1.1. Single adsorption/decomposition tests .....	97
6.1.2. Multi-cycle tests .....	101
6.1.3. Multi cycles tests in the presence of oxygen.....	106
6.2 Preliminary FTIR test of NO adsorption/decomposition.....	111
Conclusions.....	114
<b>CONCLUSIONS</b> .....	115
<b>APPENDIX A</b> – Infra Red spectroscopy of probe molecules on solid catalysts.....	118
<b>References</b> .....	121

## Abstract

Direct decomposition of NO to N<sub>2</sub> and O<sub>2</sub> would in principle constitute the most attractive solution to remove NO<sub>x</sub> since it does not require the use of a reducing agent. The main limitation to the application of this reaction is the slow kinetics. Indeed, the Cu-ZSM5, the only catalyst able to activate the NO decomposition providing reaction rates three orders of magnitude higher than the other catalysts at fairly low temperatures, shows lower performance compared to those reported for the traditional SCR process. In addition, the deactivation by water represents another unsolved issue common to the use of Cu-ZSM5 in all De-NO<sub>x</sub> processes.

This PhD thesis focuses on these two aspects proposing an alternative way to carry out the process which overcomes the kinetic limits associated to a continuous flow process and analyzing the effect of water mostly on the adsorption of NO.

The catalyst is prepared by incorporating metal cations into zeolite according to ion exchange procedure. Lanthanum has been exchanged in addition to copper to provide better hydrothermal stability to the zeolite.

The PhD work can be divided into three main sections: 1) a very fundamental study of the copper sites and their interaction with NO carried out at Bulgarian Academy of Science using FTIR spectroscopy at low temperature; 2) a quantitative and qualitative investigation of the adsorption capacity of the zeolite under condition close to that of flue gases (higher temperature and presence of water) and 3) the development of a novel experimental rig for a non-steady-state process to overcome the kinetic limitation.

A detailed investigation of the copper sites and of the nature and evolution of the NO adsorbed species with time has been performed by in-situ FTIR using a IR cell cooled at 100K studying both <sup>14</sup>NO adsorption and <sup>14</sup>NO+<sup>15</sup>NO co-adsorption. In addition to the well-known nitrosyl species on Cu<sup>2+</sup> and Cu<sup>+</sup>, two kinds of Cu<sup>3+</sup>-NO mononitrosyls have been detected produced as a result of disproportionation of Cu<sup>2+</sup> ions from associated sites: Cu<sup>2+</sup>-O-Cu<sup>2+</sup> → Cu<sup>+</sup>-O-Cu<sup>3+</sup>. In the presence of NO, the Cu<sup>3+</sup>-NO complexes are reduced to Cu<sup>+</sup>-NO and Cu<sup>2+</sup>-NO. At low temperature, the Cu<sup>3+</sup>-NO mononitrosyls are able to accept a second NO ligand forming thus Cu<sup>3+</sup>(NO)<sub>2</sub> species. The new findings support the hypothesis that Cu<sup>+</sup> ions are active sites in NO decomposition and the dinitrosyl species, reaction intermediates.

A preliminary study of the adsorption of NO and co-adsorption with water has been carried out in a continuous flow reactor at temperatures close to those typical of flue gases in order to determine the adsorption capacity of the catalyst under real conditions and the effect of water in the absence or presence of O<sub>2</sub> in the feed. TPD experiments have been performed after each adsorption test monitoring all the desorbed NO<sub>x</sub> species.

The effect of water on NO adsorption on LaCu-ZSM5 has been also qualitatively studied by in-situ FTIR identifying the copper sites for NO adsorption displaced by water.

Water has been found to displace NO from copper sites, strongly reducing its adsorption, except for nitrate-like species which are partially preserved also in the presence of water. O<sub>2</sub> addition limits the negative effect of water because it increases the nitrates formation.

Lanthanum co-exchange results in improving the NO adsorption capacity of the zeolite both in the absence and in the presence of water. The relative thermal stability of NO and H<sub>2</sub>O adsorbed species have been also determined. At about 300°C water is removed from zeolite, while NO is still adsorbed on copper as bridged nitrates.

The novel process proposed in this thesis is based on both good adsorption and catalytic properties of the Cu-exchanged ZSM5. The decomposition reaction is carried out under unsteady state (batch) conditions after the zeolite has been saturated with NO. Indeed, the limitations to high NO conversion, related to a NO partial pressure determined by combustion gas emissions, can be theoretically overcome carrying out the reaction in a closed system desorbing large amount of NO in a suitably small volume. To this end a proper experimental rig for testing the feasibility of a cyclic process has been designed and developed. The test procedure involves i) adsorption of NO (in a typical concentration of flue gases from stationary or mobile sources) on LaCu-ZSM5 at 50 °C up to saturation of the zeolite, ii) catalysts heating under batch conditions up to the decomposition temperature (480°C), iii) catalyst cooling down to NO adsorption temperature again.

It has been verified that in the step i) NO can be effectively adsorbed on LaCu-ZSM5 up to the zeolite saturation and the adsorption proceeds through a complete removal of NO<sub>x</sub> from the gas phase. In the step ii) NO is converted into N<sub>2</sub> and O<sub>2</sub> which are the only products exiting the reactor regenerating at the same time the zeolite which is ready for a new cycle after cooling down the system back to the adsorption temperature. The adsorption/decomposition cycles can be repeated without any catalyst deactivation even in the presence of O<sub>2</sub>.

It must be pointed out that a very high NO conversion, much higher than those obtained under flowing (steady state) reaction conditions, is reached in all cycles and that no NO emissions have been detected in all steps of the process.

# **Chapter 1**

## **Introduction**

In the 20<sup>th</sup> century, the increase of the worldwide population has led to a consequent increase of the energy demand and, as a consequence to a higher employment of the natural resources causing an increase of the environmental pollution.

Among the most important pollutant gases there are sulphur oxides, nitrogen oxides, unburned hydrocarbons and carbon monoxide. In order to reduce the emission of these substances, that are produced both by industries and vehicles emissions, new technologies and greener processes have nowadays been studied.

The nitrogen oxides are considered the primary pollutants of the atmosphere, since they are responsible for such environmental problems like photochemical smog, acid rain, tropospheric ozone, ozone layer depletion and even global warming caused by N<sub>2</sub>O. Further to the above, they cause many health problems in humans exposed to high concentrations of these gases. Because of environmental and human health problems caused, the laws on NO<sub>x</sub> emissions are increasingly strict and the NO<sub>x</sub> abatement's study remains a current topic.

The techniques used for the abatement of NO<sub>x</sub> are numerous; for example the Selective Catalytic Reduction (SCR) is mostly addressed to stationary sources whereas the Non selective Catalytic Reduction (NSCR) is suitable for mobile source (conventional gasoline engines).

The catalytic decomposition of NO into N<sub>2</sub> and O<sub>2</sub> would probably represent the most attractive way to remove NO<sub>x</sub> since it does not require the use of a reducing agent. However, the Cu-ZSM5, still representing the most promising catalyst for this reaction, suffers from many limitations that drastically prevent any practical application. Indeed, although the Cu-ZSM5 provides reaction rates for NO decomposition three orders of magnitude higher compared to other catalysts, even at fairly low temperatures, these values are lower than those reported for the traditional SCR reaction. As a consequence, that would entail the use of huge catalyst volume to obtain NO conversion comparable to that achieved through SCR process. However, the catalytic activity of Cu-ZSM5 towards NO<sub>x</sub> decomposition, even if low, is order of magnitude higher than those showed by other materials and, as a consequence, this catalyst represents a “model system” for NO<sub>x</sub> decomposition reaction.

## 1.1 NO<sub>x</sub> sources

The nitrogen oxides are a class of compound including: N<sub>2</sub>O, NO, NO<sub>2</sub>, N<sub>2</sub>O<sub>3</sub>, N<sub>2</sub>O<sub>4</sub> and N<sub>2</sub>O<sub>5</sub>. The abbreviation “NO<sub>x</sub>” usually relates to nitrogen monoxide (NO) and nitrogen dioxide (NO<sub>2</sub>). The most common nitrogen oxides sources are: (i) stationary sources, such as the thermoelectric plants, domestic heating systems, (ii) mobile sources, related to vehicles emissions. In Fig. 1, it is possible to observe that the bigger amount of the nitrogen oxides emissions are due to the mobile sources.

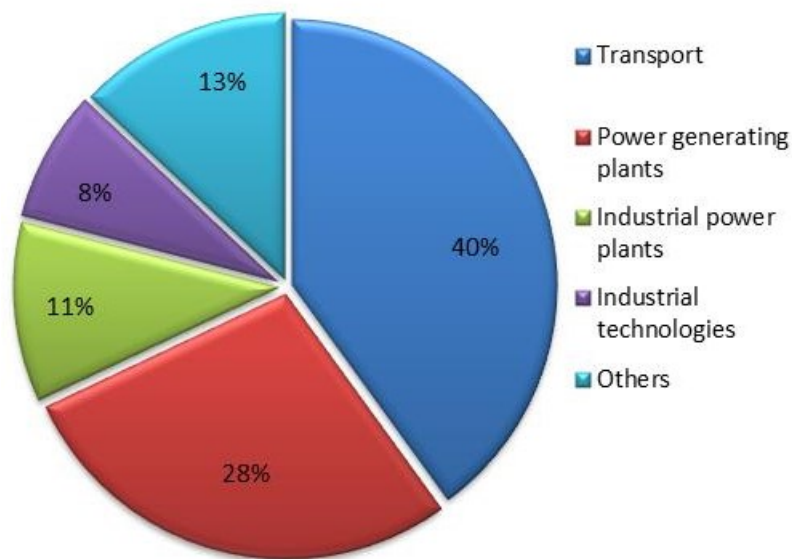


Fig. 1 – Nitrogen oxides emissions sources (Skalska et al. (2010))

Three reaction paths, each having unique characteristics, are responsible for the formation of NO<sub>x</sub> during the combustion processes (Roy et al., 2009):

- *Thermal NO<sub>x</sub>*, which are formed by the combination of atmospheric nitrogen and oxygen at high temperatures (1800 K).



The majority of NO is formed by the reaction between nitrogen and oxygen following the mechanism proposed by Zeldovich (Zeldovich, 1946) and occurring via radicals.

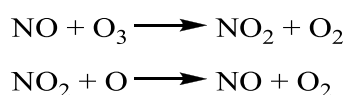


The amount of the produced NO<sub>x</sub> is not related to the fuel nature, but only to the molecular nitrogen and oxygen amount and to the combustion temperature.

- *Fuel NO<sub>x</sub>*, that are formed by the oxidation of fuel-bound nitrogen (FBN), this mechanism is temperature independent.
- *Prompt NO<sub>x</sub>*, which are formed by the reaction of fuel-derived hydrocarbon fragments with atmospheric nitrogen.

## 1.2 NO<sub>x</sub> effects and regulation limits

The nitrogen oxides emissions are one of the main responsible for the atmospheric pollution, especially in the industrialized countries. As a matter of fact, both NO and NO<sub>2</sub> give place, in the atmosphere, to a series of chemical and photochemical reactions producing nitric and nitrous acids, that contribute to the acid rains and to the photochemical smog (Centi and Perathoner, 1995). Moreover, nitrogen oxides contribute to the ozone destruction, by the reactions reported below.



About the human health risks caused by nitrogen oxides, in Tab. 1 both the TLV-TWA (Threshold Limit Value - Time Weighted Average) and their effects are reported (Centi and Perathoner, 1995).

**Tab. 1** – TLV-TWA and related effect to nitrogen oxides exposure

<b>Compound</b>	<b>TLV-TWA (ppm)</b>	<b>Effect</b>
<b>NO</b>	25	Not irritating, toxic by reacting with hemoglobin
<b>NO<sub>2</sub></b>	3	Irritating, it can cause cough, headache and gastrointestinal diseases
<b>N<sub>2</sub>O</b>	50	It contributes to green house and ozone hole, it can cause polyneuropathy and myelopathy

By considering that the major contribution to the nitrogen oxide emissions is due to the vehicles emissions, and by considering all the described effects on both human health and environment, the UE has established strict regulations for the vehicles sold in the UE countries, the so called “Euro” regulations, since 1991.

These regulations are periodically updated and the limits in the pollutant emissions are always lower and lower. In Tab. 2, the European standard emissions for the vehicles are reported for various pollutants.

**Tab. 2** – European standard emissions for vehicles (g/Km)

Diesel	Date	CO	HC + NO <sub>x</sub>	NO <sub>x</sub>	PM
Euro 1	07/1992	2.72	0.97	-	0.14
Euro 2	01/1996	1.0	0.7	-	0.08
Euro 3	01/2000	0.64	0.56	0.50	0.05
Euro 4	01/2005	0.50	0.30	0.25	0.025
Euro 5	09/2009	0.50	0.23	0.18	0.005
Euro 6	09/2014	0.50	0.17	0.08	0.005

For the above reasons, the abatement of these pollutants is demanding. In particular, the abatement of nitrogen oxides is a great interest research topic for both the academic and the industrial sectors.

As regards the stationary sources, DL 152/2006 for the industrial plants and DL 133/2005 for incinerators must be taken into account, the Italian standard are reported in Tab. 3.

**Tab. 3** – Italian standard emissions: average daily (mg/Nm<sup>3</sup>)

Pollutant	Incineration	Combustion plants	Cement factory
Total ashes	10	5	50
SO <sub>2</sub>	50	35	600
NO <sub>x</sub>	200	100	1800-3000
CO	50	-	-

### 1.3 NO<sub>x</sub> abatement routes

Two main strategies can be adopted for NO<sub>x</sub> abatement and related to primary and secondary measures. In the first case, by adopting proper reaction condition and configuration, NO<sub>x</sub> formation can be reduced. As an example, among the new developed technologies, an important innovation is represented by ovens with low NO emission; these minimize the formation of NO<sub>x</sub> and operate at lower combustion temperature and controlled flame stoichiometry, thus reducing the NO<sub>x</sub> emission by 40%. However, some side effects have been detected, such as the increase of carbon in the ashes, an increase in the CO formation, as well as problems related to corrosion and formation of slags.

The second approach (secondary abatement) consists in the abatement of NO<sub>x</sub> by reacting with other reagents, eliminating or modifying the nitrogen oxides to compounds not harmful to health or the environment.

The techniques used for the abatement of NO<sub>x</sub> are numerous; the most common methods to reduce the concentration of nitrogen oxides from gas streams are described below. The Selective Catalytic Reduction (SCR) is mostly addressed to stationary sources whereas the Non selective Catalytic Reduction (NSCR) is suitable for mobile sources (conventional gasoline engines) and the NO<sub>x</sub> storage/reduction (NSR) is used for vehicles with diesel engines.

#### 1.3.1. Selective Catalytic Reduction (SCR)

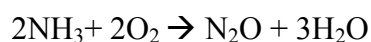
The SCR technique adopts a reducing agent in order to perform two reactions, in which the NO<sub>x</sub> react with the reducing agent, such as ammonia, to give molecular nitrogen.



This method has been used since 1970 in Japan in industrial plants and was subsequently introduced worldwide due to its efficiency, selectivity and economy. The temperature at which the reactions take place is between 200-400 °C (Gómez-García et al., 2005) depending on the type of used catalyst. In these reactions, the ammonia is chemisorbed on the catalyst and reacts with the NO<sub>x</sub> present in the gas phase. The most used catalysts for these reactions are based on metal oxides (V<sub>2</sub>O<sub>5</sub>/TiO<sub>2</sub>, V<sub>2</sub>O<sub>5</sub>-WO<sub>3</sub>/TiO<sub>2</sub>). The plant cost for a SCR is strictly related to the cost of the catalytic bed needed to the reaction.

The SCR disadvantages are (Radojevic, 1998):

- NH<sub>3</sub> emissions (called NH<sub>3</sub> slip), which cause unpleasant odors and damage to the human health. The values of NH<sub>3</sub> slip in the SCR are less than 5ppm, but it is possible to obtain values of NH<sub>3</sub> slip between 0.5 - 2 ppm.
- Emission of N<sub>2</sub>O due to the ammonia oxidation. The produced N<sub>2</sub>O contributes to the greenhouse effect and global warming increase.



- Formation of ammonium salts if in the gaseous stream SO<sub>2</sub> is present. This compound is oxidized and then reacts with the ammonia. The produced salts can poison the catalyst and corrode the equipment. This effect can be reduced by minimizing the NH<sub>3</sub> slip and placing the SCR after a FGD system (Flue Gas Desulfurization).



- The catalyst can be deactivated by the deposition of ashes, or poisoned by heavy metals or oxidized metals compounds. This effect can be reduced by minimizing the soot.

As a promising technique, Iwamoto (Iwamoto et al., 1991) initiated the selective catalytic reduction (SCR) of NO with hydrocarbon in the presence of excess oxygen. Methane, as the main component of natural gas, is cheap and abundant. Originally the selective catalytic reduction with hydrocarbons was found to proceed with the C<sub>≥2</sub> hydrocarbons and Co- and Ni-containing zeolites were reported to operate with methane. Therefore, the SCR of NO with methane has drawn a lot of attention. In the past years, both zeolite (Li et al., 1992) and solid acid loaded catalysts (Yadav et al., 1999) have been used for the SCR of NO with methane.



Even if the SCR is mostly addresses to stationary sources, since 2006 this technology is available on heavy-duty vehicles. Pure ammonia is a toxic and irritant gas, so the reducing agent taken into account is an aqueous solution of 32.5% weight urea. Also in this case the major problem with ammonia-SCR for the NO<sub>x</sub> treatment is the release of NH<sub>3</sub> not used at the exit of the exhaust-line.

The main goal of the ammonia-SCR DeNO<sub>x</sub> system is to obtain a maximum of DeNO<sub>x</sub> efficiency and to keep in control/manage the release of NH<sub>3</sub> in the exhaust-line. The main drawback with ammonia-SCR for the NO<sub>x</sub> emitted by mobile sources is the danger associated to the ammonia storage.

### 1.3.2. NO<sub>x</sub> storage/reduction (NSR)

The NSR can be used in an engine which operates alternately in lean or in rich combustion conditions.

During the lean combustion, NO<sub>x</sub> are oxidized and stored on the catalyst; successively the engine is operated under rich combustion conditions, and NO<sub>x</sub> are released and reduced by hydrocarbons and carbon monoxide.

The catalyst is generally formed by Pt/BaO/Al<sub>2</sub>O<sub>3</sub>, where alumina is the support, used for its high surface area, while Pt is the redox catalyst and BaO provides for the storage capacity.

During the lean combustion, NO is oxidized on the Pt surface to NO<sub>2</sub>. As soon as this product is formed either can be adsorbed on the surface of Pt or returns to the gas phase (Fig. 2).

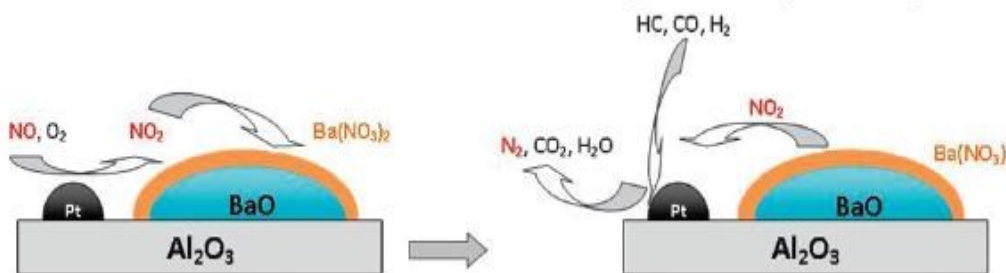


**Fig. 2** – An illustration of the possible mechanism of the NO<sub>x</sub> storage/reduction on a typical Pt/BaO/Al<sub>2</sub>O<sub>3</sub> catalyst (Liu and Gao, 2011)

Successively, NO<sub>2</sub> can react in two alternative ways on the surface of barium oxide: (i) it disproportionates into nitrates and NO, and stored as nitrate; (ii) oxidized to nitrates and stored.

During the rich combustion, the decomposition of the nitrates occurs to NO<sub>2</sub>, that can be reduced to N<sub>2</sub> by reaction with hydrocarbons, carbon monoxide or hydrogen on the Pt particles. Therefore, with this last operation it is possible to obtain the removal of NO<sub>x</sub> and the regeneration of the catalyst (Yu et al., 2009). About the catalyst, the crucial point is the efficiency of the adsorbent material. In general, this material should have a high capacity for trapping NO<sub>x</sub>, a high selectivity towards NO<sub>x</sub> in a complex mixture of gas, a desorption temperature quite low and a high resistance to SO<sub>2</sub> poisoning (Gómez-García et al., 2005).

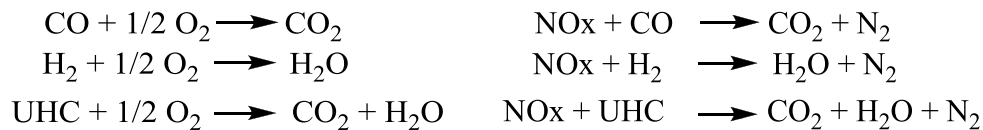
However, the limits of NSR are several:

- The catalysts are efficient only at temperatures above 250°C (when Pt is active)
- During start-up and the first minutes of use of the vehicle there is no catalytic activity
- There is a decrease of the reducing properties after few cycles of accumulation and a reduction due to variations in the structure of the material, caused by the conditions of temperature and humidity present in the catalytic converter.
- The presence of sulfur in fuel poisons the catalyst.

### 1.3.3. Non-selective catalytic reduction (NSCR)

The NSCR is a process in which the reduction of NO<sub>x</sub> to N<sub>2</sub> is simultaneous to the oxidation of carbon monoxide (CO) and unburned hydrocarbons (HC) into CO<sub>2</sub> (Heck, 1999).

Therefore, the reducing species (CO and HC) do not selectively react with NO<sub>x</sub>, the oxidation to CO<sub>2</sub> with O<sub>2</sub> is favored. For this reason, it is necessary to work at O<sub>2</sub> concentrations close to the stoichiometric value in the combustion chamber.



The catalyst is called TWC (Three Way Catalyst), so defined because capable of breaking down simultaneously three pollutant species; the catalyst life lasts about 10 years. This catalyst is based on platinum and rhodium and can be deactivated due to deposits of ash and, in some cases, to thermal sintering.

The main disadvantage of the NSCR is linked to the high cost of the control system of the fuel supply and the catalyst, based on noble metals.

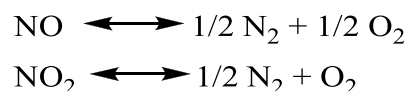
## **Chapter 2**

### **NO direct decomposition**

## 2.1 NO direct decomposition

Direct decomposition of nitrogen oxides ( $\text{NO}_x$ ) into  $\text{N}_2$  and  $\text{O}_2$  ( $2\text{NO} \rightarrow \text{N}_2 + \text{O}_2$ ) offers the most ideal route for  $\text{NO}_x$  removal by catalysis.

From a thermodynamic point of view,  $\text{NO}$  and  $\text{NO}_2$  are unstable. The related  $\Delta G^\circ$  values are both negative and are respectively equal to  $-86 \text{ kJmol}^{-1}$  and  $-51 \text{ kJmol}^{-1}$ .



Despite this thermodynamic instability,  $\text{NO}$  is kinetically very stable. Therefore, a catalyst should be used to activate this reaction at relatively low temperature. The direct  $\text{NO}$  decomposition to  $\text{N}_2$  and  $\text{O}_2$  could be the easiest way to reduce the nitrogen oxides emissions because it is not necessary to add other reagents. Nevertheless, a suitable catalyst and/or system should be developed.

Several catalysts have been studied for  $\text{NO}$  decomposition. During the last years, several materials ( $\text{La}_{2-x}\text{Ba}_x\text{NiO}_4$ ,  $\text{BaO/Ce-Fe}$ ), operating at high temperature, have been proposed (Zhu et al. 2008, Hong et al. 2010) but their application seems impractical. As a matter of fact, these catalysts show significant activity only above  $600^\circ\text{C}$ , as reported by Garin et al. (2001), and conversion higher than 80% above  $800^\circ\text{C}$ .

The most investigated catalyst for  $\text{NO}$  decomposition is copper-exchanged ZSM5, whose working temperature is below  $500^\circ\text{C}$ . No other similar formulations of catalyst (copper over other zeolites or mesoporous materials, or ZSM5 exchanged with other transition metals) exhibits a detectable activity in  $\text{NO}$  decomposition (Li et al., 1991, Li et al., 1992). The strong limitation of  $\text{Cu-ZSM5}$  is the very poor durability in the presence of steam and oxygen.

There are many papers dealing with catalytic decomposition of  $\text{NO}$ . The catalysts for  $\text{NO}$  decomposition reported so far can be classified into four groups: noble metals, metal oxides, perovskite and zeolites.

### - Noble metals

In the 1920s, it was reported that direct  $\text{NO}$  decomposition proceeded on the surface of platinum ( $\text{Pt}$ ) at above  $800^\circ\text{C}$  (Green and Hinshelwood, 1926), but research in this direction fell away because the catalytic activity was insufficient and alternative catalysts to platinum were not forthcoming.

- Metal oxides

Many kinds of metal oxides have been reported as the decomposition catalysts for NO. Among them, transition metal oxides generally show good activity. However, to obtain an acceptable level of catalytic activity very high operating temperatures ( $\sim 1000\text{ }^{\circ}\text{C}$ ) are required, this high temperature cause problems of sintering which excludes the use of these catalysts in practical applications. Another problem related to this high temperature is the heating of the flue combustion gas that means additional process cost.

- Perovskites

The perovskites-type catalysts are possible candidates for NO decomposition catalysts because they easily desorb oxygen. These materials adopt a structure based on the  $\text{ABO}_3$ -type oxide shown in Fig. 3, in which A (large ions such as rare earths and alkaline earths) and B (small transition metals) cations are coordinated by twelve and six  $\text{O}^{2-}$  ions, respectively. The perovskite-type oxides exhibit catalytic activities in the high-temperature region from  $500$  to  $850\text{ }^{\circ}\text{C}$  and are sustainable over long-term operation at the high temperatures required for NO decomposition ( $700\text{--}800\text{ }^{\circ}\text{C}$ ). Oxides adopting the perovskite-type structure expand the possibility of catalyst design, because the original ions at both the A- and B-sites can be replaced by other ions with similar ionic size and valence, while maintaining the original structure (Imanaka and Masui, 2010).

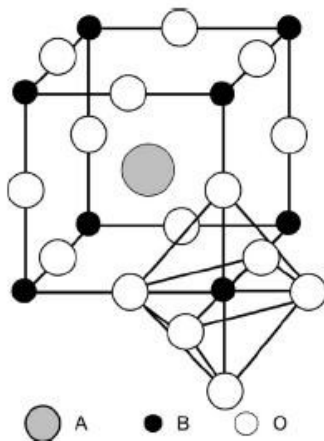


**Fig. 3** – Crystal structure of the  $\text{ABO}_3$ -type perovskite oxide

The perovskite-type catalysts show a  $\text{N}_2$  yield of 70% or more for NO decomposition in the absence of coexisting gases. The advantage of these perovskites is the stability of the structure at high temperatures, while the disadvantage is that the reaction is strongly inhibited by the presence of oxygen and carbon dioxide.

## 2.2 NO direct decomposition on Cu-ZSM5

In order to carry out the  $\text{NO}_x$  direct decomposition, many groups in the '80s have focused their attention on finding a good catalyst. In 1986, the group of Iwamoto found that the Cu-ZSM5 catalyst was more active by several orders of magnitude than all the others catalysts studied and it showed a significant activity in the range 673-773 K (Fig.4). Cu-ZSM5 decomposition activity is unique and stable, but not sufficient under practical conditions (Iwamoto et al., 1991).

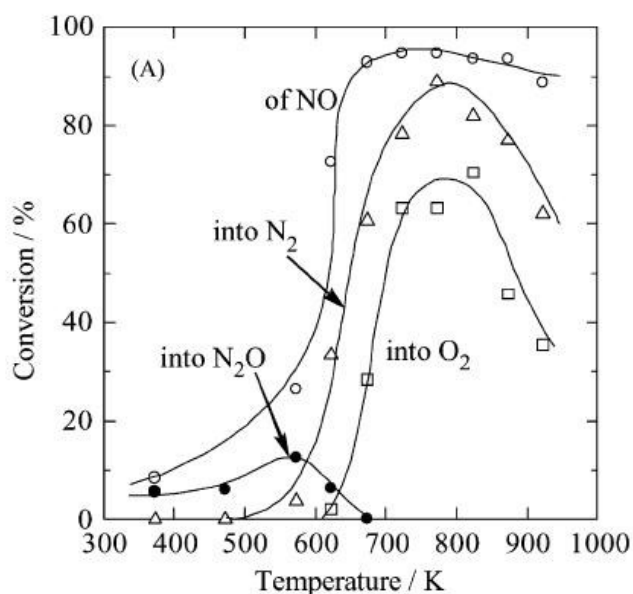


Fig. 4 – Effect of temperature on the decomposition

Iwamoto and co-workers focused special attention to the effect of temperature, observing that  $\text{N}_2$  conversion trend versus temperature presents a maximum value that depends on the Si /Al ratio and the percentage of copper exchanged (Iwamoto and Hamada, 1991).

From this point one of the most investigated catalysts for NO decomposition was copper-exchanged ZSM5.

In 1994, Iwamoto and Yahiro confirmed the activity of this catalyst. In 1991, Li and Hall showed that the rate is controlled by the oxygen desorption. The effect of copper content on conversion has been studied by Iwamoto (Iwamoto and Hamada 1991), who found that at 30% exchange the conversion was just over 20% at 450°C but rose to > 90% at 100% exchange. The Si/Al ratio also has an influence. In the same year Zhang and Flytzani-Stephanopoulos reported that the presence of co-cations enhanced the activity of the catalyst and proposed that they stabilize the active copper sites.

The order of reaction with respect to NO was found to be unity in the operating temperature range 320-550°C (Iwamoto and Hamada 1991, Zhang and Flytzani-Stephanopoulos 1996).

In 2001, Pirone et al. proposed, in the same temperature range, a reaction order with respect to NO in the range 1.24-1.74. Adequate residence times are required for the reaction to proceed (Iwamoto et al. 1991).

### **2.3 Oxygen and water effect on the NO direct decomposition on Cu-ZSM5**

One of the main drawbacks with Cu-ZSM5 is the presence of water vapour in the feed which causes deactivation generally associated to copper shifting to inactive positions (Zhang et al., 1996). However, modifications of this catalyst are further desirable to improve the reduction performance.

The cause of the deactivation is still debated (Kharas et al. 1993, Kucherov et al. 1995, Yan 1996, Zhang 1996, Kucherov, V. 1997, Iwamoto et al. 1997, Quincoces et al. 1999), being its phenomenology strictly related to the operating conditions of testing (temperature, water vapor pressure, time of exposition to wet mixtures).

The presence of water vapour has an inhibiting but reversible effect on the NO decomposition for short time of exposition to wet mixtures (Iwamoto and Hamada 1991, Li and Hall 1991, Iwamoto et al. 1991) whereas sulfur dioxide totally poisons the catalyst (Iwamoto and Hamada 1991).

Kharas et al. (1993), through a combined XRD, EXAFS, and catalytic analysis, concluded that the irreversible deactivation observed under real decomposition conditions (for long exposition time to wet mixtures) was not due to the degradation of the zeolitic framework but to sintering of copper ions to form CuO and Cu<sub>2</sub>O, which grow primarily inside the zeolite, with a partial loss of micropores volume. Catalysts deactivated by water vapour can be partially restored to activity by heating to ~ 500°C (Li and Hall 1991).

Palella et al (2006) has demonstrated that by exchanging Cu-ZSM5 with rare earth cations, especially La, it is possible to achieve a better hydrothermal stability (see Fig. 5).

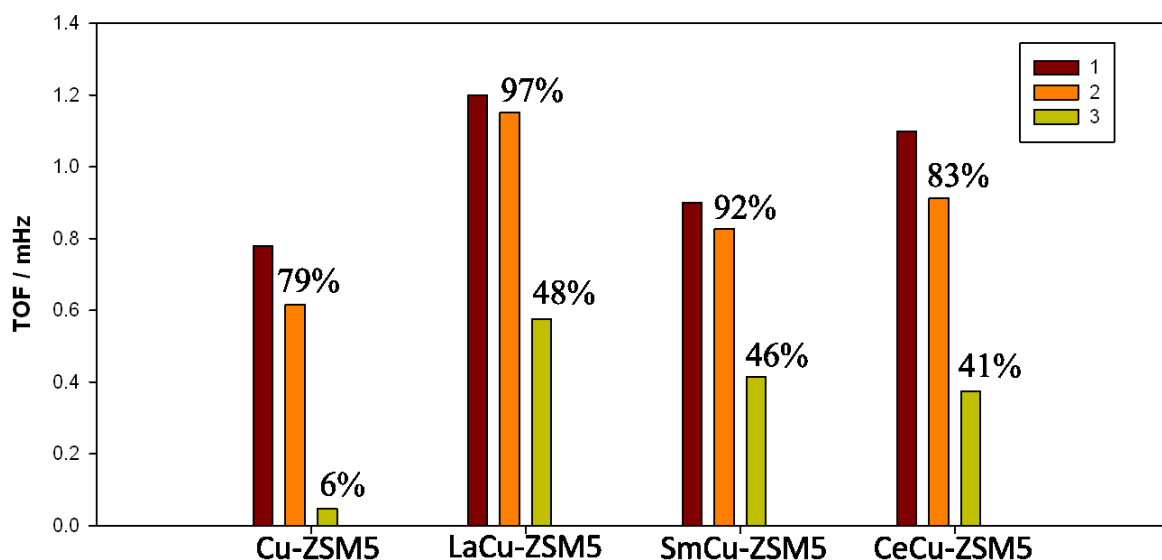


**Fig. 5** – Effect of the aging treatments on the TOF of NO decomposition evaluated under dry conditions at 450°C for CuRE-Z and Cu-Z samples. (Fresh sample (1), after 80 min under reaction mixture in the presence of 2 vol % of H<sub>2</sub>O (2), after further 15 h in the presence of 2.5 vol % at 500°C (3) (Palella et al (2006))

The other problem for the Cu-ZSM5 is the presence of oxygen during the decomposition, this oxygen can be related to the type of gas stream to be treated (combustion exhaust contain about 10% of O<sub>2</sub>) or can be produced by the decomposition reaction itself. The first experimental results on the decomposition in the presence of oxygen are reported by Iwamoto and Hamada (1991).

As it can be seen by the following figure, NO conversion to N<sub>2</sub> as function of temperature decreases when O<sub>2</sub> concentration increases.

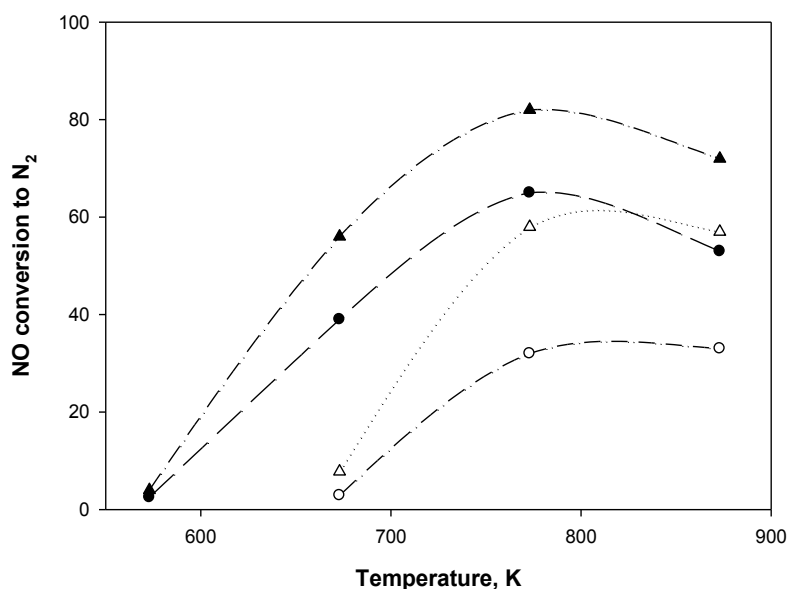


**Fig. 6** - Conversion of NO to N<sub>2</sub> as a function of temperature for a NO concentration equal to 20000 ppm. Tests are carried out with two types of zeolites Cu-ZSM5: Si / Al = 72 and Cu 3.6% wt (▲) and (Δ), Si / Al = 35 and Cu 3.9% wt (●) and (○). The feed contains O<sub>2</sub> at different concentrations: (▲) 0%, (Δ) 5%, (●) 0%, (○) 5%

Concerning the kinetics, from the early '90s several NO decomposition rate studies on Cu-ZSM5 have been reported in literature (Iwamoto et al 1986, 1989; Li and Hall 1991; Campa et al. 1994, Schay et al. 1993, Pirone et al. 2001, Seyedeyn-Azad and Zhang 2005) in order to establish the relationship between the reaction rate and the O<sub>2</sub> concentration.

Li and Hall proposed the power-law rate equation reported below.

$$r = k \cdot [NO]^n \cdot [O_2]^m$$

Where [NO] and [O<sub>2</sub>] are respectively the NO and O<sub>2</sub> concentration during the decomposition test, while n (= 1) and m (= -0.5) are the reaction orders of NO and O<sub>2</sub> respectively.

The authors suggested that NO adsorption becomes unfavorable as temperature increases, leading to a decrease in the concentration of these intermediates at higher temperatures. For this reason, reaction orders have been considered variable with temperature: the O<sub>2</sub> dependence became weaker and the NO dependence increased slightly with by increasing temperature.

The reaction orders values have been obtained by parameter estimation analysis on NO<sub>x</sub> decomposition tests. In the absence or in the presence of O<sub>2</sub> and at different NO concentrations value and temperatures, as reported in Fig. 7. In this way, the NO reaction order was properly estimated.

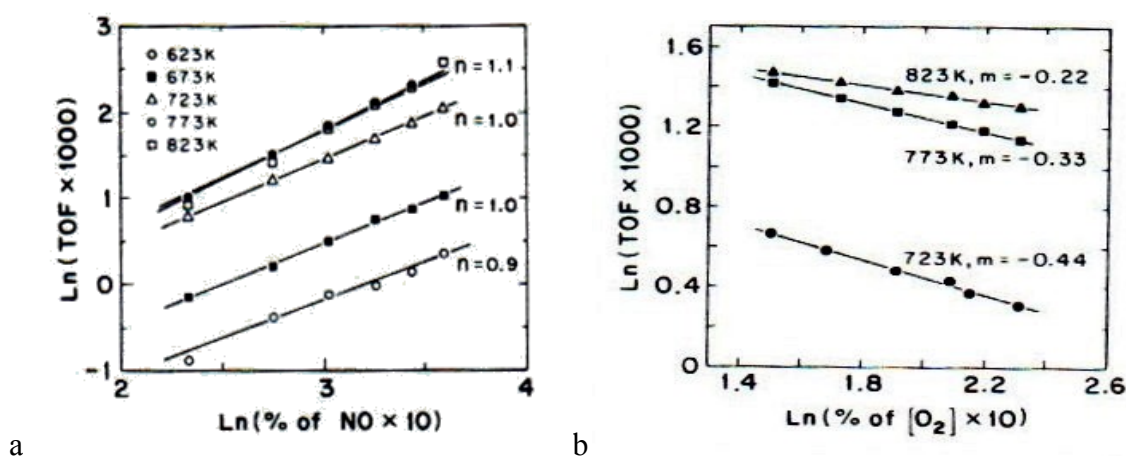


Fig. 7 – TOF (turn over frequency) as a function of NO concentration for a O<sub>2</sub> concentration equal to 0% (a) and 2 % (b). Li and Hall (1991)

The main result of Li and Hall (1991) was to determine an expression for NO decomposition rate on Cu-ZSM5-26-166 reported below.

$$r = \frac{d[N_2]}{dt} = \frac{k \cdot [NO]}{1 + K \cdot [O_2]^{1/2}}$$

In this expression  $r$  is the decomposition rate [ $s^{-1}\cdot\text{site}^{-1}$ ],  $k$  the kinetic constant [ $s^{-1}\cdot\text{site}^{-1}\cdot(\text{mol/liter})^{-1}$ ] and  $K$  the adsorption equilibrium expressed in constant  $(\text{mol/l})^{-1/2}$ .

However, the kinetic model proposed by Li and Hall is not able to predict the presence of a maximum in the NO decomposition as a function of temperature. This maximum has been found experimentally for the first time by Iwamoto et al. (1991). In order to solve this problem Pirone et al. in 2001 determined the reaction orders ( $m$  and  $n$ ) in a temperature range between 400 and 520°C. Pirone et al. proposed a model rather complex, starting from already published kinetic models, that is able to describe the experimental data also in correspondence of the maximum.

The mentioned model has been developed on the basis of the interpretation of some direct decomposition test performing by varying oxygen concentration (0-5000 ppm). The results of these tests have been reported in Fig.8.

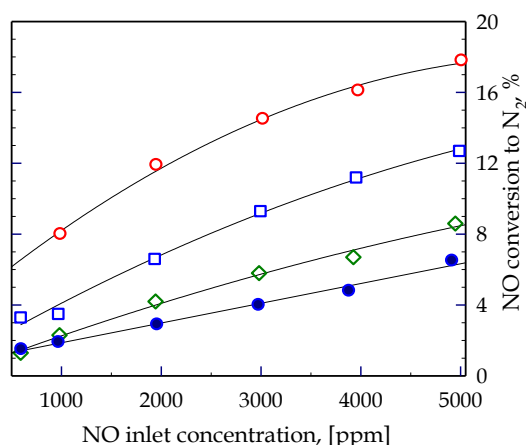
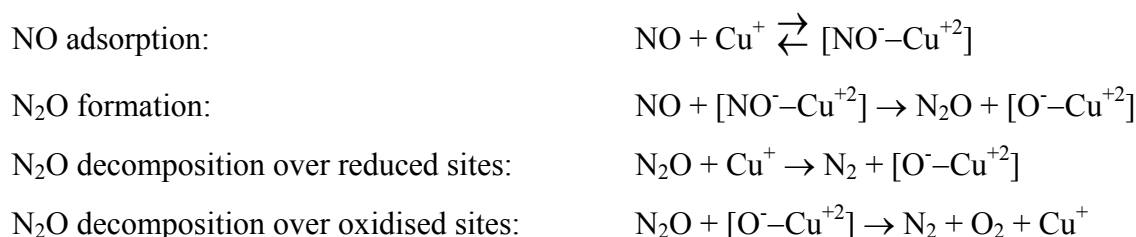


**Fig. 8** – Conversion of NO to N<sub>2</sub> as a function of NO concentration at 500°C.

The feed contains O<sub>2</sub> at different concentrations: (○) 0, (◻) 1000, (◇) 2000, (●) 5000 ppm; W/F = 0.21 g·s·cm<sup>-3</sup> (Pirone et al. 2001)

Pirone et al. demonstrated that oxygen inhibits the NO decomposition rate and that this phenomenon is also present for low values of oxygen concentration in the feed.

Finally, they proposed a mechanism for the direct decomposition and the related expression of the reaction rate. The proposed mechanism is characterized by the formation of N<sub>2</sub>O as a key step.



$$r_{N_2} = \frac{k_s K_{NO} [Cu_{tot}] \cdot p_{NO}^2}{1 + K_{NO} \cdot p_{NO} + K_{O_2} \cdot p_{O_2}^{0.5}}$$

In their paper, Pirone et al. showed the comparison between experimental and simulated data at two NO concentration in the feed (2000 ppm and 5000). It is possible to observe from Fig.9 that there is a good agreement between the experimental and simulated data.

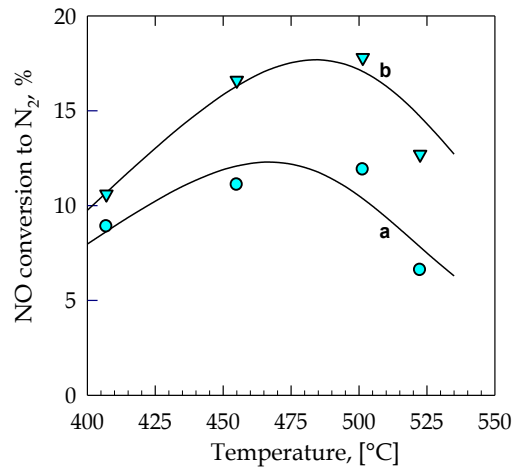


**Fig. 9** – Effect of temperature on NO conversion to N<sub>2</sub> for two representative values of the inlet NO concentration: a) 2000, b) 5000 ppm (Pirone et al. 2001)

## 2.4 Cu-ZSM5

Exchanged zeolites with transition metals are the most promising class of catalysts for NO decomposition. Zeolites are microporous crystalline solids with well-defined structures. Generally they contain silicon, aluminum and oxygen in their framework and cations, water and/or other molecules within their pores.

The zeolites structures have channels and cavities permeable to molecules of various sizes, these structures are based on TO<sub>4</sub> tetrahedra, where T is an aluminum or silicon atom.

The most studied zeolite for the NO direct decomposition is ZSM5 (Fig. 10) and in particular Cu-ZSM5.

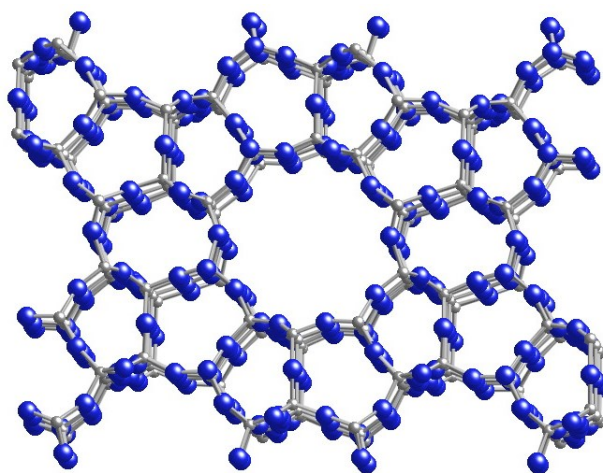


Fig. 10 – ZSM5 crystal structure

ZSM5 is a crystalline aluminosilicate having an unit cell  $M_{x/n}[(AlO_2)_{96-x}(SiO_2)_x] \cdot 16H_2O$  prepared from aqueous solution by templated crystallization, where M is a metal cation with a positive charge that can be exchanged into the zeolite. The hydrated crystals are activated by calcination before use. The structure of the resulting crystal contains oxygen ion tetrahedral with either  $Si^{4+}$  or  $Al^{3+}$  at the center, forming regular channels of diameter  $\sim 5.5 \text{ \AA}$  and cavities dimension  $\sim 9 \text{ \AA}$ . These dimensions allow straight-chain and smaller branched hydrocarbons to enter the channels. The BET surface area is typically  $300\text{-}400 \text{ m}^2\text{g}^{-1}$ . Charge neutrality demands an additional positive charge for every  $Al^{3+}$  in the lattice, in fact the presence of  $AlO_2^-$  produce a residual negative charge in the crystal lattices that are compensated by cations such as sodium located in the pores and bonded to  $AlO_2^-$  by electrostatic forces. The metal M is sodium (or  $H^+$ ) during initial preparation, but this can be exchanged for other metals by subsequent treatment with a solution of the appropriate cation. An impressive number of publications have been devoted to characterizing the Cu-ZSM5 catalyst with respect to the NO decomposition. However, the nature of the active sites is still unclear and is the subject of extensive debate.

One of the main characteristics of Cu-ZSM5 is the "self-reduction" of Cu(II) to Cu(I), occurring even in nitrogen atmosphere at 673 K and, therefore, without a reducing gas.

This reduction has been associated with the spontaneous desorption of  $O_2$  at high temperature, even though the mobility of framework oxygen and the rates of dehydroxylation are very low in these conditions. This phenomenon has been studied by Iwamoto and his co-workers (1986, 1991); subsequently Li and Hall (1991) gave a more plausible explanation of this facile copper reduction, proposing that Cu(II) cations are linked to extralattice oxygen (ELO) which can be much more easily removed with a thermal activation than framework oxygen. The ELO is not part of the zeolite structure, but is, in some way, bonded to the copper ions in the oxidized state ( $Cu^{+2}$ ).

In 1993, Valyon and Hall were able to obtain the reduced catalyst, with a pretreatment of Cu-ZSM5 at 350° C; in the same work the authors indicated a temperature equal to 300° C, as self-reduction temperature of the catalyst, in agreement with Li and Hall (1990).

In 1993, Valyon and Hall confirmed the hypothesis that the self-reduction is caused by the desorption of atoms of ELO (recombined in the form of O<sub>2</sub> gas) that the Cu-ZSM5 desorbs in quantities greater than those released by similar catalysts, in a stream of inert or vacuum high temperature. In the same paper the authors also proposed that the oxygen latter is involved in the decomposition reaction. This hypothesis has been proved by measures of isotopic exchange.

Another hypothesis (Bell et al., 1997) about the self-reduction was that a part of the reduced sites were produced during pre-treatment of the sample by dehydration of dimeric and/or oligomeric copper species, according to the following reaction:



Then, the so-obtained chains of Cu (II) ions linked by oxygen atoms can desorb O<sub>2</sub>, leading to reduced copper sites.

## 2.5 N<sub>x</sub>O<sub>y</sub> adsorbed species

The NO adsorption on copper sites causes the formation of different N<sub>x</sub>O<sub>y</sub>-copper species which may coexist on the catalyst surface. The study of these species and their evolution with time and temperature is very useful to understand the adsorption and decomposition mechanisms; the NO adsorption was considered a key-step for the formation of the reaction intermediates in DeNO<sub>x</sub> reactions (Solans-Monfort et al. 2000, Lisi et al. 2012).

The NO adsorbed species were studied in several papers, even if the results proposed by different authors are quite contradictory.

The species that are generated by the interaction of NO with the Cu-ZSM5 (Cu<sup>+1</sup> and Cu<sup>+2</sup>) are numerous (e.g. mono-nitrosyl, di- nitrosyl and nitrates) (Aylor et al., 1995; Henriques et al., 1998; Konduru and Chuang, 1999a, 1999b; Hadjiivanov , 2000).

The determination of the nature of N<sub>x</sub>O<sub>y</sub> adspecies is difficult for some reasons, one is the large number of compounds which may coexist on the surface.

A useful method to study these species is the Infra Red Spectroscopy; nevertheless, interpretation of the results is not trivial due to the coincidence of some bands from the spectra of different nitrogen-oxo compounds. Another problem is that the IR bands arising from the skeletal vibrations of zeolites do not allow observation of important bands of surface species in the 1300–1000 cm<sup>-1</sup> region (Hadjiivanov 2000).

Many reports on NO adsorption on Cu-ZSM5 revealed formation of nitrosyls of Cu<sup>2+</sup> and Cu<sup>+</sup> cations. The Cu<sup>+</sup>-NO mononitrosyls are observed at around 1815–1807 cm<sup>-1</sup>.

These species are able to accommodate a second NO molecule thus forming dinitrosyls ( $\nu_s$  at ca. 1827 and  $\nu_{as}$  at ca. 1734 cm<sup>-1</sup>) (Iwamoto et al. 1992, Yahiro et al. 2001, Fanson et al. 2002, Góra-Marek et al. 2011). Note that these dinitrosyls are true (they are not cis-dimers), because they are decomposed via mononitrosyls. The Cu<sup>2+</sup>-NO species are typically observed between 1915 and 1895 cm<sup>-1</sup>. The exact band position is considered to depend on the Cu<sup>2+</sup> environment (Jang et al. 1996, Dědeček et al. 1995, Hadjiivanov 1999). No dinitrosyls of Cu<sup>2+</sup> species were reported. In addition, formation of surface nitrates and/or nitrites were noticed by many researches (Iwamoto et al. 1992, Yahiro et al. 2001, Ziolk et al. 2000). The presence of nitrates, proven by IR (Konduru et al. 1999 and 2000, Lisi et al. 2012), has been verified by other techniques too, as reported below. These species are formed over copper sites with a ratio depending on the concentration of copper pairs. The formation of nitrate species is very important, because the development of nitrate species on copper sites is considered a key-step in the direct decomposition and in the selective catalytic reactions.

Hadjiivanov et al. (1996) studied the adsorption of NO<sub>x</sub> and NO+O<sub>2</sub> co-adsorption on Cu-ZSM5-37 (11% CuO) using FTIR spectroscopy at 180°C. In particular, they found that the NO<sub>2</sub> adsorption and NO+O<sub>2</sub> co-adsorption lead to the formation of the some types of nitrate. In the presence of oxygen, the NO is converted to nitrate according to the following scheme:



Nitrate formation has been observed also during NO<sub>2</sub> adsorption, NO being a by-product by FTIR (Olsson et al., 2009) and temperature programmed desorption (TPD) measurements (Depres et al., 2003). Authors suggested that nitrates and NO production occurred by a disproportionation reaction reported below.



The formation of nitrate and their subsequent decomposition was observed also by Schay et al. (1998) through TPD of NO. In this work the authors have observed two desorption peaks simultaneously of NO and O<sub>2</sub> at 420°C, their ratio being equal to 1.

TPD has been widely used in order to study the nature of the adsorption species (Li and Armor (1991), Schay and Guzzi (1993), Sepúlveda-Escribano et al. (1993), Eränen et al. (1994), Torre-Abreu et al. (1997), Schay et al. (1998), Despres et al. (2003), Olsson et al. (2009) and Lisi et al. (2012)). A typical TPD result is reported in Fig. 11 (Lisi et al. 2012).

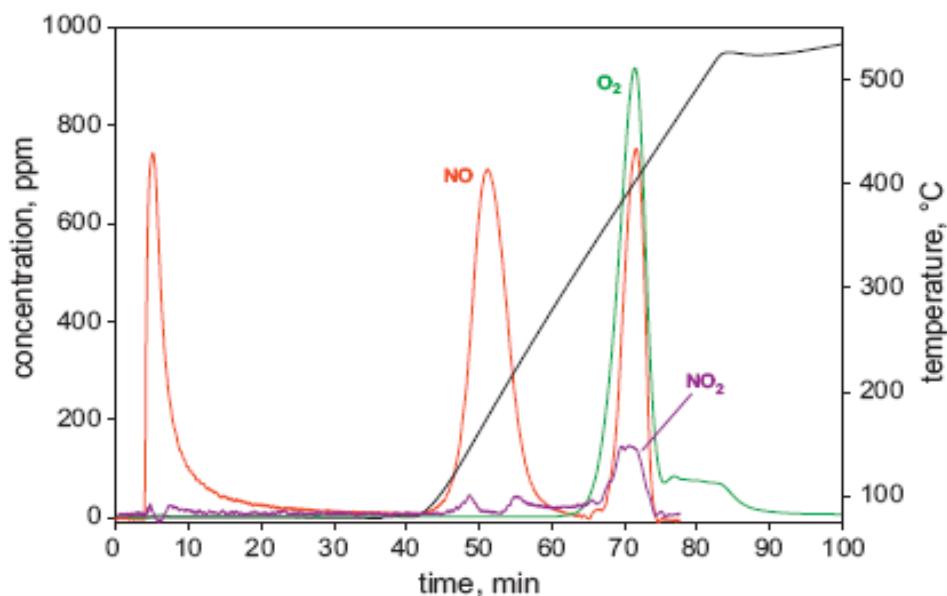


**Fig. 11** – NO, NO<sub>2</sub>, N<sub>2</sub>O and O<sub>2</sub> output concentrations during purging phase with helium and the TPD conducted after the saturation of the preoxidized Cu-ZSM5. (Lisi et al. (2012))

During the TPD the evolution of adsorbed NO into the gas phase depends on the temperature changes and presents several maxima. Five maxima have been observed by Li and Armor (1991), while other authors found a smaller number of peaks, such as Schay and Gucci (1993), Sepúlveda-Escribano et al. (1993), Eränen et al. (1994), Torre-Abreu et al. (1997), Schay et al. (1998), Despres et al. (2003), Olsson et al. (2009) and Lisi et al. (2012). Generally, the peak temperature is indicative of the stability of the different species and indicates at which temperature the adsorbed species leave the catalyst surface.

In Fig. 11, it is possible to observe a first desorption at low and constant temperature, due to the release of the physisorbed NO. When the temperature is increased, two peaks proper of NO, the first at 180°C and the second at 390°C, are detected. The first peak is more intense for catalysts with lower Si/Al ratio and it has been associated with the decomposition of mononitrosyl complexes, particularly those related to species Cu<sup>2+</sup> (Lisi et al., 2012).

The second peak is less intense by increasing Si/Al ratio and it is due to the decomposition of nitrate (NO<sup>3-</sup>) or nitrite (NO<sup>2-</sup>) adsorbed on Cu<sup>2+</sup> species, as already reported by Li and Armor (1991), Ansell et al. (1993), Zhang et al. (1993), Iwamoto (1990), Schay et al. (1998), Despres et al. (2003), Lisi et al. (2012). Generally, only NO is detected during nitrates decomposition; nevertheless, in some cases also NO<sub>2</sub> has been produced (Despres et al., 2003; Lisi et al., 2012).

In Fig. 12, adapted by Torre-Abreu et al. (1997), a shoulder is present at 200°C, that has been attributed to the NO desorption from Cu<sup>+</sup> species, in contrast to Zhang et al (1993), these last authors associated the NO desorption at 200°C at Cu<sup>2+</sup> species. According to the results reported by Lisi et al. (2012), it is probable that the single peak they detected at about 180°C corresponds to the peak and the shoulder reported by Torre-Abreu et al. (1997), thus confirming that mono-nitrosyls formed onto reduced and oxidized copper decompose at about the same temperature.

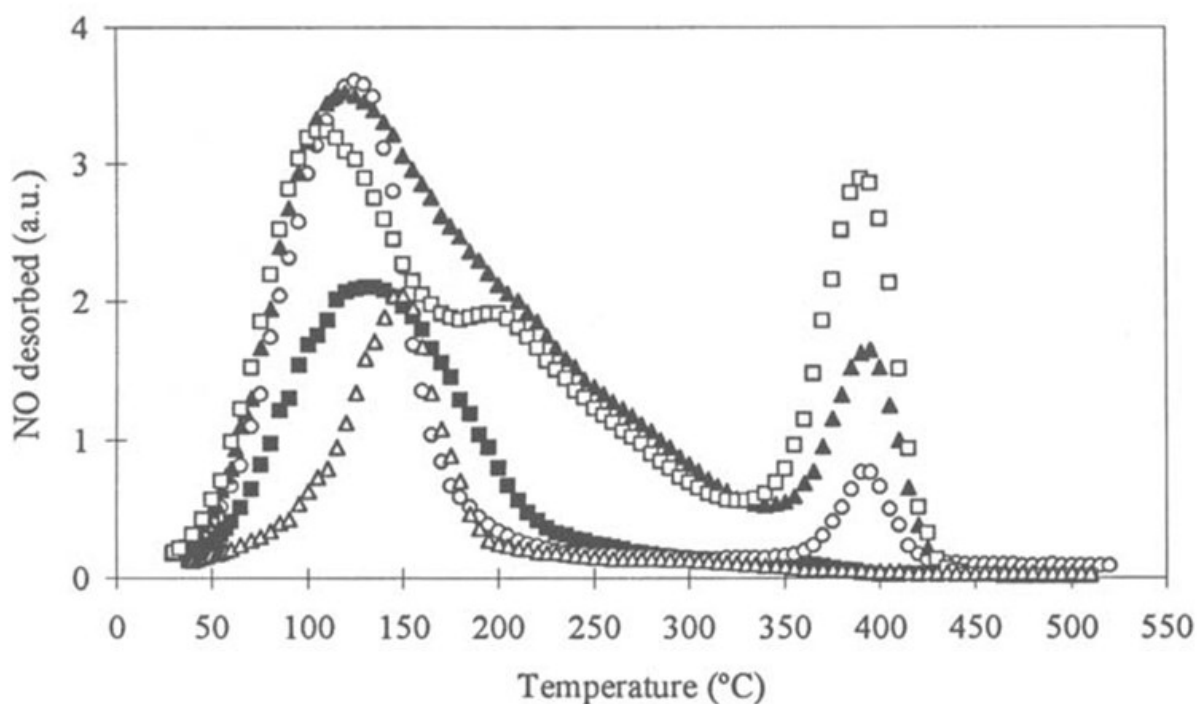


**Fig. 12** – NO adsorption over CuMFI catalysts with different Si/Al ratio and different Cu content. ( $\Delta$ ) HMF'I-27-0, ( $\blacksquare$ ) CuMFI-27-40, ( $\circ$ ) CuMFI-27-80, ( $\blacktriangle$ ) CuMFI-27-160 and ( $\square$ ) CuMFI-27-320. TPD made by Torre-Abreu et al. (1997)

Finally, the NO+H<sub>2</sub>O co-adsorption has been rarely studied. In particular, Despres et al. (2003) conducted their co-adsorption study on an over-exchanged Cu-ZSM5 (Si/Al = 40) at 200°C. They concluded that NO molecule does not adsorb on the zeolite, contrary to NO<sub>2</sub>. For this reason, they believed that NO adsorption occur only after an oxidation. The effect of water adsorption on the formation of NO<sub>x</sub> adsorbed species has been studied also by Hadjiivanov et al. (1996), in this work the authors affirmed that the nitrates are only slightly affected by water introduction in the feed.

## Thesis project

As reported before, the Cu-ZSM5 has been widely studied in the past as possible catalyst for NO decomposition because of its unique properties. Nevertheless, due to the kinetic limitation and the deactivation in the presence of water the attention towards this catalyst recently declined although the NO decomposition still represents an ideal and attractive process not requiring the use and the suitable dosage of a reducing agent.

The main limit which has been identified is the slow kinetics which would need impractical contact times (and as a consequence catalyst volume), not suitable for practical applications, to achieve the same NO conversion obtained with conventional processes. On the other hand, the NO partial pressure is unavoidably determined by the flue gas emissions and cannot be modified in order to speed up the reaction rate.

Therefore, the idea of this PhD thesis is based on the development of a periodic process, roughly inspired by the NO<sub>x</sub> Storage Reduction process and based to the good properties of the Cu-ZSM5 both as adsorbent and as catalyst. The system proposed involves NO adsorption on the zeolite at quite low temperature (50 °C) followed by the NO decomposition in static condition at the reaction temperature (480 °C). In theory the catalyst could work with a higher NO partial pressure in a time sufficient to decompose all NO into N<sub>2</sub> and O<sub>2</sub>. The occurrence of the reaction at the same time regenerates the catalysts which would be thus ready for a new adsorption cycle after cooling down to the adsorption temperature. A cyclic operation with two reactors operating in parallel, one adsorbing and another decomposing, could remove nitrogen oxides reducing the volumes necessary for the NO<sub>x</sub> abatement unit both if addressed to stationary and to mobile sources.

A preliminary detailed FT-IR study of the Cu-exchanged ZSM5 have been done through the NO adsorption and <sup>14</sup>NO + <sup>15</sup>NO co-adsorption to characterize the copper sites (Chapter 4).

Simultaneously to the study of the feasibility of this system, the effect of water vapour on the adsorption of NO has been studied since this can represent a limit to the application of the process.

The effect of the presence of water on the NO adsorption has been investigated identifying the main parameters affecting the adsorption and the chemical nature of the adsorbed species (Chapter 5).

A properly designed system with a stainless steel reactor has been developed to carry out the cyclic adsorption/decomposition process using monolith catalyst (LaCu-ZSM5). A study of the operating parameters and of the catalyst stability to repeated cycles was performed (Chapter 6).

A FTIR analysis carried out under flow conditions and temperatures very close to those taking place in the steel reactor has supported the whole investigation (Chapter 6).

## **Chapter 3**

### **Experimental section**

### **3.1 Catalysts preparation**

In the whole work, excluding adsorption/decomposition tests in the steel reactor, the catalyst was used as powder, both exchanged copper or co-exchanged with copper and lanthanum. In the adsorption/decomposition tests LaCu-ZSM5 was deposited on a ceramic monolith.

#### **3.1.1. Powder preparation**

The starting material was a NH<sub>4</sub>-ZSM5 sample was a commercial Zeolyst product (CBV-2314, SiO<sub>2</sub>/Al<sub>2</sub>O<sub>3</sub> = 23, BET specific surface area of 425 m<sup>2</sup> g<sup>-1</sup>). The sample was preliminary thermally treated 2h at 550°C under He in order to decompose ammonium and obtain the H-form of the zeolite. Copper was introduced by ion exchange from aqueous solution at 323 K for 2 h with a 20 mM solution of copper(II) acetate monohydrate (Aldrich, purity 99.8%) using a zeolite/solution ratio of 8 g l<sup>-1</sup>. After the ion exchange, the sample was centrifuged, washed twice with double distilled water, and dried at 393 K overnight. After this step the exchanged zeolite was calcined 2 h at 550 °C (10 °C min<sup>-1</sup>) under helium flow.

The LaCu-ZSM5 was prepared by a double exchange procedure. Lanthanum was firstly exchanged in a 20 mM lanthanum nitrate (Aldrich purity 99%) aqueous solution at 95 °C for 5 h.

After calcination the sample was then exchanged with copper as described before and calcined again. The copper and lanthanum concentration have been determined with an Agilent 7500 ICP-MS, the value was 1.8 and 0.16 wt% respectively.

#### **3.1.2. Structured catalyst preparation**

Structured catalysts have been prepared according to Lisi et al. (2009). Cordierite (2Al<sub>2</sub>O<sub>3</sub>·5SiO<sub>2</sub>·2MgO) honeycomb monoliths, manufactured by Corning with cell density of 400 cpsi, have been cut into cylindrical shape in order to have a length equal to 1.9 cm and a diameter of 1.7 cm. Then the monoliths have been coated by dipping them in a suspension containing water and the LaCu-ZSM5 zeolite (previously prepared according to the procedure described above). After each impregnation, the monoliths have been kept 20 minutes in an oven at 120 °C, 2 hours at 550 °C and then weighed to determine the amount of zeolite deposited. The procedure has been repeated up to reaching the desired coating amount.

## 3.2 Experimental setup

### 3.2.1. Experimental setup for NO adsorption/decomposition cyclic tests

A schematic overview of the realized experimental setup useful to study the NO adsorption and the decompositions test over the ZSM5 based catalyst is reported in Fig. 13.

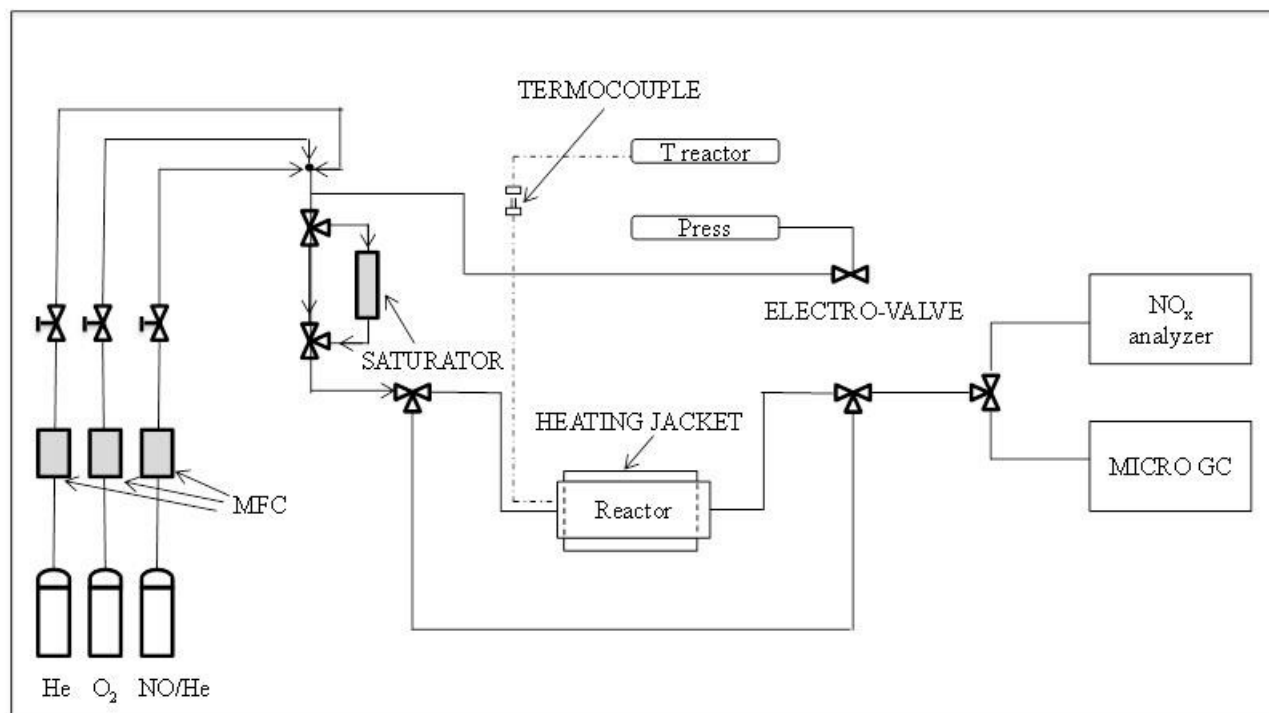


Fig. 13 – Experimental setup for the adsorption/decomposition tests

The feed mixture was obtained by mixing high purity gases (He 99.999%; O<sub>2</sub> 99.95%) and NO/He mixture (1 vol%; 100 ppmv NO<sub>2</sub> impurity). The flow-rate of each stream was controlled by a dedicated mass flow-controller (BROOKS MFC SLA5850S). The feed mixture can pass through a saturator (U-tube (d.i.= 20 mm) loaded with glass wool soaked in bi-distilled water) to introduce water vapour in a given concentration determined by the temperature.

The gas analysis system has been designed to measure NO, NO<sub>2</sub>, N<sub>2</sub>O, N<sub>2</sub> and O<sub>2</sub> species, that are the species that may be formed during the adsorption and decomposition of nitrogen monoxide. The concentration of nitrogen oxide, nitrogen dioxide and nitrous oxide in both the gaseous stream inlet and outlet was measured by a continuous analyzer (EMERSON X-STREAM XEGP). This analyzer based on the principle of IR spectrophotometry can detect the NO and NO<sub>2</sub> concentrations. The same analyzer also allows the simultaneous analysis of N<sub>2</sub>O using the same principle of operation, but by measuring the absorption of UV radiation.

The range of concentrations of NO, NO<sub>2</sub> and N<sub>2</sub>O measurable by the instrument is respectively up to 10000, 1000 and 3000 ppm.

Other gaseous species are measured by a Micro Gas Chromatograph (VARIAN CP4900), placed in parallel to the previous analyzers. This apparatus carries out measurements in a short time (45-60 s), so this analysis can be considered almost continuous.

The MicroGC is constituted by two analytical channels. Channel A is provided with a Mol Sieve 5 Å (MS5A) column with backflash, that preventing the entry of CO<sub>2</sub> present in the flue gas are able to saturate the column stationary phase in the column, with resulting in low efficiency. This channel analyzes O<sub>2</sub> and N<sub>2</sub>. Channel B is provided with a Pora Plot U (PPU) column that measures species such as CO<sub>2</sub> and N<sub>2</sub>O.

The data measured by the NO<sub>x</sub> analyzer are continuously recorded on a personal computer, using a data acquisition system developed in LabView.

To prevent the water vapor reaches the analyzers, downstream of the reactor has been inserted in a chemical trap consists of a U-tube (d.i.= 20 mm) filled with pellets of CaCl<sub>2</sub>.

The reactor and the heating system are different according to the type of test and are described in the following paragraphs.

#### **3.2.1.1. Reactor for NO adsorption**

The reactor for the NO adsorption experiments (Fug. 14) is a quartz pipe of 70 cm length and 1.0 cm internal diameter. Inside this quartz cylinder another quartz cylinder (d.i.=6 mm) is inserted in order to create an annulus between the reactors in which the gaseous mixtures can pass and reach the powder catalyst. A porous septum inside the reactor is inserted to support the powder catalyst. In the second cylinder the bottom is closed and a K-type thermocouple (Chromel-Alumel) makes the measurements of the axial temperature.

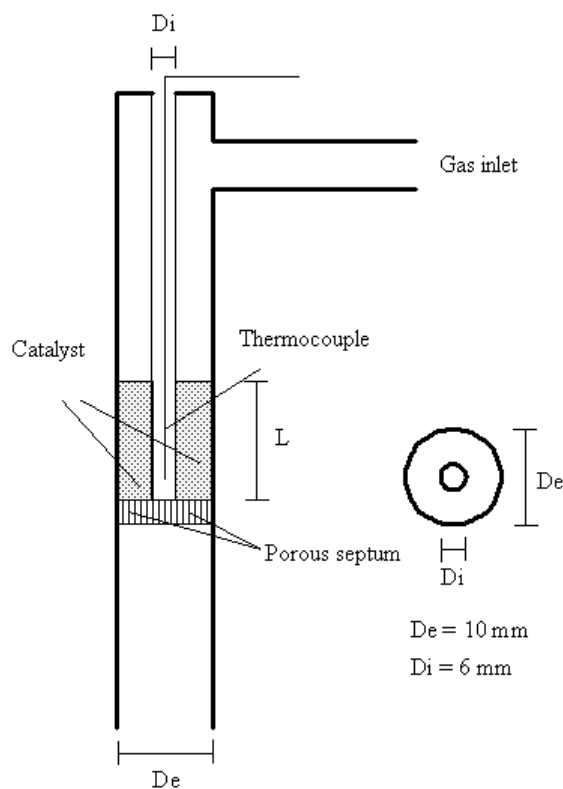


**Fig. 14** – Quartz reactor

The quartz reactor is put in a 60 cm long electrical heating (LENTON LTD mod.PTF 12/38/500). This oven is equipped with three temperature control device (TCD) EURO THERM 808, each of these manages a single resistor and ensures overall isothermal zone 40 cm long. Inside the catalytic bed a good isothermicity is guaranteed as given that the axial dimensions of the bed are by far lower than the corresponding dimensions of the oven.

On the other hand the thermal effects due to the adsorption heating are negligible, because of the low concentrations of the reagents.

### **3.2.1.2. Reactor for NO decomposition tests**

Before carrying out NO decomposition tests under batch condition, the maximum pressure reachable in the reactor has been estimated. The NO decomposition reaction to nitrogen and oxygen, takes place without change of the number of moles from reagent to products. For this reason, the increase of the reactor pressure during the reaction can be due to the temperature rise from adsorption temperature ( $50^\circ\text{C}$ ) to the decomposition temperature ( $480^\circ\text{C}$ ) and to the possible NO desorption before decomposition occurs.

By using the ideal gas state equation, it is possible to calculate the maximum pressure during the decomposition, by fixing the reactor volume (0.088 dm<sup>3</sup>), the amount of NO adsorbed per gram of zeolite at 50 °C (60 μmol), evaluated from the previous tests, and the initial pressure (1.4 atm).

$$P_{dec} = \frac{n_2 \cdot T_{dec}}{n_1 \cdot T_{ads}} \cdot P_{in}$$

where:

$n_1$ : initial μmols at  $T_{ads}$

$n_2$ : μmols at  $T_{dec}$  (sum of  $n_1$  and the adsorbed μmols)

$T_{ads}$ : adsorption temperature

$T_{dec}$ : decomposition temperature

The value of the maximum pressure during the decomposition results to be equal to 3 atm ( $P_{dec}$ ). The real pressure should be lower due to the not uniform distribution of temperature inside the reactor (the peripheral elements are at lower temperature).

For this reason, the batch reactor to be used for adsorption-decomposition tests should be made in stainless steel because the value of pressure reached during the NO decomposition step does not recommend the use of glass-like reactor and of the corresponding fittings.

The reactor is a stainless steel tube of 28 cm length and 1” diameter. Immediately before and after the reactor two three-ways valves are placed in order to isolate the reactor from the gas stream. A scheme of the reactor is reported below (Fig.15).



Fig. 15 – Steel reactor

At the outlet of the reactor, before the three-way valve, a pressure transducer (Dwyer series 628, range 0-300 psig) is positioned in order to monitor the pressure during the decomposition test. The reactor is electrically heated by using an easily removable heating jacket connected to a temperature controller).

This reactor will be operated under unsteady state condition; in the first part of the experiment NO adsorption will be performed until catalyst saturation. Afterwards the reactor inlet and outlet will be closed and later decomposition will be performed in order to regenerate the catalyst.

Before carrying out NO adsorption/decomposition tests, the contribution of the amount of NO, contained in the gas phase inside the steel reactor, have been determined. In order to calculate the micromoles of gas contained in the reactor it is useful to consider several parameters evaluated from the previous tests. These parameters are the pressure inside the reactor (1.4 atm), the adsorption temperature (323 K) and the volume of the reactor ( $0.088 \text{ dm}^3$ ). It is possible to calculate the micromoles of NO, contained in the gas phase inside the steel reactor, considering that the NO concentration in the gas phase is 800 ppm. The NO amount calculated ( $3.74 \text{ } \mu\text{mol}$ ) is negligible compared to the amount of NO adsorbed by the catalyst at  $50 \text{ } ^\circ\text{C}$  ( $60 \text{ } \mu\text{mol/g}_{\text{cat}}$ ). So it can be considered that the amount of NO contained in the reactor (NO adsorbed + NO in the gas phase) is about equal to the NO adsorbed with an error of 6%.

Before starting with the experiments the stain steel reactor has been thermally characterized. The reactor has been filled with 14 cordierite monoliths (length 1.9 cm; diameter 1.7 cm) without catalyst, then the reactor has been electrically heated to a given temperature flowing a He stream ( $5 \text{ l/h}$ ). The temperature was measured at various reactor lengths moving a thermocouple along the reactor to obtain a temperature profile. Figure 16 shows that an almost isothermal zone exists in the middle of the reactor and is about 5 cm long. As a consequence, in order to perform experiments under controlled conditions, no more than 2 coated monoliths located in the center of the reactor can be used because the temperature sharply declines moving towards the end sides.

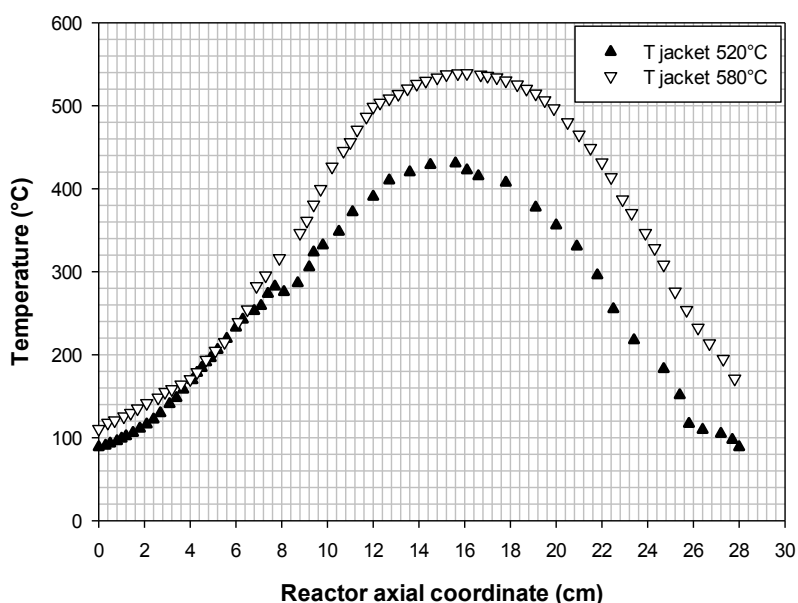


**Fig. 16** – Temperature profile recorded at different reactor's length

In order to confirm this result, the two central ceramic monoliths have been substituted with two ZSM5-coted monolith and four thermocouples have been placed in the centers of each monolith, and at the inlet and outlet section as shown in Fig.17.

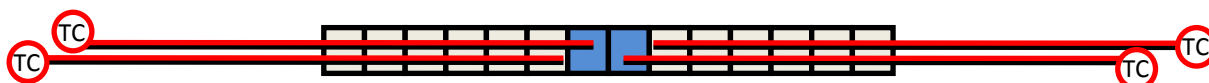


**Fig. 17** – Thermocouples positions

Then, the temperature of the heating jacket has been changed and the monoliths temperatures have been recorded; the results are reported in the following table (Tab.6).

**Tab. 4** – Thermal tests

<b>T jacket (°C)</b>		19	65	100	500	520	550	600
<b>Thermocouple</b>	<b>Reactor axial coordinate (cm)</b>	<b>Temperature (°C)</b>						
1	12 (inlet)	18.6	50.0	71.7	438	460	491	549
2	13 (middle)	18.7	50.7	71.5	445	467	498	552
3	15 (middle)	18.5	50.8	71.5	443	465	497	551
4	16 (exit)	18.5	49.9	71.5	433	456	487	550

The temperature values measured in the middle of the catalyst are practically equal, while those of the inlet and the outlet of the monoliths are slightly (c.a. 1 °C) lower in the T jacket range 500-600 °C. This result suggests that the monoliths are placed in the middle of the reactor, i.e. in the pseudo-isothermal zone according to the previous results.

### **3.2.2. Experimental setup for FTIR measurements**

CO and NO were used as probe molecules for characterization of the Cu-ZSM5 sample. Two different apparatus have been used for FTIR experiments that will be described in details in the next paragraph.

#### **3.2.2.1. IR experimental setup for Cu-ZSM5 characterization**

These FTIR experiments have been carried out at the “Institute of General and Inorganic Chemistry - Bulgarian Academy of Sciences” with the supervision of Prof. Konstantin I. Hadjiivanov. Cu-ZSM5 has been studied through FTIR experiments using a Nicolet Avatar 360. The IR transmission spectra were recorded with an appropriate software (OMNIC) useful for the spectra acquisition and elaborations. The spectra were recorded accumulating 64 scans at a spectral resolution of  $2\text{ cm}^{-1}$ . Self-supporting pellets (ca.  $10\text{ mg cm}^{-2}$ ) were prepared from the sample powders and treated directly in a purpose-made IR cell (see Fig. 18b) allowing measurements in the temperature range 100–300 K.

The cell was connected to a vacuum-adsorption apparatus, reported in Fig. 19, allowing a residual pressure below  $10^{-3}\text{ Pa}$ . Prior to the adsorption measurements, the samples were activated by heating in air at 673 K for 1 h followed by evacuation at the same temperature (see Fig. 18a).

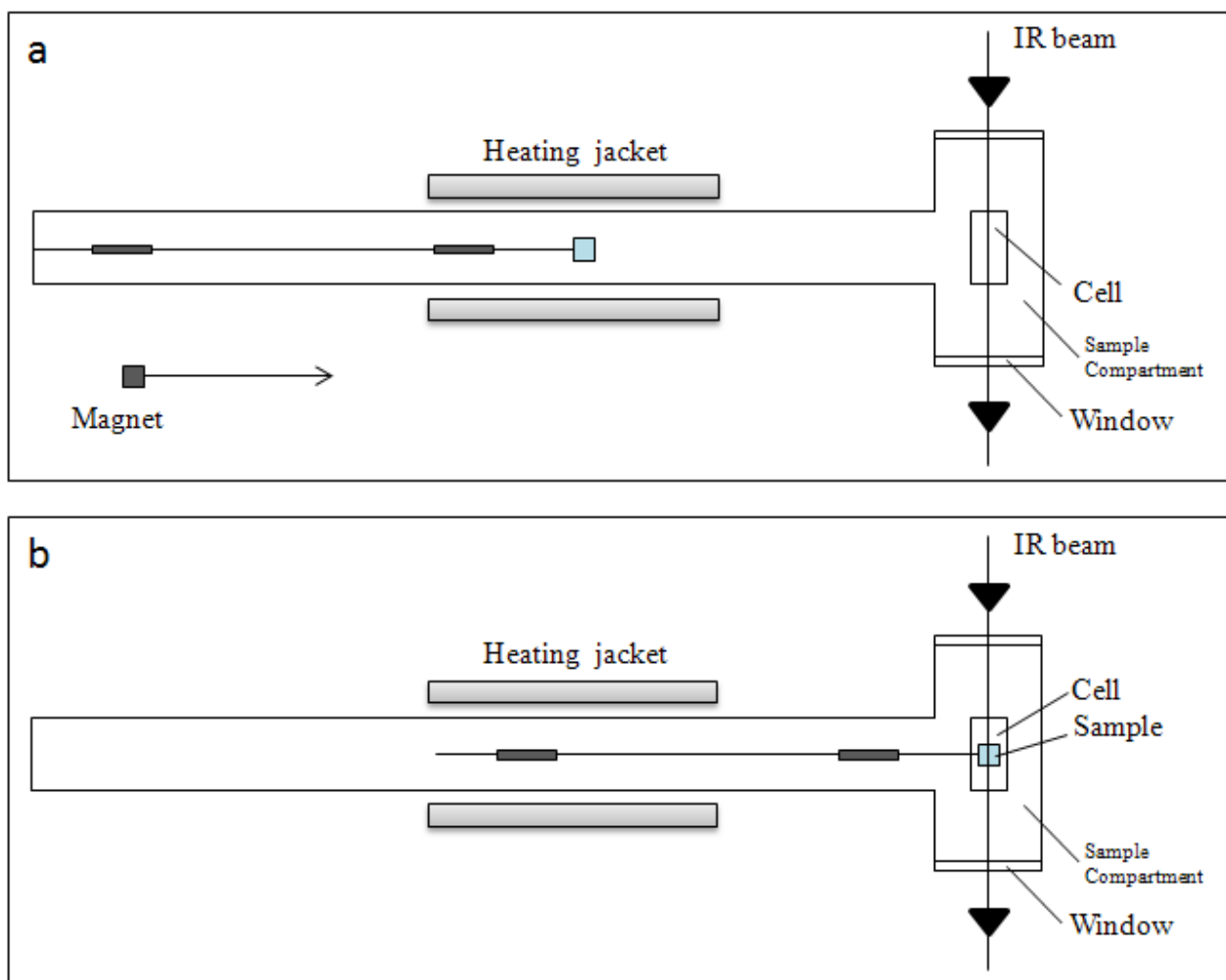


**Fig. 18** – IR cell: a) heating phase; b) IR measurement phase

The special feature of this cell is that it can work at low temperatures (100 K) cooling the sample compartment with liquid nitrogen.

The feeding stream mixture of the cell is obtained by using three separate bottles, containing gas mixtures of high purity. NO (purity of > 99.0%) was obtained from Messer Griesheim GmbH.  $^{15}\text{NO}$  was purchased from ISOTEC INC. Matheson Tri Gas Company ( $^{15}\text{NO}$  (99 %)/He; molar ratio of 1:10). Carbon monoxide (99.5 %) was supplied by Merck. Before use, carbon monoxide passed through a liquid nitrogen trap to remove the carbon dioxide impurity.

A schematic overview of the vacuum-adsorption apparatus is reported below.

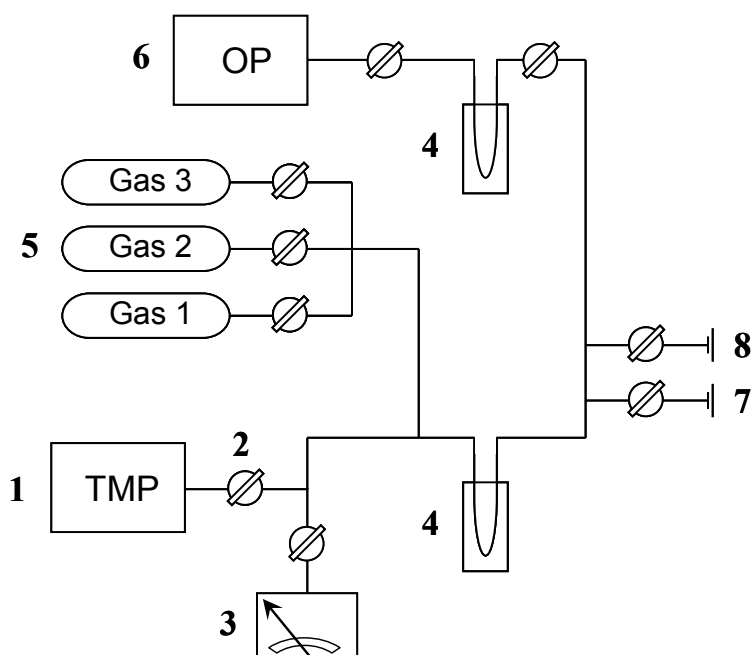


**Fig. 19** – Vacuum-adsorption apparatus: (1) turbo-molecular pump, (2) vacuum valve, (3) pressure gauge, (4) liquid nitrogen trap, (5) balloons, (6) oil vacuum pump, (7) connection to the IR cell, (8) connection to the atmosphere or additional devices

A suitable vacuum ( $P > 10^{-3}$  Pa) was reached in two steps; the first is an evacuation with the oil vacuum pump. This pump is able to remove the air inside the cell, but the reached vacuum values are not good enough. The second step is another evacuation with the turbo-molecular pump and the residual pressure is below  $10^{-3}$  Pa.

### 3.2.2.2. IR experimental setup for co-adsorption of NO and H<sub>2</sub>O

NO and H<sub>2</sub>O co-adsorption on LaCu-ZSM5 under flow conditions and at high temperature has been qualitatively studied through FTIR experiments using a Perkin Elmer Spectrum GX spectrometer. A personal computer with an appropriate software (Spectrum PE application) was used for the spectra acquisition and elaborations.

A schematic overview of the experimental setup to study the co-adsorption of NO and water over LaCu-ZSM5 catalyst is reported in Fig. 20.

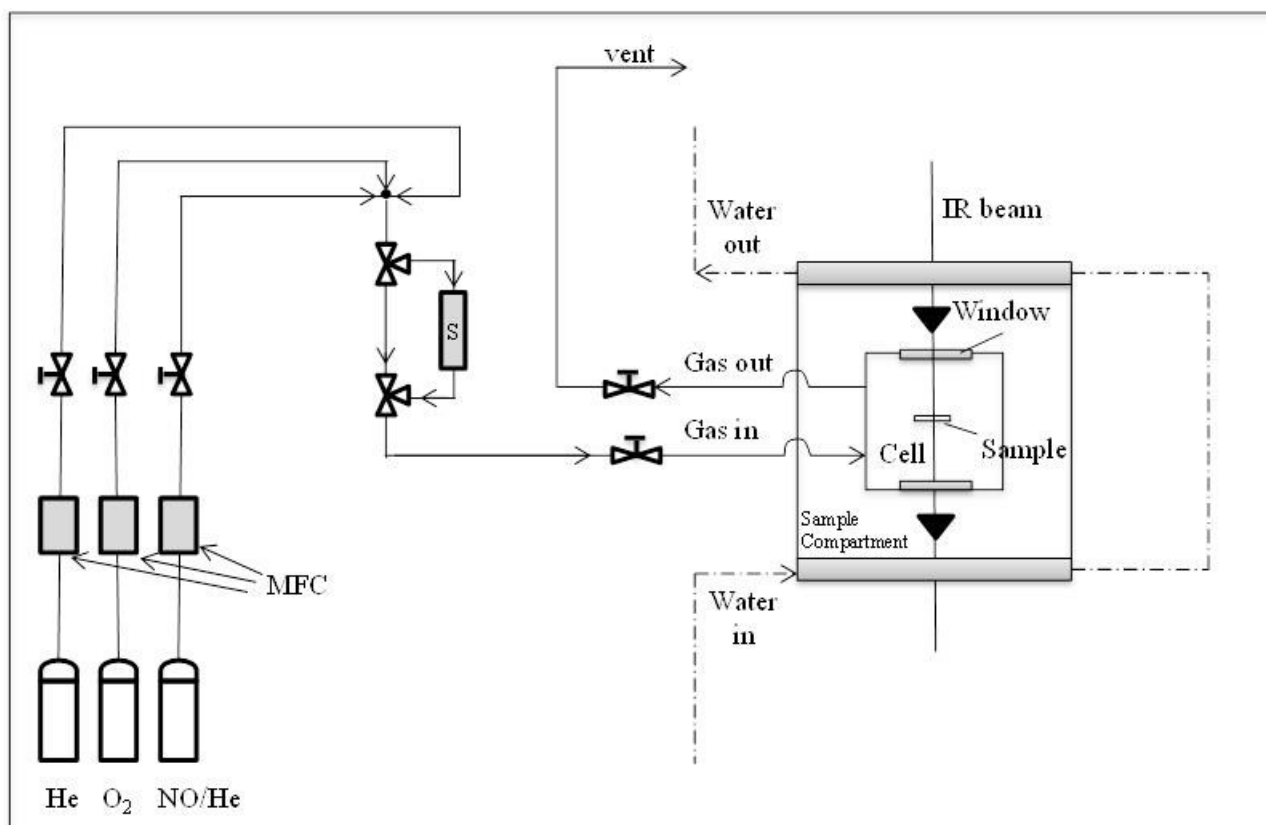


**Fig. 20** – Scheme of the laboratory plant for IR transmission experiments

The spectrometer was equipped with a liquid-N<sub>2</sub> cooled MCT detector FTIR spectra were recorded with a spectral resolution of 4 cm<sup>-1</sup> averaging each spectrum over 50 scans. A LaCu-ZSM5 self-supported disc (i.d. 13 mm) was placed into a high temperature and high pressure cell (Specac) equipped with a ZnSe windows and connected to mass flow controlled gas lines.

The ZnSe window allows operation at high temperature and in the presence of water as well. Sample temperatures of up to 800 °C can be reached and the cell can operate at pressures from vacuum to 1000 psi for in-situ reaction studies.

The detector MCT (mercury cadmium telluride) can be used for wavelengths comprised between 12500-400 cm<sup>-1</sup>, this detector has a high acquisition speed and higher sensitivity compared to DTGC (detector commonly used). The cell is supplied with a dedicated automatic digital temperature controller.

A cooling system with circulating water prevents excessive heating of the outer compartment of the cell during the test. An important feature of the cell used is that it can operate under flow conditions, also.

The feeding mixture was obtained by mixing high purity gases, He 99.999%; O<sub>2</sub> 99.95% was supplied by Sol, and NO/He mixture, 1 vol% NO and 100 ppmv NO<sub>2</sub> purchased from Rivoira.

The cell picture is reported below (Fig.21).

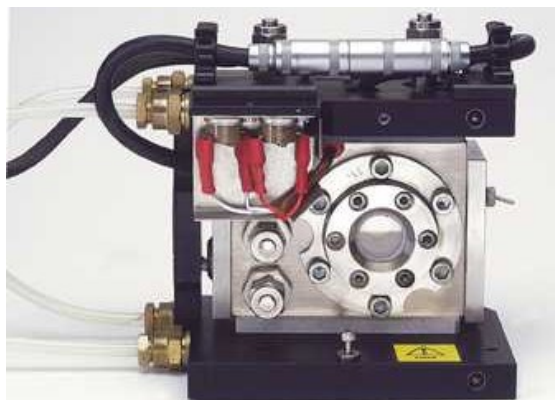


**Fig. 21** – Picture of the IR cell

## **Chapter 4**

### **Catalyst and adsorbed species characterization<sup>1</sup>**

---

<sup>1</sup> Parts of this chapter appear in M. Tortorelli, K. Chakarova, L. Lisi, K. Hadjiivanov, *Journal of Catalysis* 309 (2014) 376–385

#### 4.1 Adsorption tests

An in-situ FTIR study was performed to define the catalyst characterization and the nature of the adsorbed species. The FTIR analyses were carried out using the apparatus system described in paragraph 3.2.2.1.

The adsorption tests were carried out in three steps:

- Catalyst pre-treatment: The catalyst was pre-treated in two different ways.  
Pre-activated. The sample was pre-activated in situ at 400 °C for 15 min in air and evacuated for about 30 min at the same temperature and then cooled down to ambient temperature.  
Pre-reduction. The sample was pre-reduced in situ at 200 °C for 15 min in 50 mbar CO and evacuated at 523 K until the disappearance of the band at 2156 cm<sup>-1</sup> (Cu<sup>+</sup>-CO).  
During the pre-activation the cell was open, during the pre-reduction closed.
- Adsorption: the cell was filled with the gas mixture at 100 K or ambient temperature until catalyst saturation and then spectra collected every 2 min. During the adsorption phase the cell was closed.
- Evacuation: the cell was evacuated using the vacuum apparatus at the adsorption temperature up to ambient temperature. During this phase the vacuum valves are open.

#### 4.2 Investigation of Cu-ZSM5 using IR spectroscopy of probe molecules

For characterization of the Cu-ZSM5 sample CO and NO were used. These two probes are complementary when studying copper-containing catalysts because CO is preferentially adsorbed on Cu<sup>+</sup> sites, while NO on Cu<sup>2+</sup> ions. The monocarbonyls are characterized by a band at 2157–58 cm<sup>-1</sup>, and the dicarbonyls display  $\nu_s$  at 2178 cm<sup>-1</sup> and  $\nu_{as}$  at 2151 cm<sup>-1</sup>. Bands at 2192 and ca. 2167 cm<sup>-1</sup> (Spoto et al., 1994 and Drenchev et al., 2011) and possibly a band at 2137 cm<sup>-1</sup> (Spoto et al., 1994) are typical of tricarbonyl species.

CO is a good probe molecule for characterization of Cu<sup>+</sup> sites since it forms stable complexes with Cu<sup>+</sup> cations, whereas the Cu<sup>2+</sup>-CO species are very unstable. Cu<sup>+</sup> species are normally formed during self-reduction of copper-containing samples *in vacuo*.

The adsorption experiments were carried out at low temperature (100 K) for several reasons:

- To get information on all copper sites on the surface (CO is a weak base and at room temperature it can be adsorbed only on strong Lewis acid sites);
- To get information on the surface OH groups (at room temperatures CO cannot coordinate to surface OH groups);
- To minimize the reduction of the copper during the adsorption process (at room temperature CO can reduce the metal cations during adsorption).

#### 4.2.1. Low-temperature CO adsorption on the Cu-ZSM5

In the Cu-ZSM5 sample investigated here the copper loading is quite high and a significant part of the divalent copper ions were self-reduced to  $\text{Cu}^+$  during the second part of activation process (with the vacuum).

This is evidenced by the intense bands due to  $\text{Cu}^+$  carbonyls that were registered after low-temperature CO adsorption on activated Cu-ZSM5 sample (see Fig. 22).

Analysis of the results obtained with the activated (oxidized) sample show that at high CO coverage,  $\text{Cu}^+$  cations form tricarbonyl  $\text{Cu}^+(\text{CO})_3$  complexes characterized by bands at 2192 and 2168  $\text{cm}^{-1}$  (Fig. 22, spectrum a). The band at ca. 2140  $\text{cm}^{-1}$  is due to physically adsorbed CO. Some authors associated it with the tricarbonyl species but it does not change in concert with the bands at 2192 and 2168  $\text{cm}^{-1}$ . With the decrease of the CO coverage these two bands decrease in intensity and two new bands at 2178 and 2151  $\text{cm}^{-1}$  emerged at their expense (Fig. 22 A, spectra b-g). This indicates conversion of the tricarbonyls into dicarbonyl complexes ( $\nu_s$  at 2178 and  $\nu_{as}$  at 2151  $\text{cm}^{-1}$ ). Further evacuation leads to a loss of another CO ligand and the bands at 2178 and 2151  $\text{cm}^{-1}$  that are due to dicarbonyls start decreasing in intensity. At the same time a new band with maximum at 2156  $\text{cm}^{-1}$  appears (Fig. 2, spectra a-g). The results show that dicarbonyl complexes in their turn convert into  $\text{Cu}^+-\text{CO}$  monocarbonyls that are stable towards evacuation at 298 K (Fig. 22 B, spectrum h).

Evacuation at higher temperatures display that the band due to  $\text{Cu}^+-\text{CO}$  (2156  $\text{cm}^{-1}$ ) remained in the spectrum even after 5 min evacuation at 483 K (Fig. 22 B, spectrum j).

The band at 2112  $\text{cm}^{-1}$  is due to adsorbed  $^{13}\text{C}$ CO that is always present in small amounts in carbon monoxide.

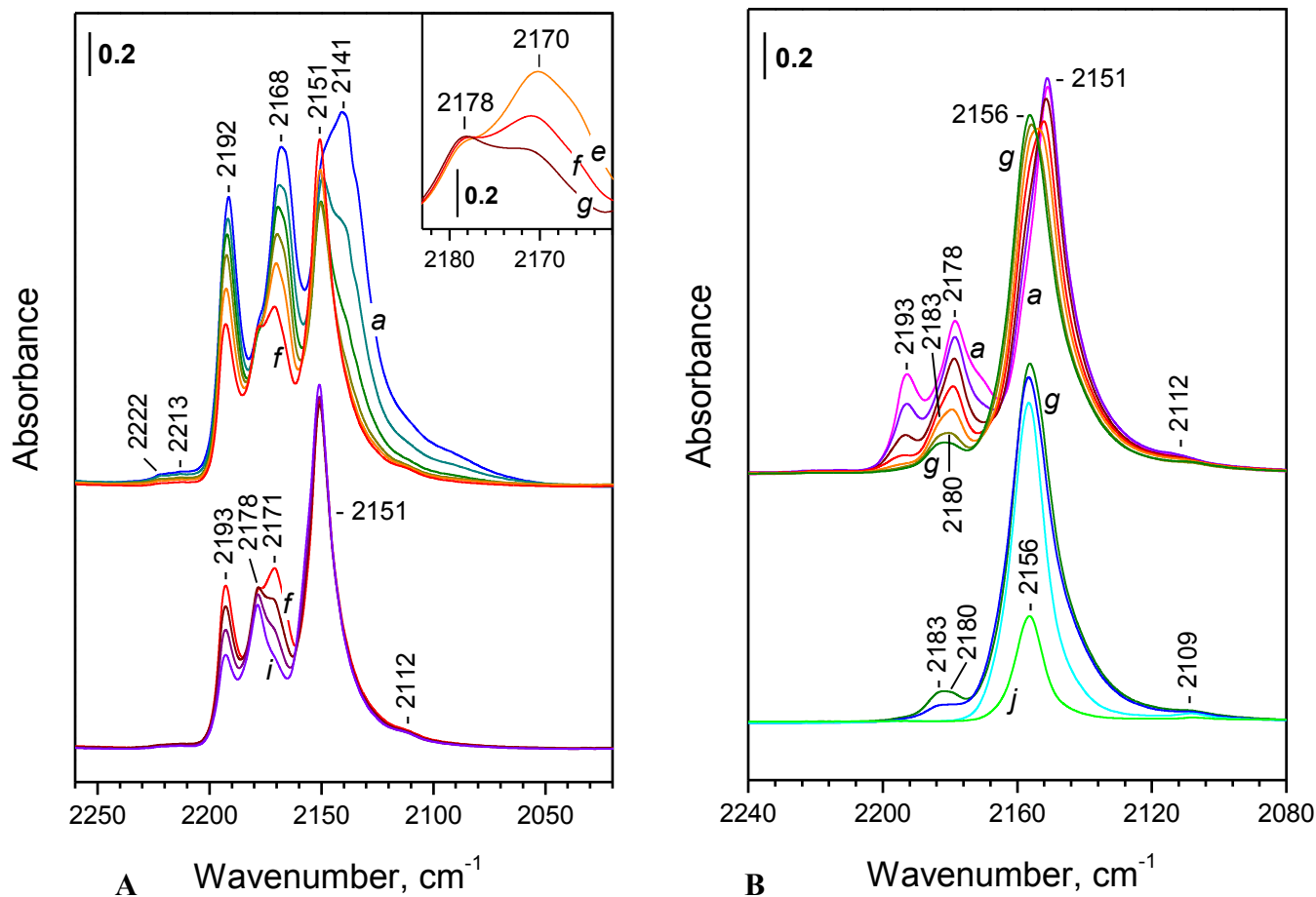


**Fig. 22** - FTIR spectra of CO (350 Pa equilibrium pressure) adsorbed on activated Cu-ZSM5 A) at 100 K (a) and evolution of the spectra during evacuation at 100 K (b-i). B) Evolution of the spectra during evacuation at 100 K (a-g), at increasing temperatures up to 298 K (h) and after 5 minutes evacuation at 398 K (i) and 483 K (j). The spectra are background and CO gas phase corrected

In order to get more information of the carbonyls of  $\text{Cu}^+$ , the Cu-ZSM5 sample was reduced in CO atmosphere. Fig. 23 shows the reduction of  $\text{Cu}^{2+}$  to  $\text{Cu}^+$  in 5 kPa CO at different temperatures (for 15 min at each temperature). Introduction of CO at ambient temperature leads to formation of dicarbonyl complexes manifesting bands at 2176 and 2151  $\text{cm}^{-1}$  (Fig. 23, spectrum a). It is visible that even at 373 K the main part of the  $\text{Cu}^{2+}$  cations is reduced to  $\text{Cu}^+$  (Fig. 23, spectrum b). At that temperature the band at 2151  $\text{cm}^{-1}$  is already saturated because of the high copper loading.

However, the increase of the amount of  $\text{Cu}^+$  ions can be monitored by the intensity of the band with maximum at 2176  $\text{cm}^{-1}$ . The further increase of the reduction temperature does not lead to a significant increase of the intensity of the carbonyl bands (Fig. 23, spectra c, d).

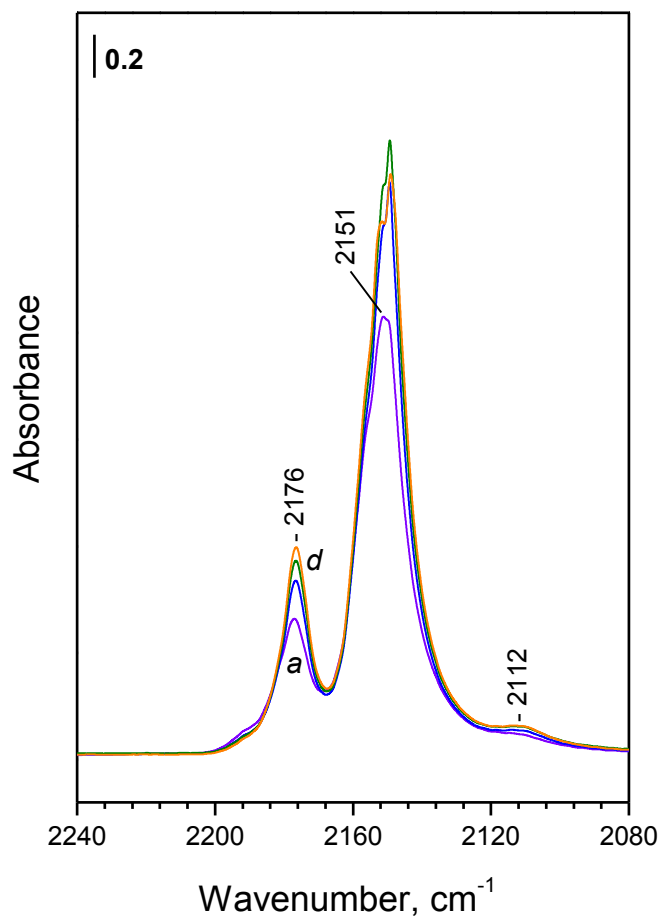


**Fig. 23** - FTIR spectra of CO (5 kPa) adsorbed on Cu-ZSM5 at ambient temperature (a) and evolution of the spectra after heating of the sample in CO atmosphere at 373 (b), 423 (c) and 473 K (d) for 15 min at each temperature. The spectra are background and CO gas phase corrected

The results obtained after low-temperature adsorption of CO on reduced Cu-ZSM5 sample are reported in Figs 24 and 25. These results are analogous to those registered with the activated sample. At high CO coverage, tricarbonyls of Cu<sup>+</sup> are formed (2191 and 2169 cm<sup>-1</sup>) (Fig. 4, spectrum a). With evacuation they are converted to dicarbonyls ( $\nu_s$  at 2178 and  $\nu_{as}$  at 2150 cm<sup>-1</sup>) (Fig. 24A, spectra b-e) and ultimately to linear complexes (2156 cm<sup>-1</sup>) (Fig. 24B, spectra a-h). Here the conversion of the tricarbonyls into dicarbonyls is more discernible with the reduced Cu-ZSM5 sample (see Fig. 24A, spectra b-e and the inset).

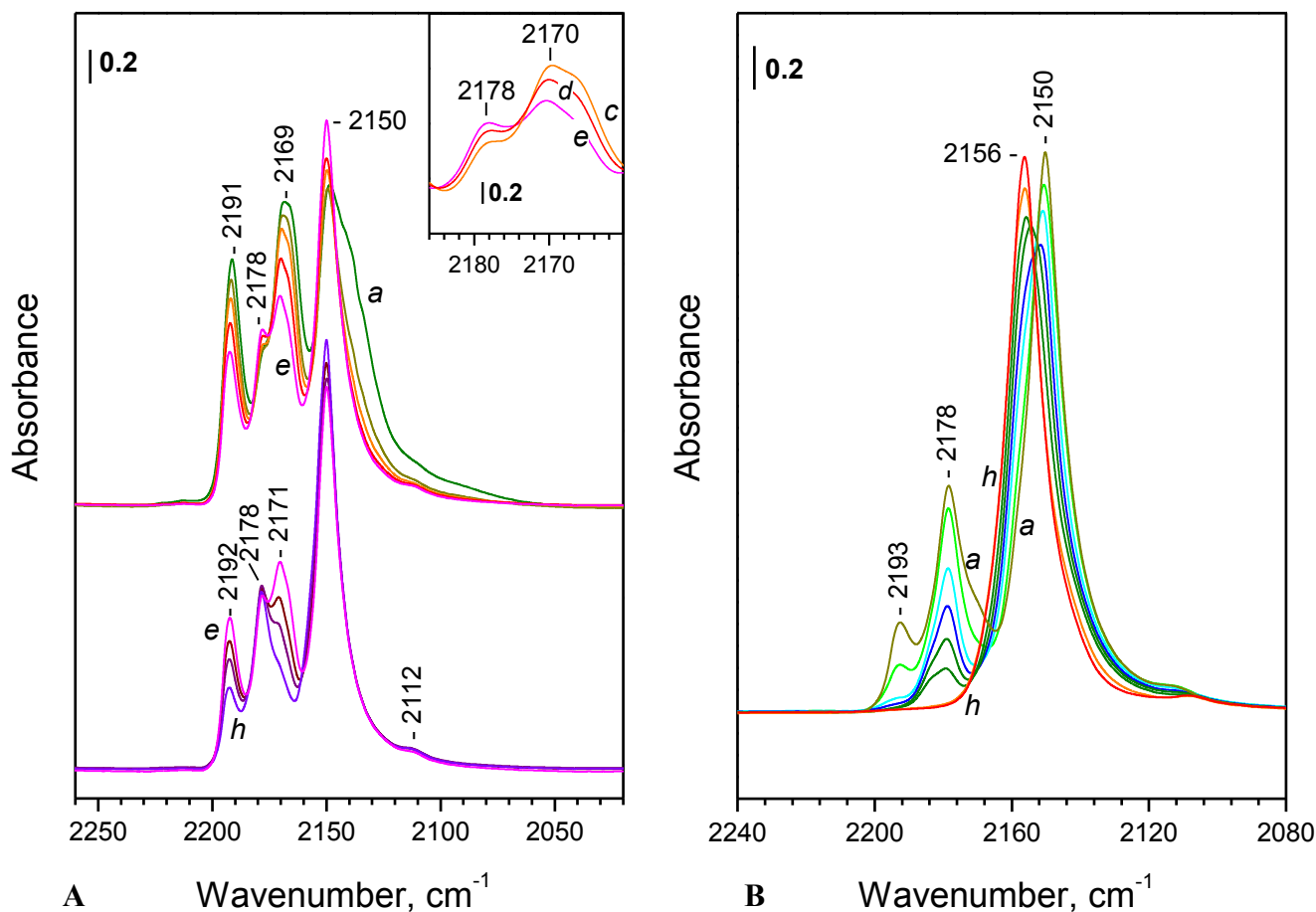


**Fig. 24** - FTIR spectra of CO (300 Pa equilibrium pressure) adsorbed on reduced Cu-ZSM5 A) at 100 K (a) and evolution of the spectra during evacuation at 100 K (b-h). B) evolution of the spectra during evacuation at 100 K (a-f) and at increasing temperatures up to 298 K (g, h). The spectra are background and CO gas phase corrected

Fig. 25 shows comparison of the spectra obtained after low-temperature CO adsorption on activate and on reduced Cu-ZSM5 sample. It is visible that the carbonyl bands of  $\text{Cu}^+$  are definitely more intense in the reduced sample. The spectra reported in Fig. 25 are characterized by three different coverages: (i) at saturation (spectra a and d), (ii) when the tricarbonyls of  $\text{Cu}^+$  are practically destructed (spectra b and e), and (iii) when only monocarbonyls exist on the sample (spectra c and f).

The spectra e and a show that all bands of the activated sample are of lower intensity except for the band at  $2193\text{ cm}^{-1}$ . That means there is an overlapping of the bands of tricarbonyls of  $\text{Cu}^+$  with another band having similar wavenumber. This band is due to carbonyls of  $\text{Cu}^{2+}$ . It is interesting that there is only one kind of  $\text{Cu}^{2+}$  carbonyls.

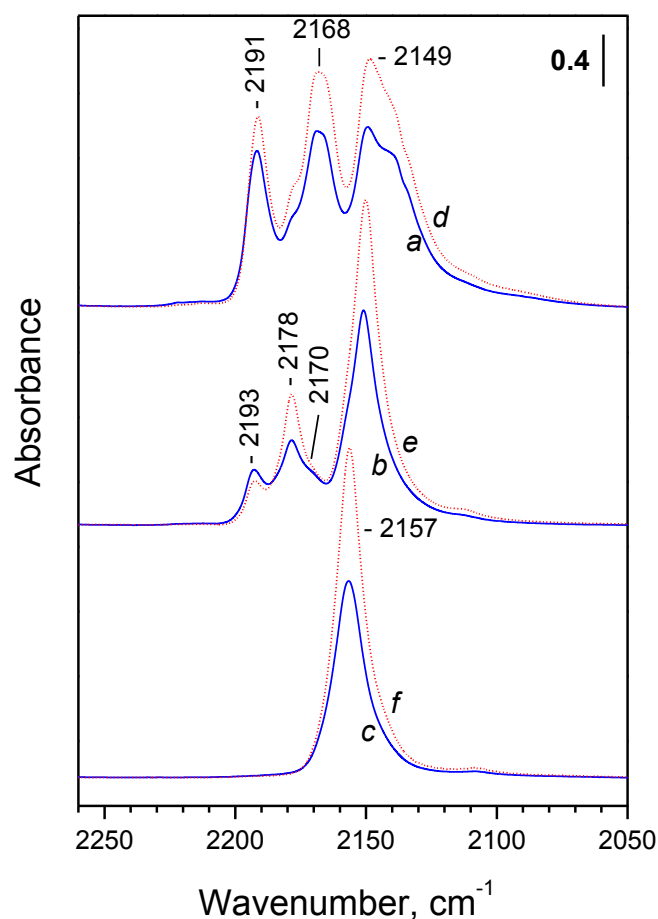


**Fig. 25** - FTIR spectra of CO adsorbed on activated (a, b, c) and CO-reduced Cu-ZSM5 (d, e, f). Equilibrium CO pressure of 500 Pa at 100 K, followed by short (a, d) and prolonged (b, e) evacuation at 100 K at and after evacuation at ambient temperature (c, f). The spectra are background corrected. The spectra are background and CO gas phase corrected

The main conclusions based on the experiments are that (i) a significant fraction of  $\text{Cu}^+$  sites exist on the activated sample (ca. 67% of the  $\text{Cu}^+$  sites detected with the CO-reduced sample) and (ii) only one kind of  $\text{Cu}^{2+}$  sites are detected by CO. The latter are monitored by the band at  $2193\text{ cm}^{-1}$  in spectra b and e. Note that this band is more intense with the activated sample. Unfortunately, it is not possible to quantify the amount of the  $\text{Cu}^{2+}$  sites because of the superimposition of the  $\text{Cu}^{2+}$ -CO band with the band at  $2192\text{ cm}^{-1}$  due to residual tricarbonyl species.

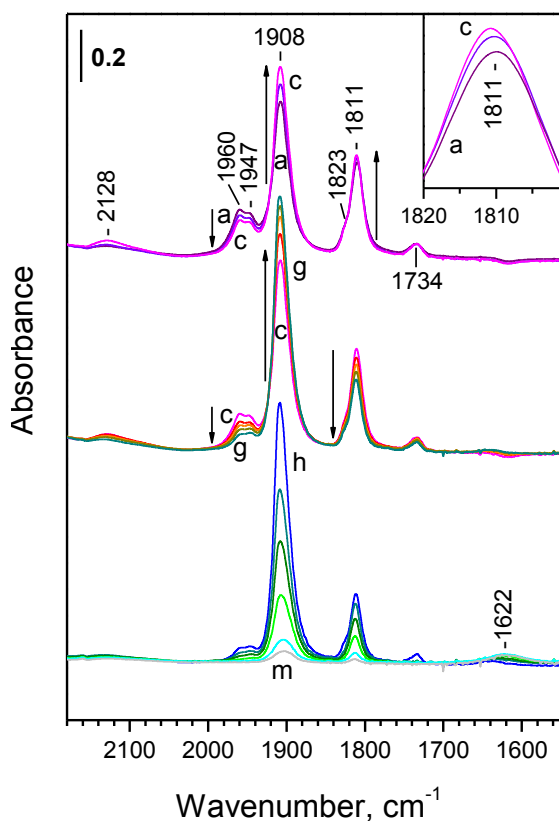
#### 4.2.2. NO adsorption on the Cu-ZSM5 at ambient temperature

After the adsorption of CO, the adsorption of NO at ambient temperature was investigated. The evolution with time of the IR spectra on the activated sample is shown in Fig. 26.

Introduction of NO (500 Pa equilibrium pressure) to the system provokes appearance of five IR bands in the nitrosyl stretching region, their maxima being at 1960, 1947, 1908, 1811, and 1734  $\text{cm}^{-1}$ . A shoulder at 1823  $\text{cm}^{-1}$  can also be distinguished (Fig. 26, spectrum a).

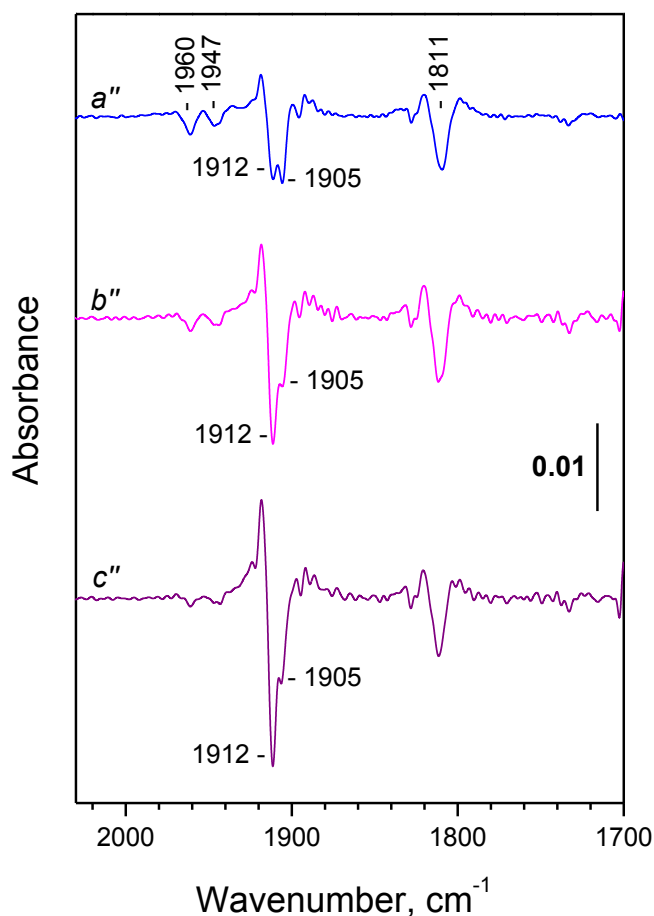
At first the bands at 1960 and 1947  $\text{cm}^{-1}$  ( $\text{Cu}^{\text{n}+}\text{-NO}$ ) decrease in intensity and bands at 1908  $\text{cm}^{-1}$  ( $\text{Cu}^{2+}\text{-NO}$ ) and 1811  $\text{cm}^{-1}$  ( $\text{Cu}^+\text{-NO}$ ) increase (Fig. 26, spectra a-c and the inset). With elapsed time the band at 1811  $\text{cm}^{-1}$  also starts decreasing and the only band that gains intensity is this at 1908  $\text{cm}^{-1}$  (Fig. 26, spectra c-g). The results show oxidation of  $\text{Cu}^+$  ions to  $\text{Cu}^{2+}$  and conversion of  $\text{Cu}^{\text{n}+}$  sites to  $\text{Cu}^{2+}$  (in other words the above results show conversion of some nitrosyl species into others.).

Evacuation at ambient temperature leads to stepwise disappearance of all bands (Fig. 26, spectra h-m). First disappear the two bands due to dinitrosyls of  $\text{Cu}^+$  (1823 and 1734  $\text{cm}^{-1}$ ) followed by those with maxima at 1960 and 1947  $\text{cm}^{-1}$ . The most stable are the bands at 1908 and 1811  $\text{cm}^{-1}$  that disappear almost simultaneous.



**Fig. 26** - FTIR spectra of NO (500 Pa equilibrium pressure) adsorbed on activated Cu-ZSM5 at ambient temperature (a), evolution of the spectra with time: after 20 (b), 60 (c), 150 (d), 210 (e), 270 (f) and 330 min (g) and during evacuation at ambient temperature (h-m). The spectra are background and gas phase corrected

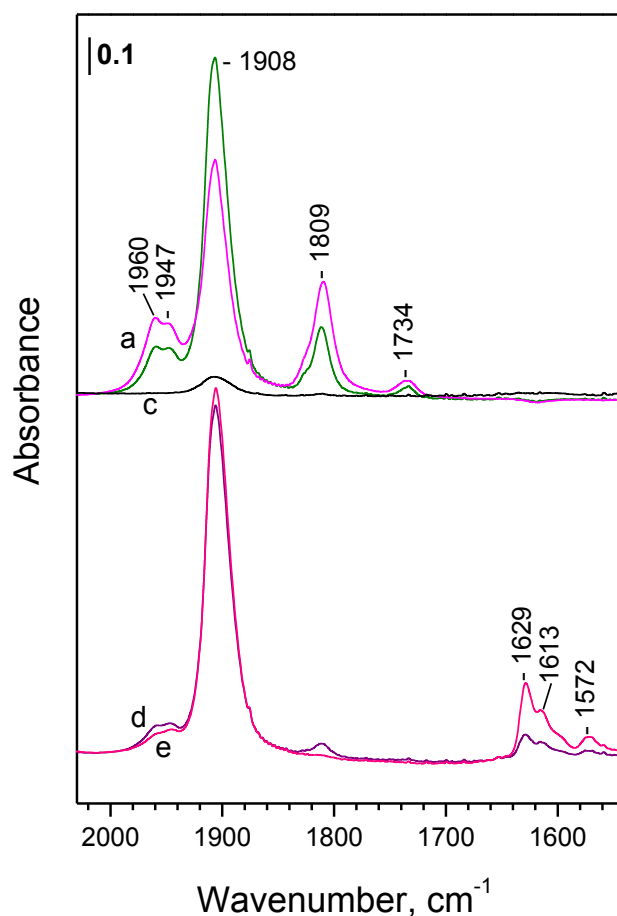
A careful inspection of the spectra suggests that the band at  $1908\text{ cm}^{-1}$  is complex and consists of at least two component located at  $1912$  and  $1905\text{ cm}^{-1}$ .



**Fig. 27** - Second derivatives of the spectra registered after adsorption of NO (500 Pa equilibrium pressure) on Cu-ZSM5 at ambient temperature (a'') and after allowing the sample to stay in NO atmosphere for 150 (b'') and 334 min (c'')

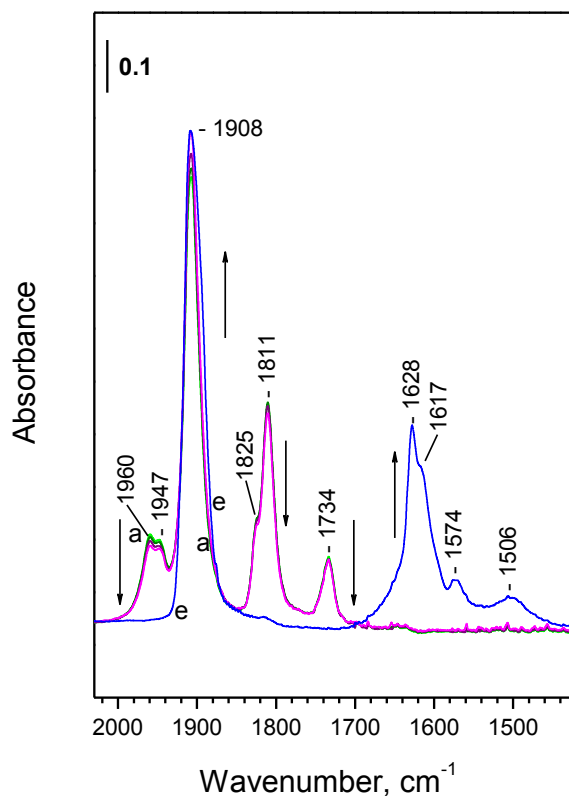
The above results show conversion of some nitrosyl species into others. In particular the both  $\text{Cu}^{2+}\text{-NO}$  ( $1912\text{ cm}^{-1}$ ) and  $\text{Cu}^+\text{-NO}$  species are formed at the expense of the HF (High Frequency) nitrosyls (Fig. 27, spectra a-c).

Additional experiments (reported in Fig. 28) revealed that the ambient temperature conversion of the HF bands to a band at  $1912\text{ cm}^{-1}$  is an irreversible process. In this experiment an evacuation of NO (at  $50^\circ\text{C}$  for 90 min) followed by a second NO adsorption does not completely restore the HF bands.



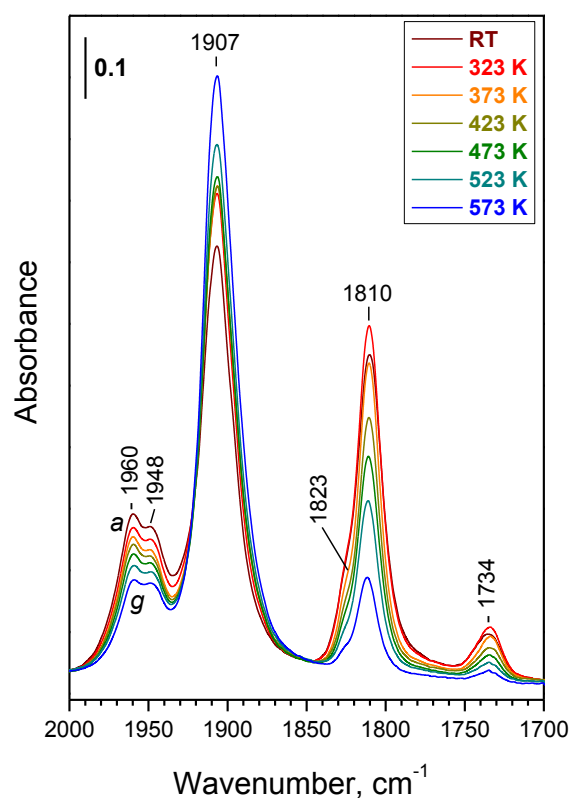
**Fig. 28** - FTIR spectra of NO (5 mbar equilibrium pressure) adsorbed on reactivated Cu-ZSM5 at RT (a), after heating at  $50^\circ\text{C}$  for 90 min (b) and after evacuation (c). Second adsorption of NO 5 mbar equilibrium pressure (d) and evolution after 3 min (e). The spectra are background and gas phase subtracted

Fig. 29 shows another NO adsorption experiment carried out in the same conditions of the first NO adsorption at ambient temperature reported but with longer adsorption time. It is visible that after 65 hours in NO atmosphere at ambient temperature the bands due to  $\text{Cu}^+$  nitrosyls ( $1825$ ,  $1811$  and  $1734\text{ cm}^{-1}$ ) and  $\text{Cu}^{\text{n}+}$  complexes ( $1960$  and  $1947\text{ cm}^{-1}$ ) disappear completely and the only bands in the spectrum are those of  $\text{Cu}^{2+}\text{-NO}$  ( $1908\text{ cm}^{-1}$ ) and nitrates ( $1700 - 1400\text{ cm}^{-1}$ ).



**Fig. 29** - FTIR spectra of NO (1 kPa equilibrium pressure) adsorbed on activated Cu-ZSM5 at ambient temperature (a), evolution of the spectra with time: after 10 (b), 30 (c) and 60 min (d) and after 65 h (e). The spectra are background corrected

Some experiments were performed in order to establish whether the different NO adsorption sites are stable at higher temperatures. The results of these experiments are reported below in Fig. 30, it is possible to observe that several species (1960, 1946, 1907  $\text{cm}^{-1}$ ) are very stables.



**Fig. 30** - FTIR spectra of NO (500 Pa equilibrium pressure) adsorbed at ambient temperature on activated Cu-ZSM5 (a) and evolution of the spectra after heating the sample in NO atmosphere for 10 min at 323 (b), 373 (c), 423 (d), 474 (e), 523 (f) and 573 (g). The spectra are background and gas-phase corrected

The assignments of the bands reported in this chapter were resumed in Tab. 5.

**Tab. 5** – Frequencies and assignment of the nitrosyl bands observed in literature (Hadjiivanov et al. (2000), Schay et al. (1998), Ziolk et al. 2000)

<b>№</b>	<b>Wavenumber of the band, cm<sup>-1</sup></b>	<b>Assignment</b>
1	2005*	(N <sub>2</sub> O <sub>2</sub> ) <sup>+</sup>
2	1960	Cu <sup>n+</sup> -NO
3	1947	Cu <sup>n+</sup> -NO
4	1912	Cu <sup>2+</sup> -NO (Cu <sup>2+</sup> ions in pyramidal configuration)
5	1900	Cu <sup>2+</sup> -NO (Cu <sup>2+</sup> ions in square planar configuration)
6	1864	v <sub>as</sub> (NO) of Cu <sup>n+</sup> (NO) <sub>2</sub>
7	1782	v(NO) of trans-(N <sub>2</sub> O <sub>2</sub> )
8	1821 and 1728	v <sub>s</sub> and v <sub>as</sub> of Cu <sup>+</sup> (NO) <sub>2</sub>
9	1810	Cu <sup>+</sup> -NO
10	1683*	Overlapping of v <sub>as</sub> (NO) of [N <sub>2</sub> O <sub>2</sub> ] <sup>+</sup> at 1687 cm <sup>-1</sup> and v(NO) of ONON at 1678 cm <sup>-1</sup>

\* The bands are registered also with ZSM5 support

### 4.2.3. NO adsorption on the Cu-ZSM5 at low temperature

The next experiment was carried out at low temperature and it was a NO adsorption on activated Cu-ZSM5 sample. The aim of this experiment is to study the nature of species formed at low temperature.

In order to distinguish unambiguously between the bands produced as a result of NO interaction with the support, before the adsorption on Cu-ZSM5 an NO adsorption at 100 K on the parent H-ZSM5 material was carried out (Fig. 31). Before this experiment, the zeolite was activated by heating for 1 h in air at 400 °C followed by 5 h evacuation at the same temperature in order to remove the ammonia and water (the commercial zeolite is in ammonium form).

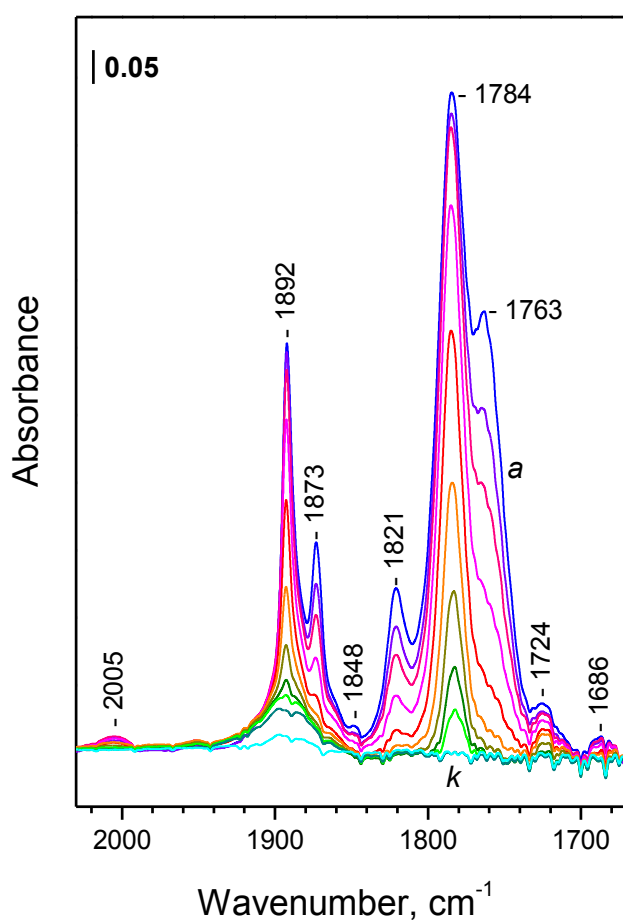


**Fig. 31** - FTIR spectra of NO (200 Pa equilibrium pressure) adsorbed on activated H-ZSM5 at 100 K (a) and evolution of the spectra during evacuation at 100 K (b-k). The spectra are background corrected

In Fig. 31 the most intense bands are at 1892, 1873, 1821, 1784 and 1763 cm<sup>-1</sup>.

The band 1892 (Fig. 31) is due to NO interacting with bridging OH groups. This band is expected with much lower intensity on the copper-exchanged sample because of the lower concentration of OH groups. In the same figure the bands at 1784 and 1763  $\text{cm}^{-1}$  are due to *trans*-( $\text{N}_2\text{O}_2$ ). At higher coverage (Fig. 31, spectrum a) bands due to *cis*-( $\text{N}_2\text{O}_2$ ) (1873 and 1821  $\text{cm}^{-1}$ ) are observed. A band at 1763  $\text{cm}^{-1}$  is detected at even higher coverage and tentatively assigned to weakly adsorbed *trans*- $\text{N}_2\text{O}_2$ .

Two low-intensity bands, at 1724 and 1679  $\text{cm}^{-1}$ , rise almost in parallel, the latter band shifting to 1685  $\text{cm}^{-1}$  with coverage increase. The bands at 1724 and the 1679  $\text{cm}^{-1}$  component are assigned to adsorbed asymmetric NONO dimer. The component at ca. 1685  $\text{cm}^{-1}$ , together with the band at 2005  $\text{cm}^{-1}$ , characterizes  $[\text{ONNO}]^+$  species (Penkova et al., 2004).

The spectrum of NO adsorption and evacuation on Cu-ZSM5 at 100 K is shown in Figs 32 and 33.

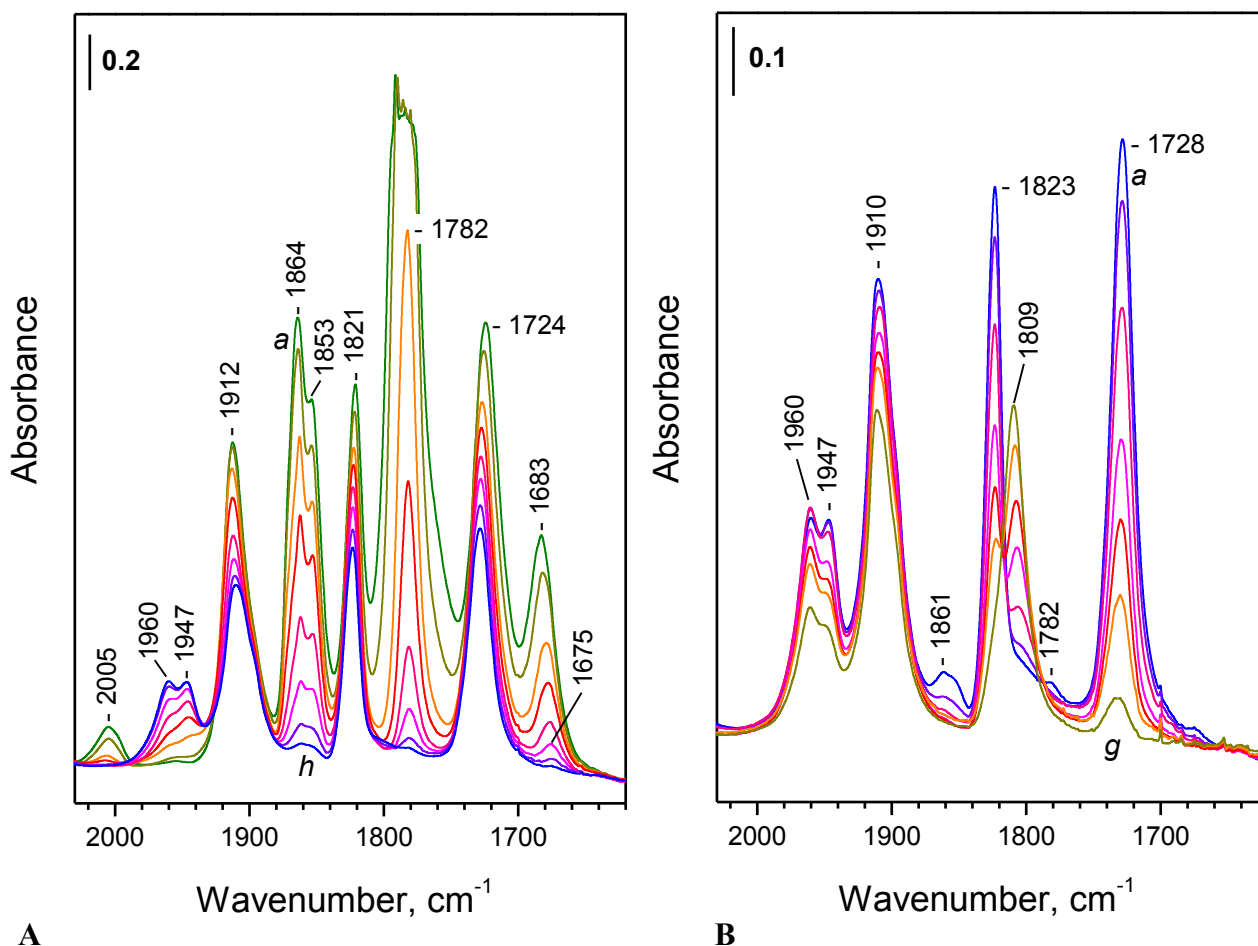


**Fig. 32** - FTIR spectra of NO (200 Pa equilibrium pressure) adsorbed on activated Cu-ZSM5 A) at 100 K (a) and evolution of the spectra during evacuation at 100 K (b-h). B) evolution of the spectra during evacuation at 100 K (a-g). The spectra are background corrected

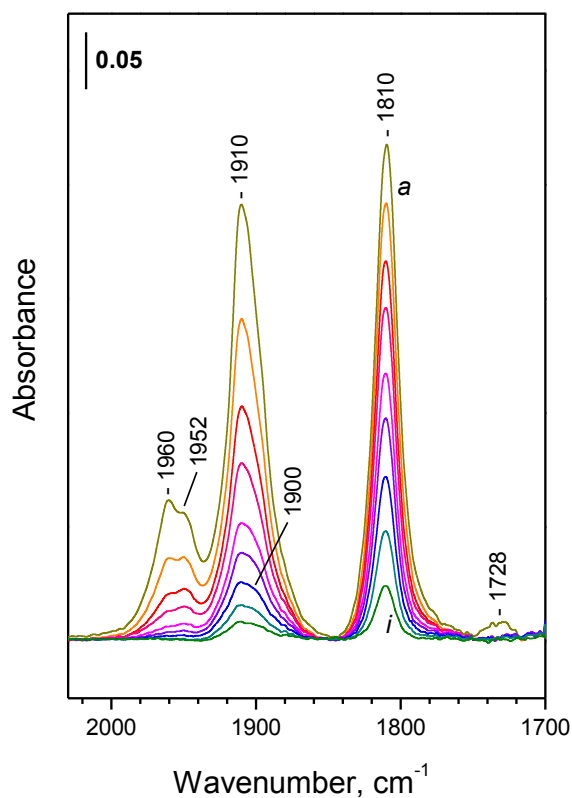


**Fig. 33** - (continuation from Fig. 32) FTIR spectra of NO (200 Pa equilibrium pressure) adsorbed on activated Cu-ZSM5 at 100 K: evolution of the spectra during evacuation at increasing temperatures (a-e) up to 298 K (f-i). The spectra are background corrected

In figures 32-33 the main bands are at 2005, 1912, 1864, 1853, 1821, 1782, 1724, and 1683  $\text{cm}^{-1}$ . The band at 1782  $\text{cm}^{-1}$  is more intense than the detection limit of the instrument, for this reason the exact position of its maximum cannot be determined. Further evacuation at 100 K (Fig. 32A, spectra b-h) caused a gradual decrease in intensity of all bands described while the bands at 2005 and 1683  $\text{cm}^{-1}$  (the latter shifted to 1675  $\text{cm}^{-1}$ ) ultimately disappeared. Simultaneously, the HF nitrosyl bands (1960 and 1947  $\text{cm}^{-1}$ ) registered during the ambient temperature experiments developed.

After this experiment, the NO adsorption test was repeated using a pre-reduced Cu-ZSM5. The catalyst was heated in 5 kPa CO at 473 K for 15 min and evacuated at 523 K. The evacuation was at high temperature in order to remove the band of  $\text{Cu}^+-\text{CO}$  (2156  $\text{cm}^{-1}$ ) that was stable towards evacuation at 483 K.

By comparing the results obtained after NO adsorption on activated and reduced Cu-ZSM5 it is possible to observe insignificant difference in the intensity of the bands (see Fig. 34). This shows that during the activation the sample was partially reduced.

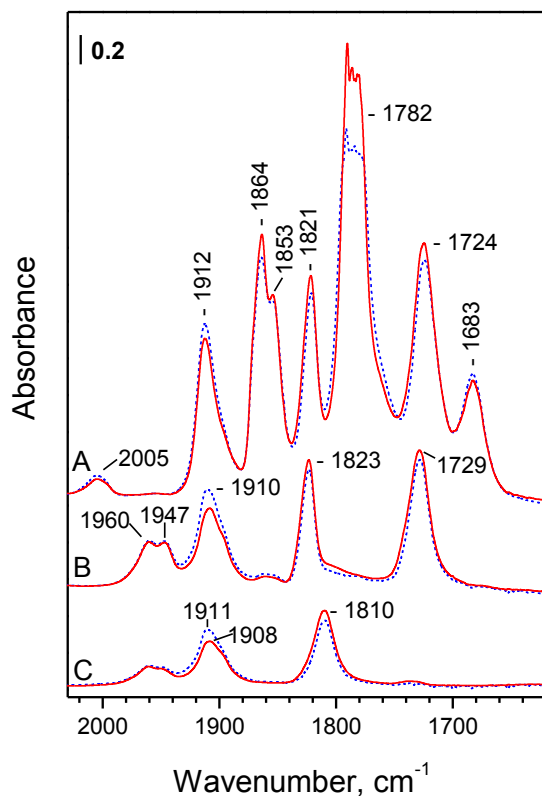


**Fig. 34** - FTIR spectra of NO adsorbed at 100 K on activated (dashed lines) and reduced (solid lines) Cu-ZSM5. Set A: spectra recorded at 200 Pa NO equilibrium pressure; set B: spectra recorded after evacuation at 100 K; set C: spectra recorded after evacuation at increasing temperatures up to 298 K. The spectra are background and NO gas phase corrected

The assignments of bands are supported by  $^{14}\text{NO}$ - $^{15}\text{NO}$  adsorption at 100 K presented in Fig. 35, the use of isotopic mixture to assign the adsorbed species will be presented in the next paragraph.

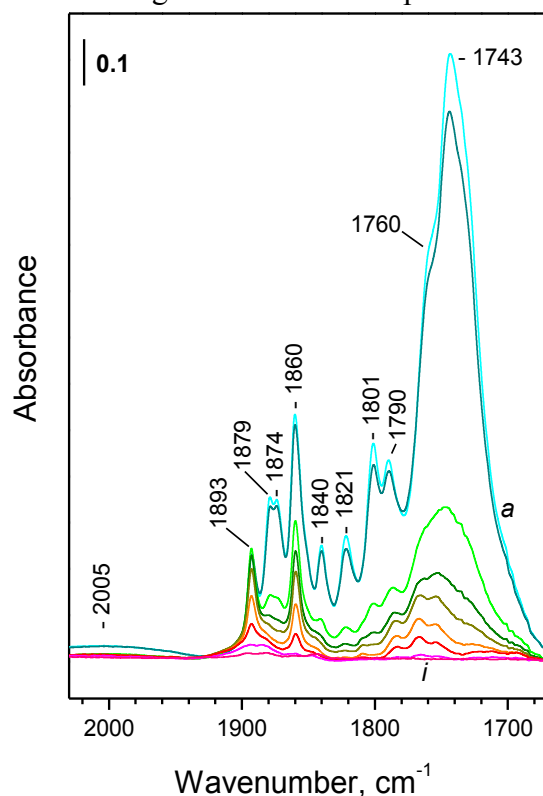


**Fig. 35** - FTIR spectra of  $^{14}\text{NO}$  and  $^{15}\text{NO}$  (200 Pa equilibrium pressure) adsorbed on activated H-ZSM5 at 100 K (a) and evolution of the spectra during evacuation at 100 K (b-i). The spectra are background corrected

In Fig. 36 the comparison between the NO adsorption at 100 K on H-ZSM5 and Cu-ZSM5 was reported.

Comparison with the spectra of NO adsorbed on the parent H-ZSM5 material (Fig. 36) shows that the bands above  $1895\text{ cm}^{-1}$  and that at  $1809\text{ cm}^{-1}$  could be associated only with copper content. The bands at  $1864$ ,  $1853$ ,  $1821$ , and  $1724\text{ cm}^{-1}$  are also connected with the presence of copper but contain some (although weak) components due to species formed on the support.

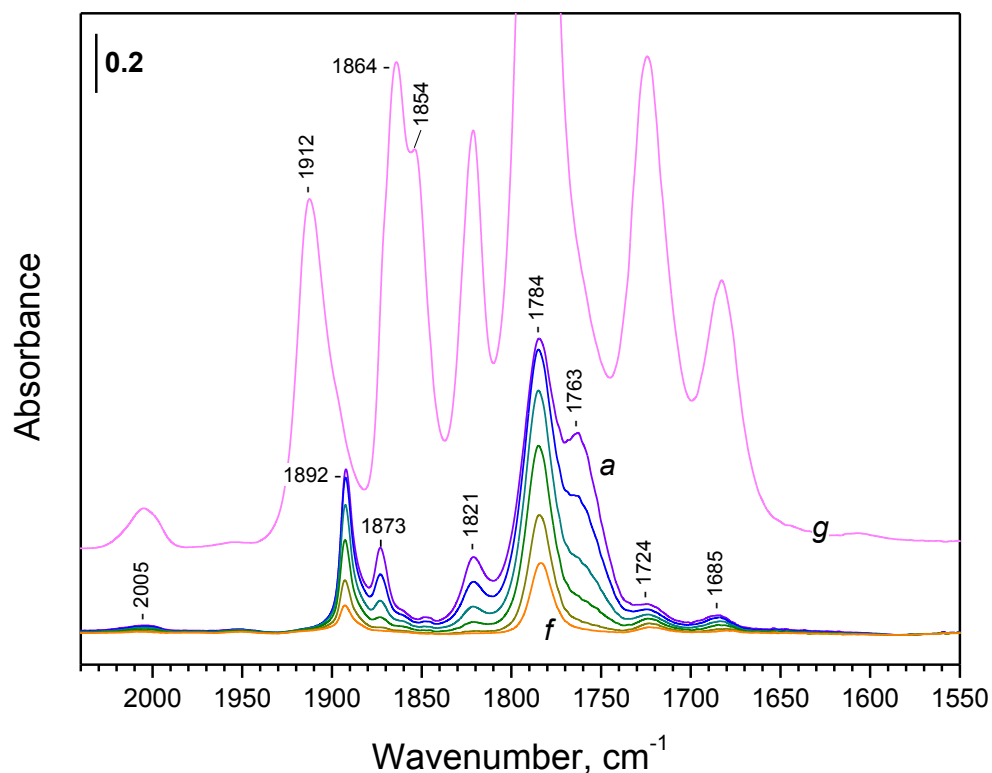


**Fig. 36** - FTIR spectra of NO adsorbed at 100 K on H-ZSM5. Equilibrium NO pressure of 200 Pa NO (a) and development of the spectra during evacuation (b-f). The spectra are background corrected. The spectrum of NO (200 Pa) adsorbed at 100 K on the Cu-ZSM5 sample is also shown for comparison (spectrum g)

### 4.3.1. Co-adsorption of $^{14}\text{NO}$ and $^{15}\text{NO}$

The next experiment was a low-temperature adsorption of  $\text{NO} + ^{15}\text{NO}$  isotopic mixture on activated Cu-ZSM5 sample and it is presented in Figs. 37 and 38. The assignment of the bands is given in Table 6.

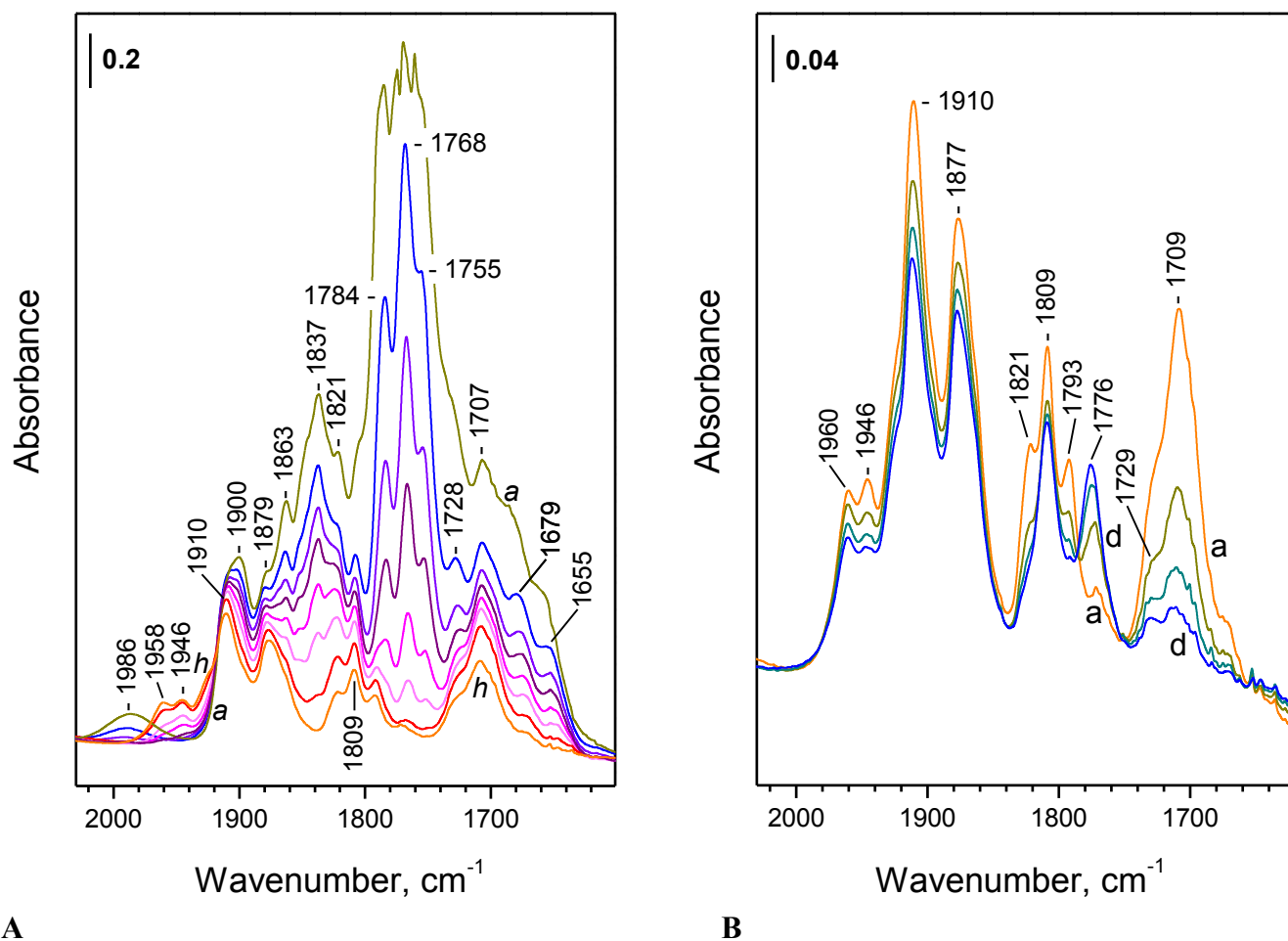


**Fig. 37** - FTIR spectra of  $^{14}\text{NO}$  and  $^{15}\text{NO}$  (200 Pa equilibrium pressure) adsorbed on activated Cu-ZSM5: A) at 100 K (a) and evolution of the spectra during evacuation at 100 K (b-h). B) Evolution of the spectra during evacuation at 100 K (a-d). The spectra are background corrected. The spectra are background corrected

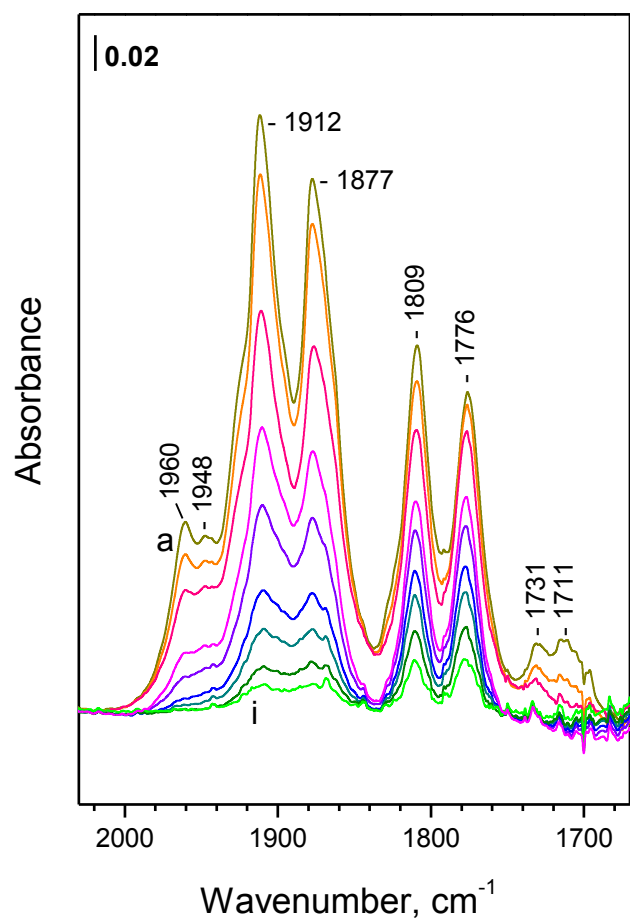


**Fig. 38** - (continuation from Fig. 37) FTIR spectra of <sup>14</sup>NO and <sup>15</sup>NO (200 Pa equilibrium pressure) adsorbed on activated Cu-ZSM5 at 100 K: evolution of the spectra during evacuation at increasing temperatures (a-h) up to 298 K (i). The spectra are background corrected

**Tab. 6** – Frequencies and assignment of the nitrosyl bands observed

<b>№</b>	<b>Species</b>	<b>Mode</b>	<b><sup>14</sup>N</b>	<b><sup>14</sup>N-<sup>15</sup>N</b>	<b><sup>15</sup>N</b>	<b>Note</b>
	<b>Copper nitrosyls</b>					
1	Cu <sup>n+</sup> -NO	v(NO)	1960	-	1925	
2	Cu <sup>n+</sup> -NO	v(NO)	1947	-	1914	Second type
3	Cu <sup>n+</sup> (NO) <sub>2</sub>	v <sub>s</sub> (NO)	1913	1902	1879	Interconverted with <b>1</b> and <b>2</b>
		v <sub>as</sub> (NO)	1864	1837	1831	
4	Cu <sup>2+</sup> -NO	v(NO)	1912	-	1878	Resolved in 2 <sup>nd</sup> derivative
5	Cu <sup>2+</sup> -NO	v(NO)	1905	-	1870	Resolved in 2 <sup>nd</sup> derivative
6	Cu <sup>+</sup> -NO	v(NO)	1810	-	1762	
7	Cu <sup>+</sup> (NO) <sub>2</sub>	v <sub>s</sub> (NO)	1824	1809	1791	
		v <sub>as</sub> (NO)	1728	1708	1699	
	<b>Other nitrosyls</b>					
8	Trans-(N <sub>2</sub> O <sub>2</sub> )	v <sub>as</sub> (NO)	1784	1767	1754	
9	ONON	v(NO)	1678	-	1651	
10	OH-NO	v(NO)	1891	-	1858	Shoulders
11	[N <sub>2</sub> O <sub>2</sub> ] <sup>+</sup>	v <sub>s</sub> (NO)	2005	1988	1969	Low concentration
		v <sub>as</sub> (NO)	1687	1671	1657	

Because the spectra of adsorbed isotopic mixtures are complex and many bands overlap, for better understanding a comparison of the real spectrum and the so-called “simulated mononitrosyl” spectrum is used (see APPENDIX A).

Fig. 39 represents comparison of the simulated spectrum and the spectrum of NO +  $^{15}\text{NO}$  adsorbed at ambient temperature. It is visible that the two spectra (Fig. 39, spectra a+b and c) coincide very well. In this case the simulated spectrum coincides with the real spectrum registered after adsorption of the isotopic mixture, this means that all bands observed correspond to N–O vibrations of mononitrosyl species (see APPENDIX A). The principal deviations are in the region (1750 – 1680  $\text{cm}^{-1}$ ) and around 1825  $\text{cm}^{-1}$  and concern the dinitrosyl species of  $\text{Cu}^+$ .

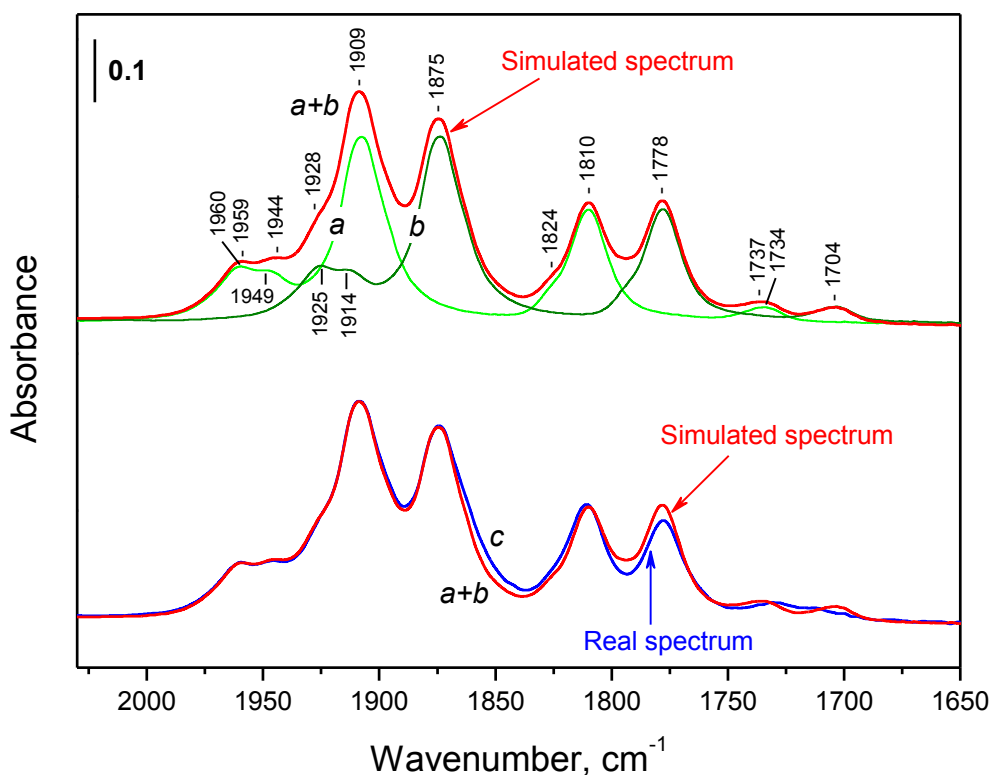


**Fig. 39** - FTIR spectra of  $^{14}\text{NO}$  and  $^{15}\text{NO}$  adsorbed and coadsorbed on Cu-ZSM5 at ambient temperature. Spectrum “a” represents the spectrum recorded after adsorption of NO (500 Pa equilibrium pressure) divided by a factor of two; spectrum “b” is obtained by shifting of spectrum “a” along X-axis by the isotopic shift factor (1.018); spectrum “c” represents the spectrum recorded after coadsorption of  $^{14}\text{NO}$  –  $^{15}\text{NO}$  (500 Pa equilibrium pressures). The spectra are background and gas-phase corrected. Some spectra are shifted along the Y-axis

Figs. 40 and 41 represent comparison of the simulated spectrum and the spectrum of NO +  $^{15}\text{NO}$  adsorbed at low temperature at low and high coverage of the isotopic mixture.

The spectra in figure 40 correspond to prolonged evacuation of about 15 min (low coverage of the isotopic mixture), whereas the spectra in Fig. 41 correspond to short evacuation of about 5 min (higher coverage of the isotopic mixture). The spectra a in Fig. 40 is chosen in order to be the last ones before the appearance of the HF bands during evacuation.

On the top part of these two figures it is possible to see the spectra of NO (a) and  $^{15}\text{NO}$  (b) adsorbed at 100 K, and the simulated spectrum that is sum of the two (a+b). At the down part of the same figures is presented the comparison between the simulated (a+b) and the real spectra (c).

It is visible from Figure 40 that the main differences between the spectra (a+b) and (c) are in the 1850 – 1625  $\text{cm}^{-1}$  region.

There are four bands with reduced intensity in the real spectrum: 1824, 1791, 1728 and 1699  $\text{cm}^{-1}$  (Fig. 40, spectrum c). These bands correspond to  $\text{Cu}^+(\text{NO})_2$  (1824 and 1728  $\text{cm}^{-1}$ ) and to  $\text{Cu}^+(\text{NO})_2$  (1791 and 1699  $\text{cm}^{-1}$ ). At the same time, in the real spectrum there are two new bands with maxima at 1809 and 1708  $\text{cm}^{-1}$ . They correspond to the complex with mixed ligands  $\text{Cu}^+(\text{NO})(\text{NO})$  (see APPENDIX A).

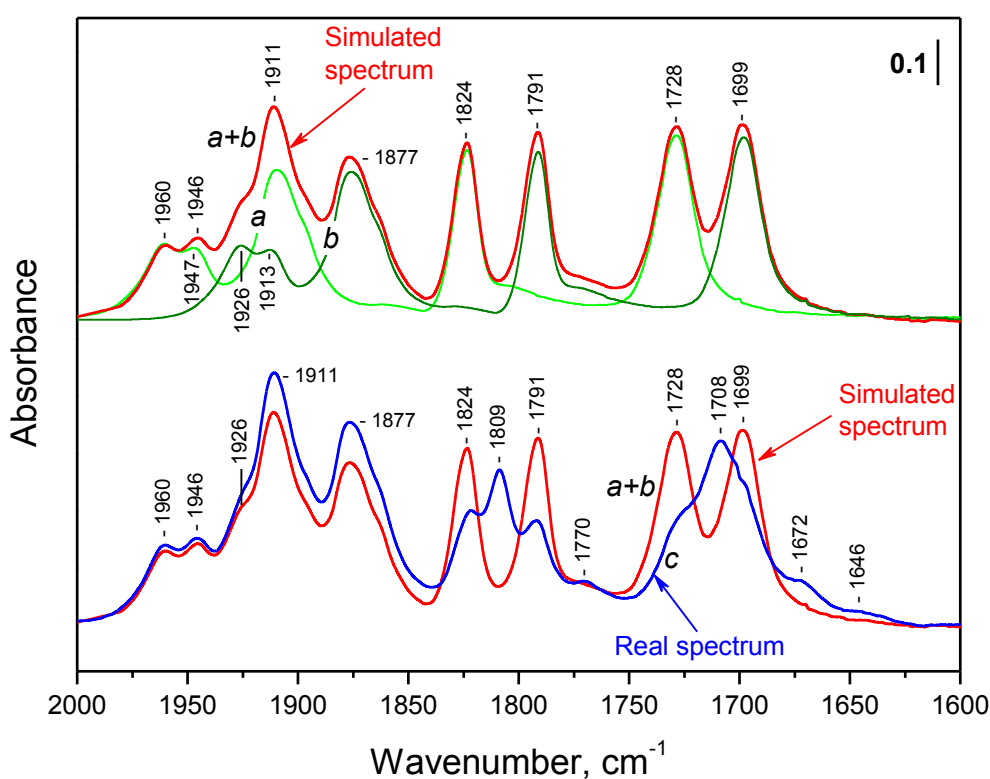


**Fig. 40** - FTIR spectra of  $^{14}\text{NO}$  and  $^{15}\text{NO}$  adsorbed and coadsorbed on Cu-ZSM5 at 100 K. Spectrum “a” represents the spectrum recorded after adsorption of NO (200 Pa equilibrium pressure, followed by a prolonged evacuation of 15 min) divided by a factor of two; spectrum “b” is obtained by shifting of spectrum “a” along X-axis by the isotopic shift factor (1.018); spectrum “c” represents the spectrum recorded after coadsorption of  $^{14}\text{NO}$  –  $^{15}\text{NO}$  (200 Pa equilibrium pressure, followed by a prolonged evacuation). The spectra are background and gas-phase corrected. Some spectra are shifted along the Y-axis

The differences below 1825  $\text{cm}^{-1}$  are due to formation of dinitrosyls of  $\text{Cu}^+$  and to trans- $(\text{N}_2\text{O}_2)$ . To facilitate the identification of  $\text{Cu}^+$  dinitrosyls bands, a part of the spectrum c from Fig. 40 (grey solid line) was reported in Fig. 41. The bands at 1678 and 1653  $\text{cm}^{-1}$  are assigned to asymmetric NO dimer (ONON).

The main part of the band at  $1913\text{ cm}^{-1}$  is due to mononitrosyl species but there is a component of the band that also located around  $1913\text{ cm}^{-1}$ , that develops when the mononitrosyl bands at  $1960$  and  $1947\text{ cm}^{-1}$  disappear (these bands are well visible in Fig. 40).

This suggests that this component is due to dinitrosyl species. There is another band with maximum at  $1864\text{ cm}^{-1}$  that also appears when the bands at  $1960$  and  $1947\text{ cm}^{-1}$  disappear.

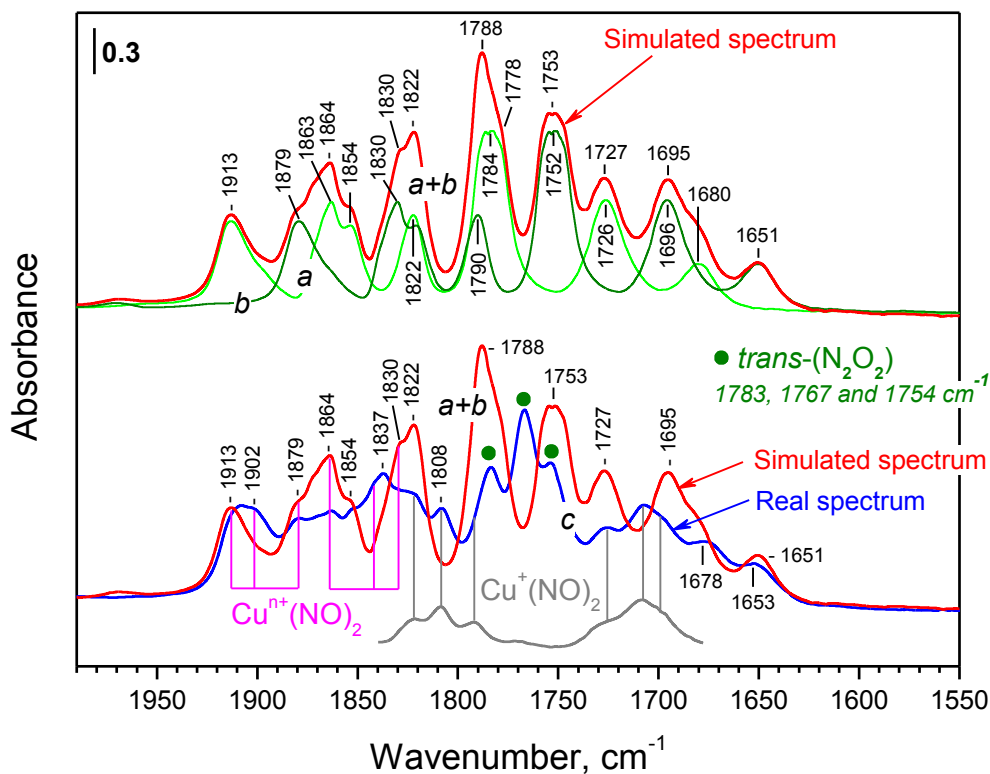


**Fig. 41** - FTIR spectra of  $^{14}\text{NO}$  and  $^{15}\text{NO}$  adsorbed and coadsorbed on Cu-ZSM5 at 100 K. Spectrum “a” represents the spectrum recorded after adsorption of NO (200 Pa equilibrium pressure, followed by 5 min evacuation) divided by a factor of two; spectrum “b” is obtained by shifting of spectrum “a” along X-axis by the isotopic shift factor (1.018); spectrum “c” represents the spectrum recorded after coadsorption of  $^{14}\text{NO} - ^{15}\text{NO}$  (200 Pa equilibrium pressure, followed by evacuation). The spectra are background and gas-phase corrected. Some spectra are shifted along the Y-axis

If the bands at  $1913$  and  $1864\text{ cm}^{-1}$  are due to dinitrosyls it is possible to use these wavenumbers in the approximate force field model (Braterman, 1975) to calculate the corresponding  $^{15}\text{NO}$  and  $[(\text{NO})(^{15}\text{NO})]$  dinitrosyl species. The calculated values coincide well with the bands in the real spectra which evidence that the mononitrosyls characterized by bands at  $1960$  and  $1947\text{ cm}^{-1}$  are converted into dinitrosyls.

These dinitrosyls are true dinitrosyls (see Fig. 42 A) and their decomposition goes through mononitrosyls. The oxidation state of copper in these complexes is  $> 1$ .

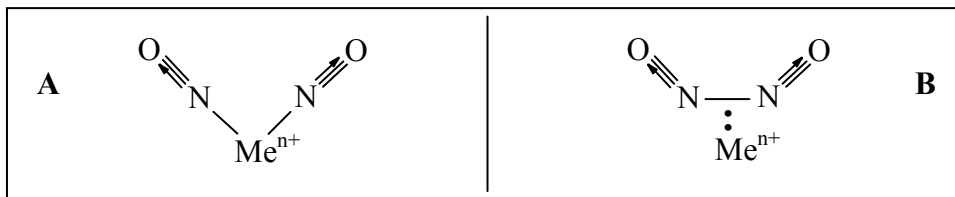


Fig. 42 - True dinitrosyls (A) and adsorbed cis-dimers (B)

After revealing the nature of the bands at  $1960$  and  $1947\text{ cm}^{-1}$ , the conversion of the same bands was studied. Two additional experiments (Fig. 43 and 44), one with NO and the other with isotopic mixture, have been performed.

In the first experiment the NO adsorption has been followed by heating at  $50\text{ }^{\circ}\text{C}$ , evacuation at ambient temperature and another NO adsorption. It is visible from Fig. 43 (spectrum d) that after this second NO adsorption the bands at  $1960$  and  $1947\text{ cm}^{-1}$  appear with intensity lower than the initial. This means that bands at  $1960$  and  $1947\text{ cm}^{-1}$  were irreversibly converted into  $\text{Cu}^{2+}\text{-NO}$  ( $1908\text{ cm}^{-1}$ ).

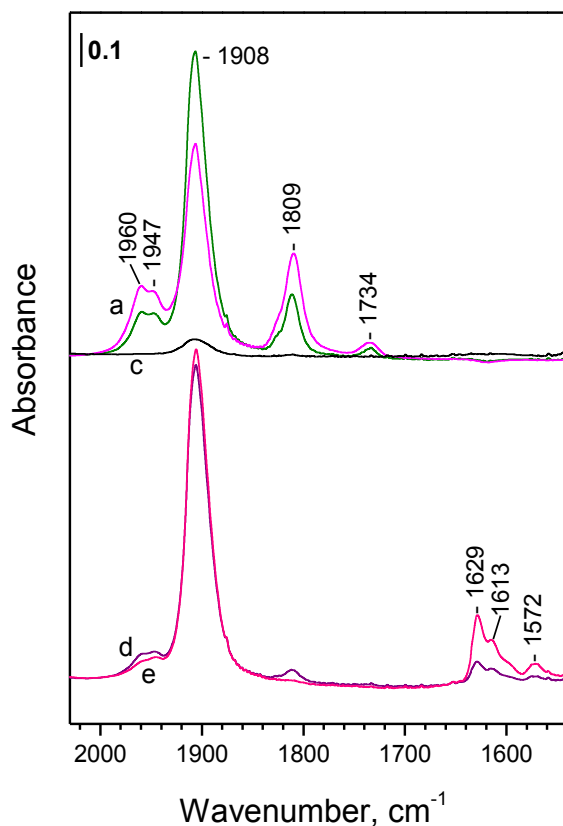
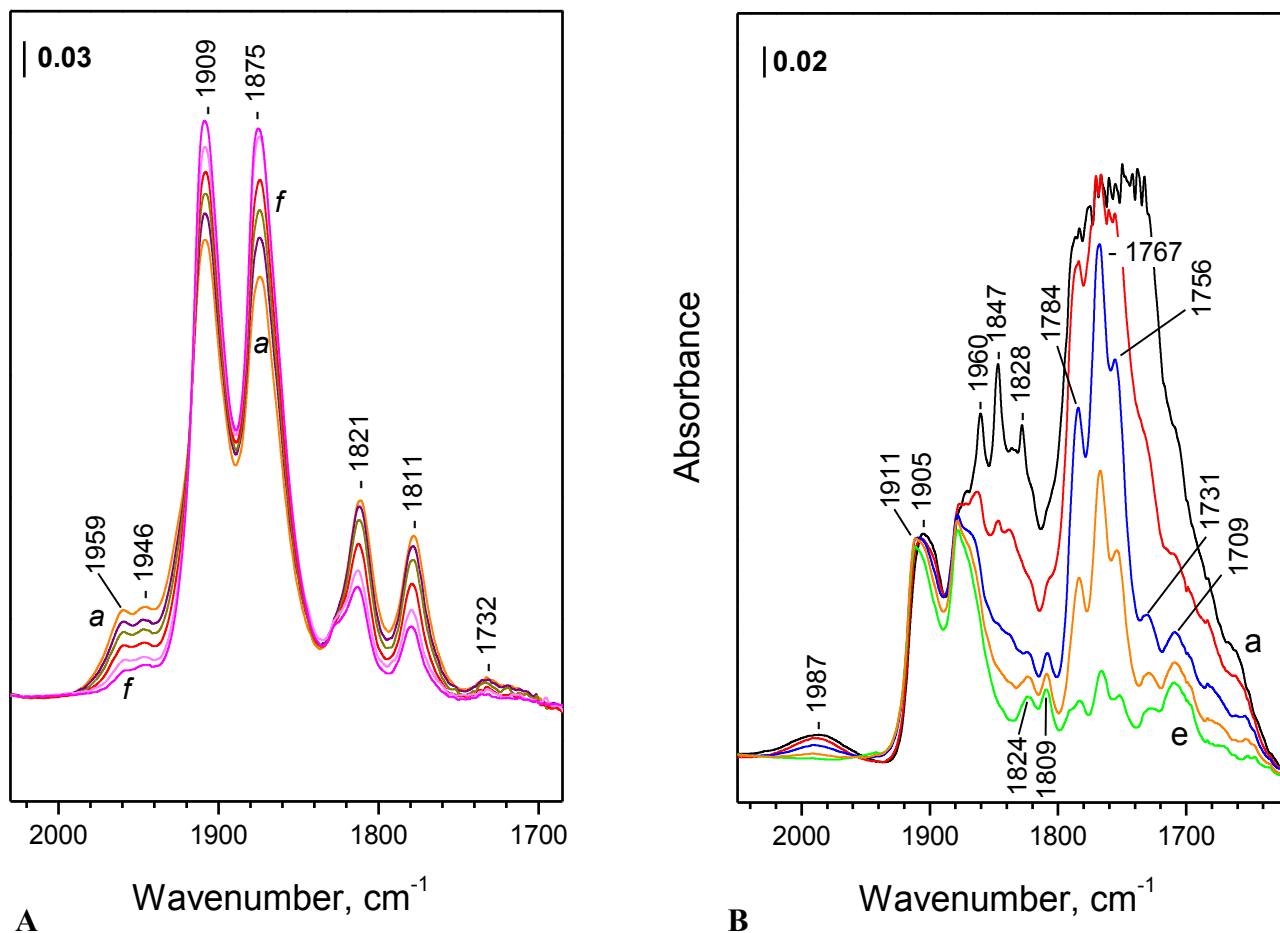


Fig. 43 - FTIR spectra of NO (500 Pa equilibrium pressure) adsorbed on activated Cu-ZSM5 at ambient temperature (a), after heating at  $323\text{ K}$  for 90 min (b) and after evacuation (c). Second adsorption of NO (500 Pa equilibrium pressure) at ambient temperature (d) and evolution after 3 min (e). The spectra are background corrected

The same experiment was repeated with the isotopic mixture, the results obtained with this adsorption are presented in Fig. 44. In this case it is possible to verify that the heating followed by a second adsorption was not able to restore the bands at 1960 and 1947  $\text{cm}^{-1}$ .



**Fig. 44** - FTIR spectra of  $^{14}\text{NO}$  and  $^{15}\text{NO}$  (500 Pa equilibrium pressure) adsorbed on activated Cu-ZSM5: A) at ambient temperature (a) and evolution of the spectra during heating at 323 K (b-f) for 5 (b), 15 (c), 30 (d), 60 (e), 90 (f) minutes. B) FTIR spectra of  $^{14}\text{NO}$  and  $^{15}\text{NO}$  (500 Pa equilibrium pressure) obtained after cooling of the sample at 100 K (a) and evolution of the spectra during evacuation at 100 K (b-e). Before cooling the sample was heated in 5 mbar  $^{14}\text{NO}+^{15}\text{NO}$  at 323 K for 90 min. The spectra are background corrected. The spectra are background corrected

In conclusion, our results revealed that the conversion of the bands at 1960 and 1947  $\text{cm}^{-1}$  ( $\text{Cu}^{\text{n}+}-\text{NO}$ ) to a band at 1912  $\text{cm}^{-1}$  ( $\text{Cu}^{2+}-\text{NO}$ ) is an irreversible process.

#### 4.3.2. The oxidation state of the copper sites in the HF mononitrosyls

The few assignments of these bands in the literature are tentatively assigned to nitrosyls of  $\text{Cu}^{2+}$  ions. However, such assignment contradicts the experimental results reported in the previous paragraphs. The frequency of the HF nitrosyls indicates a high electrophilicity of the  $\text{Cu}^{2+}$  sites which should reflect to a higher thermal stability that is opposite to the experimental observations. The ability of the HF nitrosyls to accept additional NO molecule and to form true dinitrosyls could suggest a high coordinative unsaturation of the copper sites which is again in contradiction with the stability. The development of the  $\text{Cu}^+-\text{NO}$  bands at the expense of the HF nitrosyls, in other words the reduction of  $\text{Cu}^{2+}$  to  $\text{Cu}^+$  in presence of NO, contradicts the well established fact that  $\text{Cu}^+$  sites are oxidized in NO atmosphere. Another possible assignment of the HF bands is to  $\text{Cu}^{3+}-\text{NO}$  complexes. Although not typical, oxidation state 3+ is reported in many works, though not for copper in zeolites (Mirica et al. 2004, Pham et al. 2013, Mandal et al. 1987, Pieroot et al. 2010). In particular, it is proposed that  $\text{Cu}^{2+}$  ions where the Cu–Cu distance is short, like in the case of associated  $\text{Cu}^{2+}$  sites, are able to disproportionate giving  $\text{Cu}^{3+}$  and  $\text{Cu}^+$  in order to avoid the Jahn-Teller effect (Pham et al. 2013). The assumption of 3+ oxidation state is consistent with our experimental results. Increase of the oxidation state of a cation leads to an increase of the stretching frequency of the adsorbed NO. In our case the increase of copper oxidation state from  $\text{Cu}^+$  to  $\text{Cu}^{2+}$  (2 times) reflects the increase of the stretching frequency of adsorbed NO by about  $100\text{ cm}^{-1}$ . Further increase from  $\text{Cu}^{2+}$  to  $\text{Cu}^{3+}$  (1.5 times) leads to a further increase of the frequency by  $40\text{--}50\text{ cm}^{-1}$ . It seems that the  $\text{Cu}^{3+}$  sites do not exist on activated samples but are formed as a result of interaction of the associated  $\text{Cu}^{2+}$  sites with NO. In this thesis it is found that some  $\text{Cu}^+$  sites are formed during interaction of  $\text{Cu}^{2+}$  ions with NO. Moreover, the HF bands are found only with samples where existence of associated copper sites is expected. On the other side, the irreversible conversion of the HF nitrosyls into  $\text{Cu}^{2+}-\text{NO}$  ( $1912\text{ cm}^{-1}$ ) and  $\text{Cu}^+-\text{NO}$  ( $1811\text{ cm}^{-1}$ ) can be easily explained by reduction of  $\text{Cu}^{3+}$  sites by NO. Additionally,  $\text{Cu}^{3+}$  ions have a  $d^8$  electron configuration which is expected to favour the formation of dinitrosyls.

#### 4.3.3. Adsorption of NO on CO-precovered sample

In order to study the NO-induced formation of  $\text{Cu}^+$  sites (as suggested from our results) it was studied NO adsorption on a sample with preadsorbed CO. In this case it was expected CO to block all  $\text{Cu}^+$  sites for NO adsorption (CO is preferentially adsorbed on  $\text{Cu}^+$  sites, while NO on  $\text{Cu}^{2+}$  ions). Experimental and instrumental parameters are the same like for CO or NO adsorption experiments. Before adsorption, CO and NO were additionally purified by  $\text{H}_2\text{O}$  and  $\text{CO}_2$  condensation at  $77\text{K}$  (liquid nitrogen).

The first experiment was the adsorption of CO at ambient temperature, evacuation, subsequent cooling to 100 K and adsorption of NO at 100 K on activated Cu-ZSM5 sample (see Figs. 45 and 46).

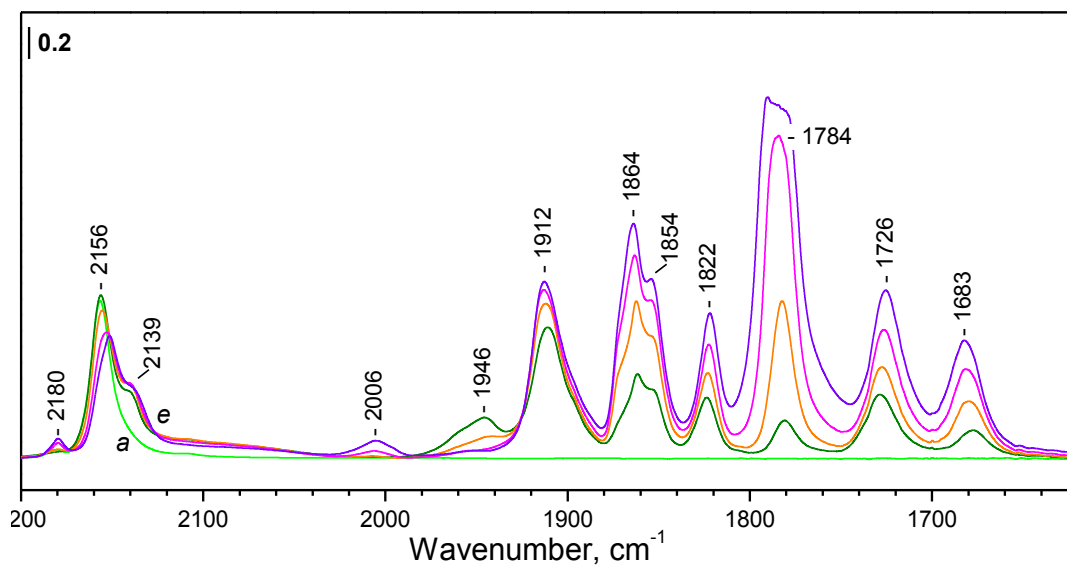


**Fig. 45** - FTIR spectra of CO and NO co-adsorbed on reactivated Cu-ZSM5: adsorption of CO (1 kPa) at RT and subsequent cooling at 100 K (a); adsorption NO (200 Pa) at 100 K (b) and evolution of the spectra with time (c-e). The spectra are background corrected

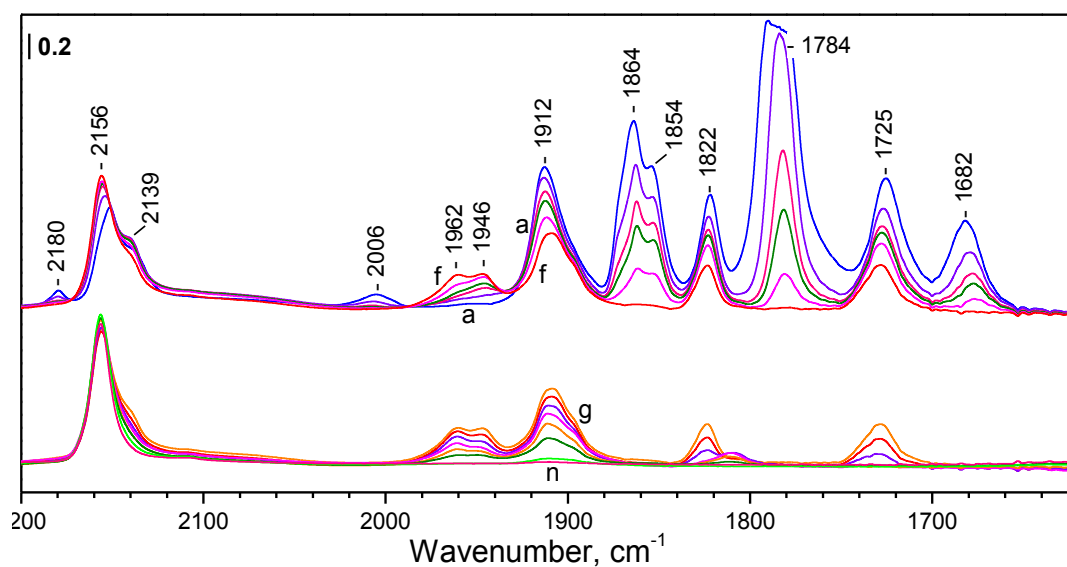


**Fig. 46** - FTIR spectra of CO and NO co-adsorbed on reactivated Cu-ZSM5: evolution of the spectra after evacuation at 100 K (a-i) and at increasing temperature (j-m) up to 298 K (n). The spectra are background corrected

In addition to the well known bands resulting from the CO and NO adsorption, a weak band at 2139  $\text{cm}^{-1}$  was also registered. This last band is due to the conversion of the band at 2156  $\text{cm}^{-1}$ , in fact the intensity of this last band decreases while the new band increases.

It is visible from Figs. 45 and 46 that the main part of  $\text{Cu}^+$  sites are engaged in formation of monocarbonyl species (2156  $\text{cm}^{-1}$ ), although small amount of dicarbonyls also existed (2180  $\text{cm}^{-1}$ ).

In order to verify unambiguously the lack of bare  $\text{Cu}^+$  sites, the sample was tested with  $^{15}\text{N}_2$ . This isotope was used in order to avoid any hindrance from atmospheric  $\text{CO}_2$ .

The low-temperature adsorption of  $^{15}\text{N}_2$  on reduced Cu-ZSM5 sample is presented in Fig. 47; the band at  $2253\text{ cm}^{-1}$  is attributed to  $\text{N}_2$  interacting with the OH groups and the band at  $2219\text{ cm}^{-1}$  is assigned to  $\text{Cu}^+-^{15}\text{N}_2$  species (the shoulder at  $2247\text{ cm}^{-1}$  probably is nitrogen physically adsorbed to the surface). Fig. 47B represents comparison of the results of this last adsorption (spectrum a) and the low-temperature adsorption of  $^{15}\text{N}_2$  on CO-precovered Cu-ZSM5 (spectrum b).

The spectrum b (Fig. 47B) contains only the band at  $2253\text{ cm}^{-1}$ . Thus, the results prove that all  $\text{Cu}^+$  sites on the sample have been blocked by CO.

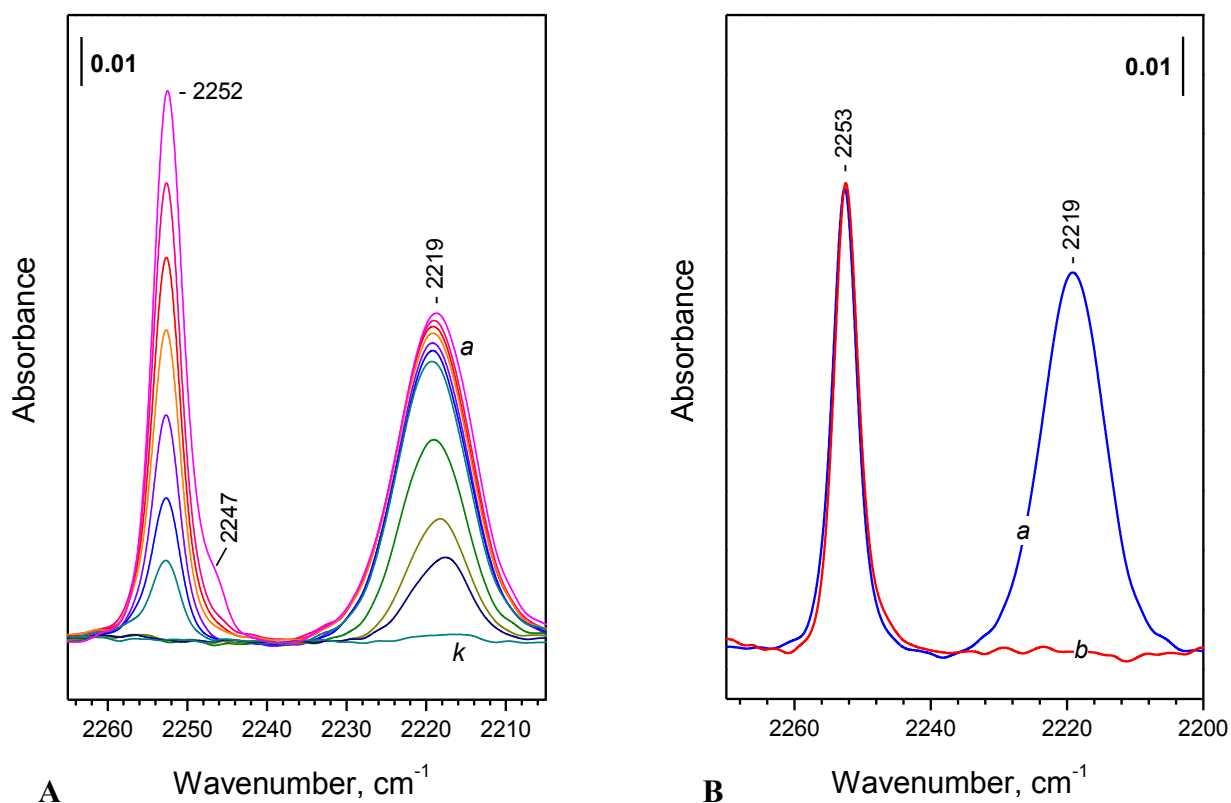


**Fig. 47** - FTIR spectra of  $^{15}\text{N}_2$  (500 Pa) adsorbed on reduced Cu-ZSM5: A) at 100 K (a); evolution of the spectra during evacuation at 100 K (b-i) and at increasing temperatures (j) up to 298 K (k). B) adsorbed at 100 K on partially reduced Cu-ZSM5 (a) and on Cu-ZSM5 precovered with CO (b). The spectra are background corrected

After verifying that the  $\text{Cu}^+$  are really blocked by CO, the subsequent experiment was the adsorption of small doses of NO at 100 K on CO-prerecovered Cu-ZSM5, followed by  $\text{O}_2$  adsorption at the same temperature and evacuation (see Figs. 48, 49 and 50).

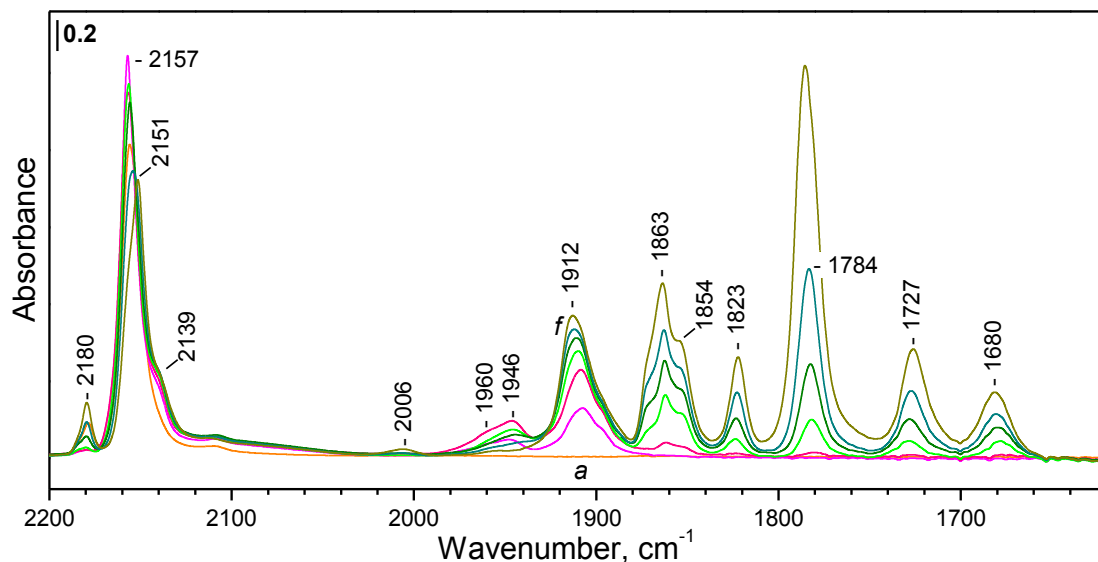


**Fig. 48** - FTIR spectra of CO and NO coadsorbed on reduced Cu-ZSM5: CO adsorption (10 kPa) at ambient temperature and subsequent cooling to 100 K (a) followed by adsorption of 2 mbar NO at 100 K (b-f). The spectra are background corrected

Fig. 48 shows evolution of the spectra with NO coverage. Immediately after the second dose of NO the bands at 1960, 1947 and 1908  $\text{cm}^{-1}$  appeared (Fig. 48, spectra b) and the bands due to dicarbonyls (2151 and 2180  $\text{cm}^{-1}$ ) almost disappeared, while the principal CO band at 2157  $\text{cm}^{-1}$  developed.

The results show the increase of the concentration of the  $\text{Cu}^+$  sites and transfer of one CO molecule from the dicarbonyl complexes to a  $\text{Cu}^+$  site newly formed.

With increasing coverage of NO (Fig. 48, spectra c) the bands at 2005, 1912, 1863, 1854, 1823, 1784, 1727 and 1680  $\text{cm}^{-1}$  developed, in the same spectra the band of  $\text{Cu}^+\text{-CO}$  species (2157  $\text{cm}^{-1}$ ) started to decrease in intensity and a band at 2180  $\text{cm}^{-1}$  (dicarbonyls) developed. In addition, a shoulder at 2139  $\text{cm}^{-1}$  was also formed.

Góra-Marek and Datka (2011) have attributed this shoulder (reported by them at 2137  $\text{cm}^{-1}$ ), together with a band at 1890  $\text{cm}^{-1}$ , to  $\text{Cu}^+(\text{CO})(\text{NO})$  species. However, in our experiments it was recorded spectra where the band at 2139  $\text{cm}^{-1}$  developed without a concomitant band at 1890  $\text{cm}^{-1}$ . Therefore, the band at 2139  $\text{cm}^{-1}$  was assigned to  $\text{Cu}^+(\text{CO})(\text{H}_2\text{O})$  species. Water is produced as a side product from the formation of  $\text{NO}^+$  and  $[\text{ONNO}]^+$ .

In the second part of this experiment  $\text{O}_2$  was fed to verify that the band at 2139  $\text{cm}^{-1}$  was due to  $\text{Cu}^+(\text{CO})(\text{H}_2\text{O})$ . In fact, reacting with NO oxygen forms  $\text{N}_2\text{O}_3$  which interacts with the bridging hydroxyls producing water; if this hypothesis is correct the band at 2141  $\text{cm}^{-1}$  should increase.

In Fig. 49 it is possible to see that the band at 2141  $\text{cm}^{-1}$  increases during the  $\text{O}_2$  adsorption.

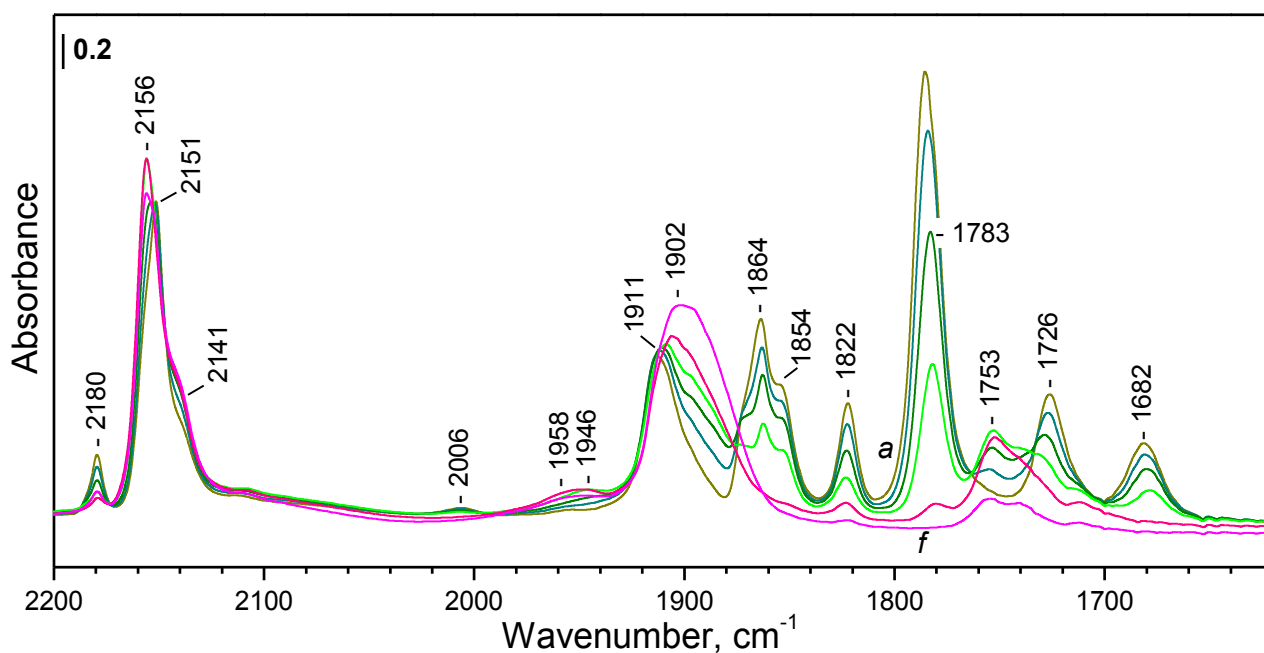


**Fig. 49** - (Continuation of Fig. 48) FTIR spectra of CO, NO and  $\text{O}_2$  co-adsorbed on reduced Cu-ZSM5: CO adsorption (10 kPa) at ambient temperature and subsequent cooling to 100 K followed by adsorption of 2 mbar NO at 100 K (a); adsorption of  $\text{O}_2$  in doses at 100 K (b-f). The spectra are background corrected

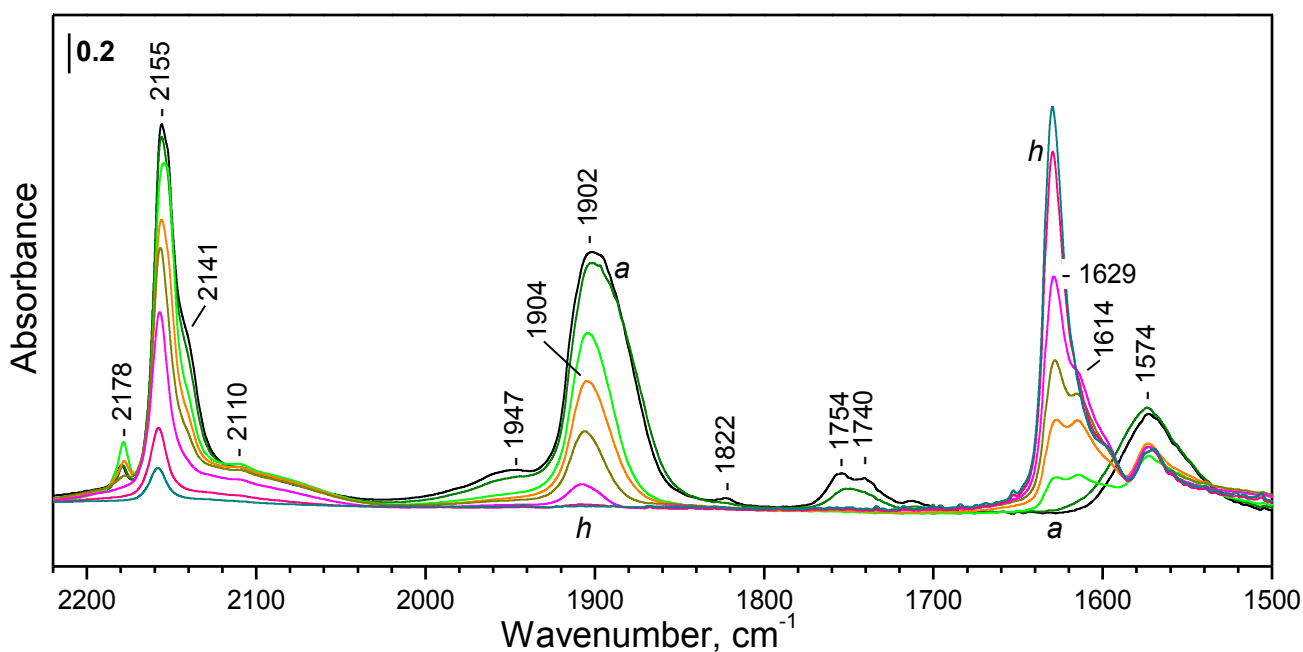
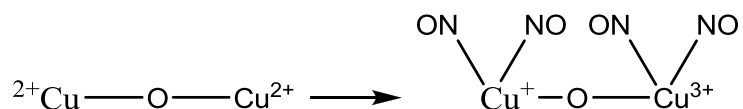


**Fig. 50** - (Continuation of Fig. 49) FTIR spectra of CO, NO and  $\text{O}_2$  co-adsorbed on reduced Cu-ZSM5 (a) and evolution of the spectra during evacuation at 100 K (b) and at increasing temperature (c-g) up to ambient temperature (h). The spectra are background corrected

## Conclusions

In conclusion the adsorption of NO on an over-exchanged Cu-ZSM5 sample ( $\text{SiO}_2/\text{Al}_2\text{O}_3 = 23$ ) leads to formation of nitrosyls of  $\text{Cu}^{2+}$  and  $\text{Cu}^+$  and dinitrosyl of  $\text{Cu}^{3+}$  ions. The  $\text{Cu}^{3+}$  ions do not exist on activated sample but are produced as a result of interaction of NO with associated  $\text{Cu}^{2+}\text{-O-Cu}^{2+}$  sites. The repulsion of two NO molecules on copper ion having an odd number of electrons as in  $\text{Cu}^{2+}$  is overcome by the formation of  $\text{Cu}^+$  and  $\text{Cu}^{3+}$  (disproportionation) in the complex reported below.  $\text{Cu}^+$  and  $\text{Cu}^{3+}$  both have the electron configuration promoting the formation of dinitrosyls.



The ability of  $\text{Cu}^{3+}$  (and  $\text{Cu}^+$ ) ions to form dinitrosyls is favored by the electron pairing in the complexes, contrary to the  $\text{Cu}^{2+}$  ions that form only mononitrosyls.

Moreover, the new findings that  $\text{Cu}^+$  sites are formed during interaction of  $\text{Cu}^{2+}$  ions with NO and the ability of  $\text{Cu}^{3+}$  ions to form dinitrosyls favor the hypothesis that dinitrosyl species are intermediates in NO decomposition.

# Chapter 5

## NO adsorption<sup>2,3</sup>

---

<sup>2</sup> Parts of this chapter appear in G. Landi, L. Lisi, R. Pirone, G. Russo, M. Tortorelli, *Catalysis Today* 191 (2012) 138– 141

<sup>3</sup> Parts of this chapter appear in M. Tortorelli, G. Landi, L. Lisi, G. Russo, submitted to *Micro and Mesoporous Materials*

## 5.1 Adsorption tests

NO adsorption experiments were carried out feeding a gas mixture NO/He (20 L/h) in the temperature range 50-150 °C to a flow quartz reactor (paragraph 3.2.1.1) containing an over-exchanged Cu-ZSM5 or LaCu-ZSM5. The quantitative analysis was carried out using the apparatus system described in paragraph 3.2.1. The powder catalyst (about 1g) with a particle size of 200-400 µm was placed in the reactor.

The adsorption was carried out until catalyst saturation, then the gas mixture was substituted with He flow (20 L/h) carrying out a TPD by heating the reactor at 10 °C/min up to 500 °C.

The NO adsorption test was repeated 4 times for each catalyst with a different feed mixture. In this way, the effect of the H<sub>2</sub>O presence and the co-presence of O<sub>2</sub> and H<sub>2</sub>O were studied. Before each NO adsorption experiment, the catalyst was pre-reduced 2 h at 550 °C in a He flow (20L/h).

The difference among the tests was in the composition of the feeding mixture (see Tab. 7).

**Tab. 7** – Composition of the feeding mixture for each cycle.

<b>Test</b>	<b>Composition</b>
<b>1</b>	800 ppm NO/ He
<b>2</b>	800 ppm NO/2%H <sub>2</sub> O/He
<b>3</b>	800 ppm NO/1%O <sub>2</sub> / He, 2%H <sub>2</sub> O after 80 min
<b>4</b>	800ppm NO/1%O <sub>2</sub> /2% H <sub>2</sub> O/ He

In Figs. 51-58 the concentration of NO, NO<sub>2</sub> and N<sub>2</sub>O as a function of time, for the four NO adsorption test on Cu-ZSM5 at 125 °C, are reported. The trend of NO, NO<sub>2</sub> and N<sub>2</sub>O concentration is qualitatively the same at the other temperatures and for LaCu-ZSM5 as well. At the end of each TPD a decomposition test was performed, to prove that the catalyst was not deactivated.

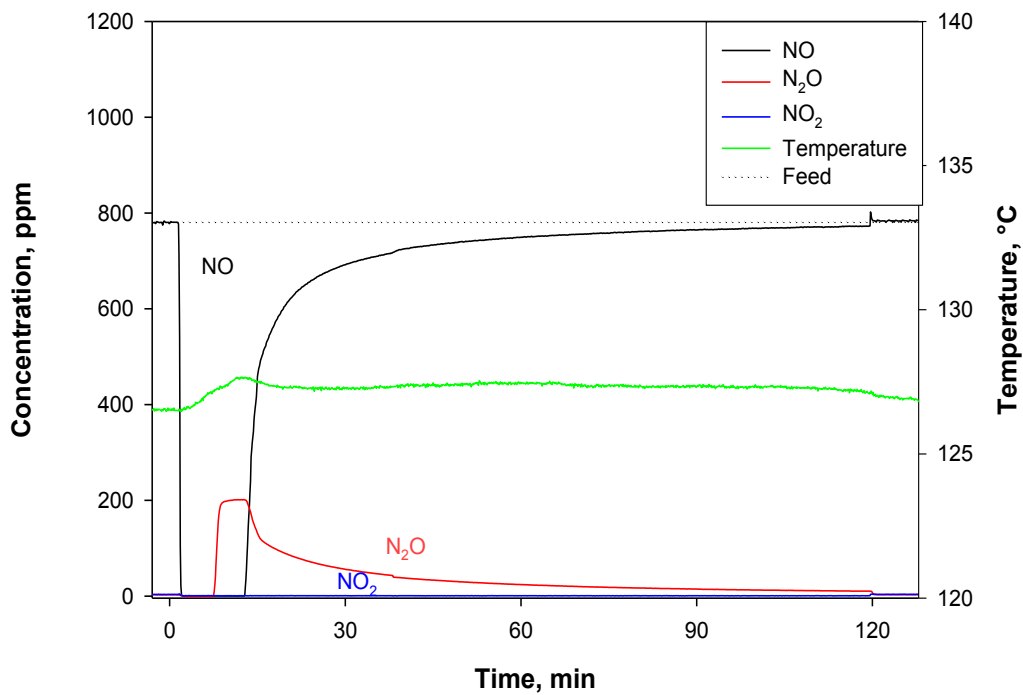


**Fig. 51** – NO, NO<sub>2</sub>, N<sub>2</sub>O and O<sub>2</sub> output concentrations during the adsorption test (feed=NO/He) at 125 °C on Cu-ZSM5

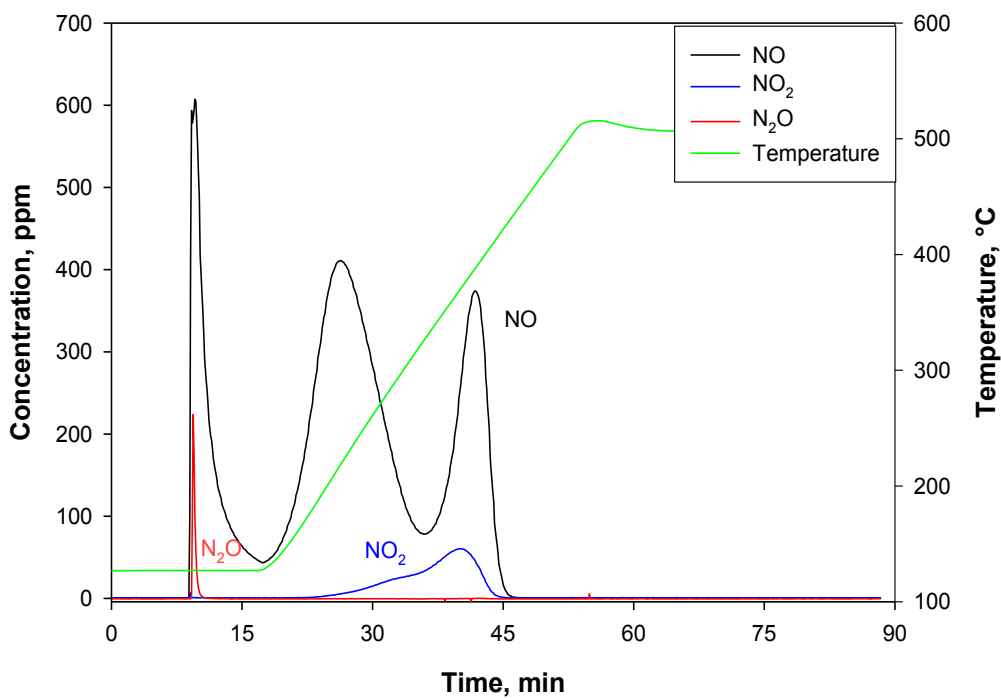


**Fig. 52** – NO, NO<sub>2</sub>, N<sub>2</sub>O and O<sub>2</sub> output concentrations during purging phase with helium and the TPD conducted after the saturation of the pre-reduced Cu-ZSM5

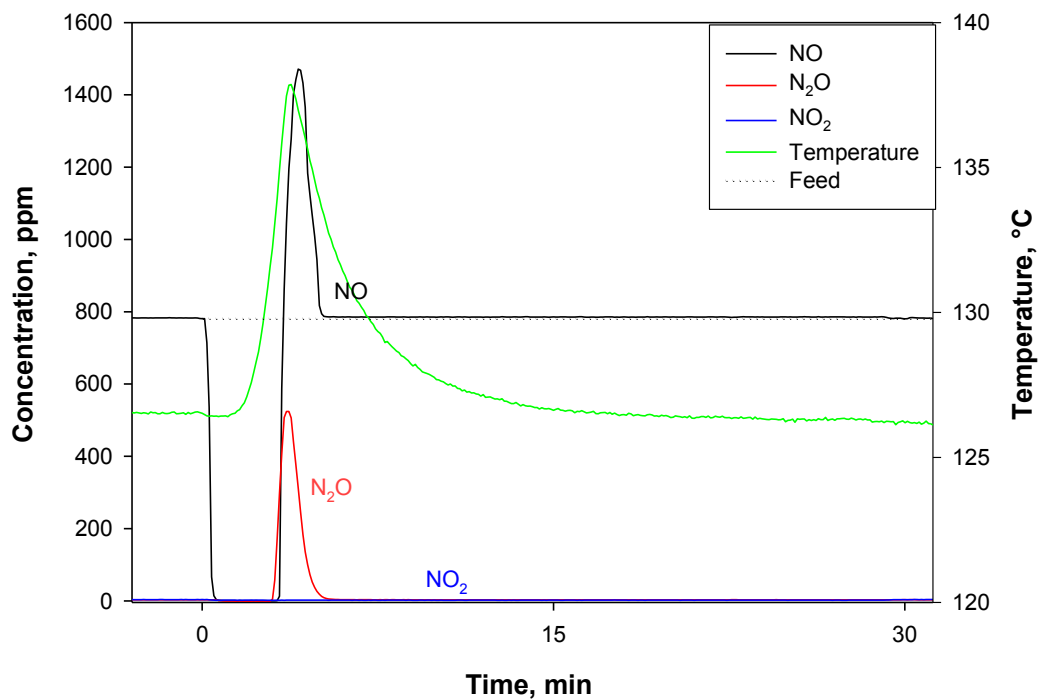


**Fig. 53** – NO, NO<sub>2</sub>, N<sub>2</sub>O and O<sub>2</sub> output concentrations during the adsorption test (feed=NO/He/H<sub>2</sub>O) at 125 °C on Cu-ZSM5

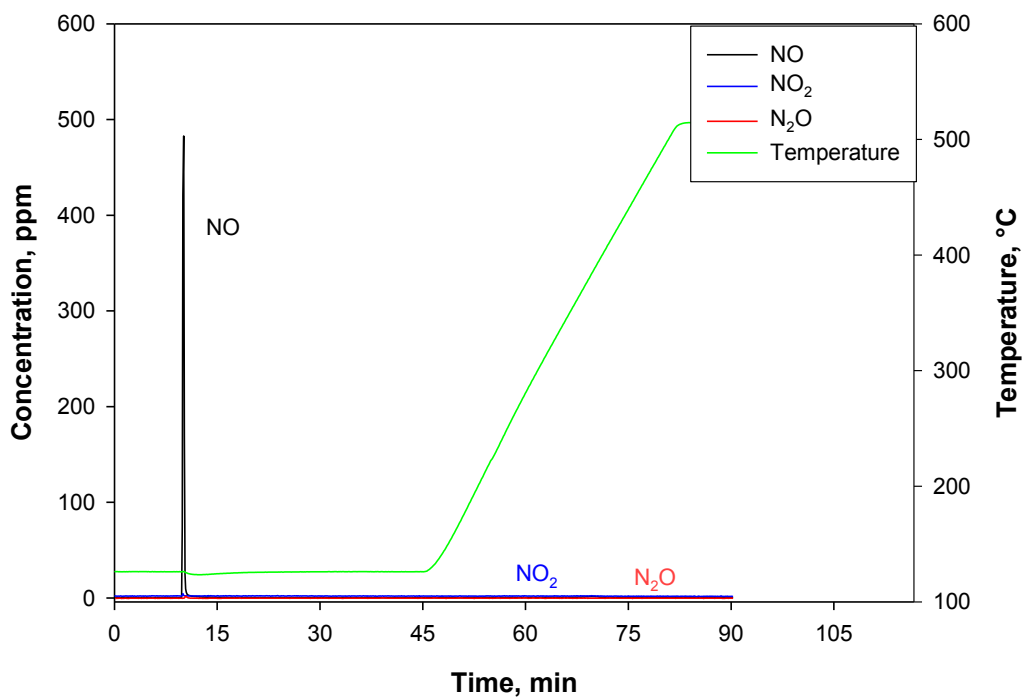


**Fig. 54** – NO, NO<sub>2</sub>, N<sub>2</sub>O and O<sub>2</sub> output concentrations during purging phase with helium and the TPD conducted after the saturation of the pre-reduced Cu-ZSM5

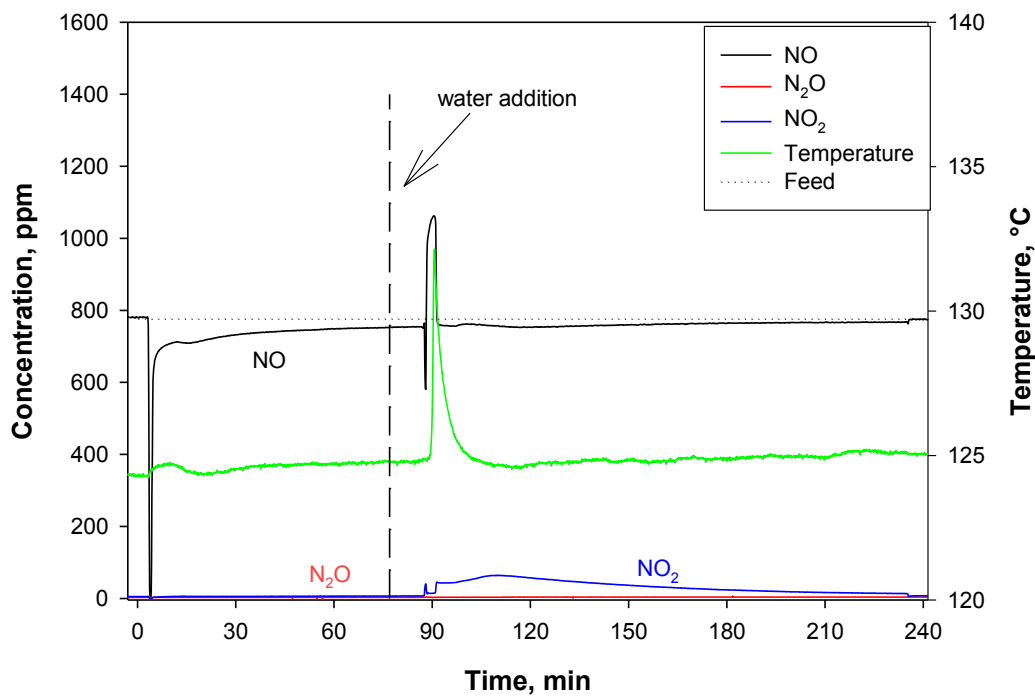


**Fig. 55** – NO, NO<sub>2</sub>, N<sub>2</sub>O and O<sub>2</sub> output concentrations during the adsorption test (feed=NO/He/O<sub>2</sub> and H<sub>2</sub>O after 80 min) at 125 °C on Cu-ZSM5

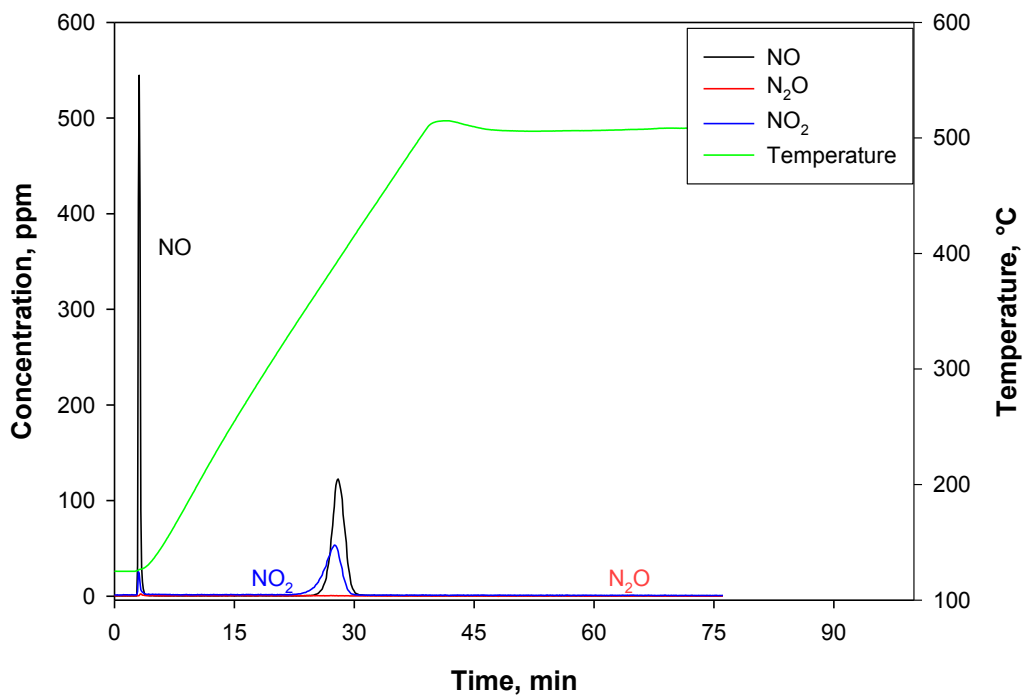


**Fig. 56** – NO, NO<sub>2</sub>, N<sub>2</sub>O and O<sub>2</sub> output concentrations during purging phase with helium and the TPD conducted after the saturation of the pre-reduced Cu-ZSM5

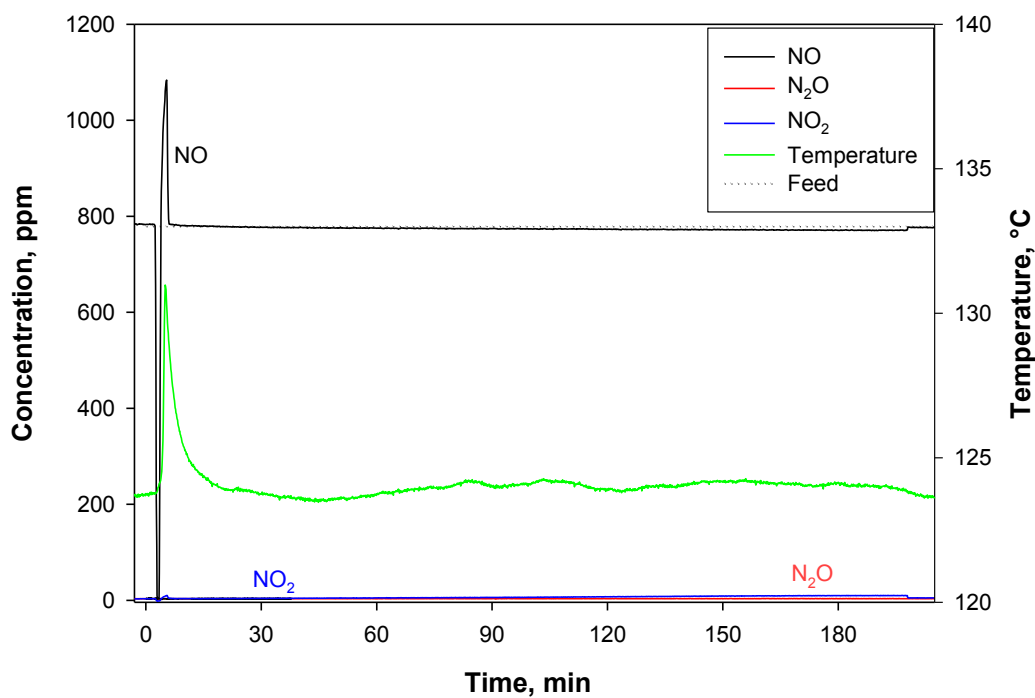


**Fig. 57** – NO, NO<sub>2</sub>, N<sub>2</sub>O and O<sub>2</sub> output concentrations during the adsorption test (feed=NO/He/O<sub>2</sub>/H<sub>2</sub>O) at 125 °C on Cu-ZSM5

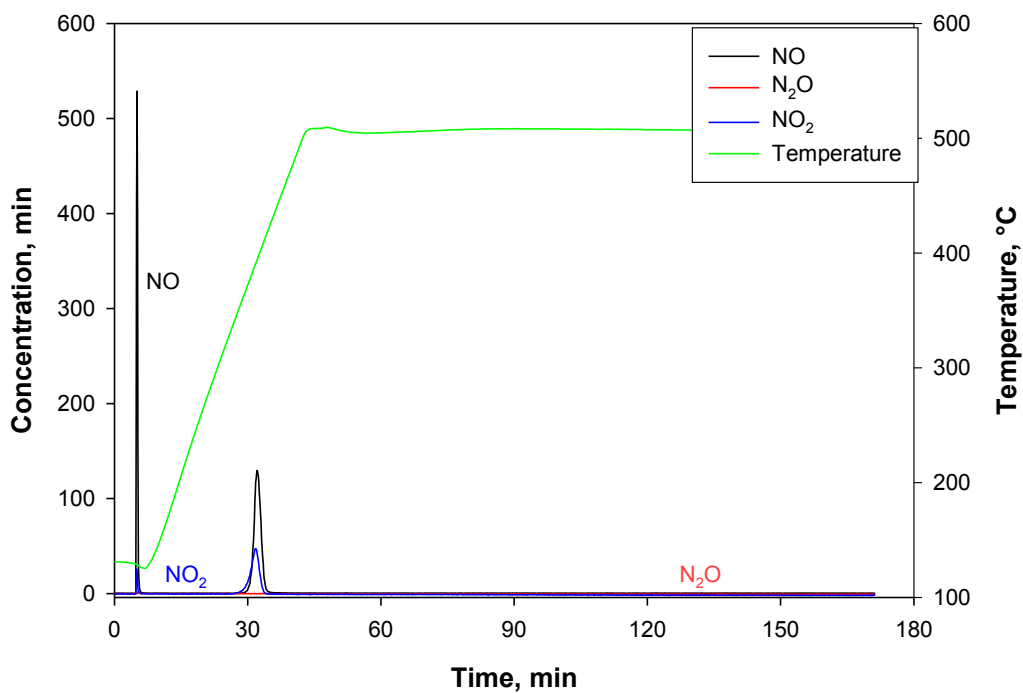


**Fig. 58** – NO, NO<sub>2</sub>, N<sub>2</sub>O and O<sub>2</sub> output concentrations during purging phase with helium and the TPD conducted after the saturation of the pre-reduced Cu-ZSM5

In the first adsorption test the feed was simply by 800 ppm NO/ He, the NO adsorption time lasted about 10 minutes, during the adsorption phase N<sub>2</sub>O was produced and its level slowly decreased after catalyst saturation (Fig. 51). The reason of N<sub>2</sub>O formation was the reduction of NO caused by copper oxidation.

When the zeolite was purged with He a physical adsorbed NO peak was detected and then, when the temperature was enhanced, two main NO peaks were observed at about 200 and 380 °C respectively (Fig. 52). In phase with the last NO emission an about equimolar amount of O<sub>2</sub> (not reported) and a lower NO<sub>2</sub> quantity were detected.

In the second experiment the presence of water in the feed (Fig. 53) strongly reduced NO adsorption. In Fig. 53 it was possible to observe a fast NO and N<sub>2</sub>O desorption after about 3 minutes which suggests a displacement of both NO and N<sub>2</sub>O by water. At the same time in addition to the two desorption peaks, there was a temperature peak that revealed a temperature increase of about 10 °C which accounted for a higher exothermicity of water adsorption compared to NO<sub>x</sub> species.

In the corresponding TPD (Fig. 54) there was only the first peak suggesting that copper sites were chemical bonded with water.

During the third NO adsorption test (Fig. 55) the amount of adsorbed NO was reduced by the water addition in the feed. After 80 minutes water vapour was added to NO/He/O<sub>2</sub>; at 90 minutes it was possible to observe two desorption peaks (NO and NO<sub>2</sub>) probably due to a water displacement (like in the second test).

By observing the Fig. 55, it was possible to note that during the third adsorption experiment the N<sub>2</sub>O was not present. The reason of this absence is connected with the presence of O<sub>2</sub> in the feed which prevails as oxidant with respect to NO in the gaseous mixture.

In the third TPD (Fig. 56), in addition to the peak of reversibly adsorbed NO, the NO desorption peak at 380 °C is detectable. This last peak reveals the nitrate formation during the adsorption phase, caused by oxygen presence in the feed.

By concluding, in the last test (Fig.57) the oxygen presence reduced the amount of NO displaced by water.

The last TPD (Fig. 58) was very similar to the third; the reason of this similarity could be that water cannot displace the nitrate species which then successfully to compete with water for the same copper site.

In Fig. 59 the amount of NO<sub>x</sub> (μmol/g<sub>cat</sub>) desorbed in the TPD analyses following the performed experimental tests with both Cu-ZSM5 and LaCu-ZSM5 at each adsorption temperature was reported.

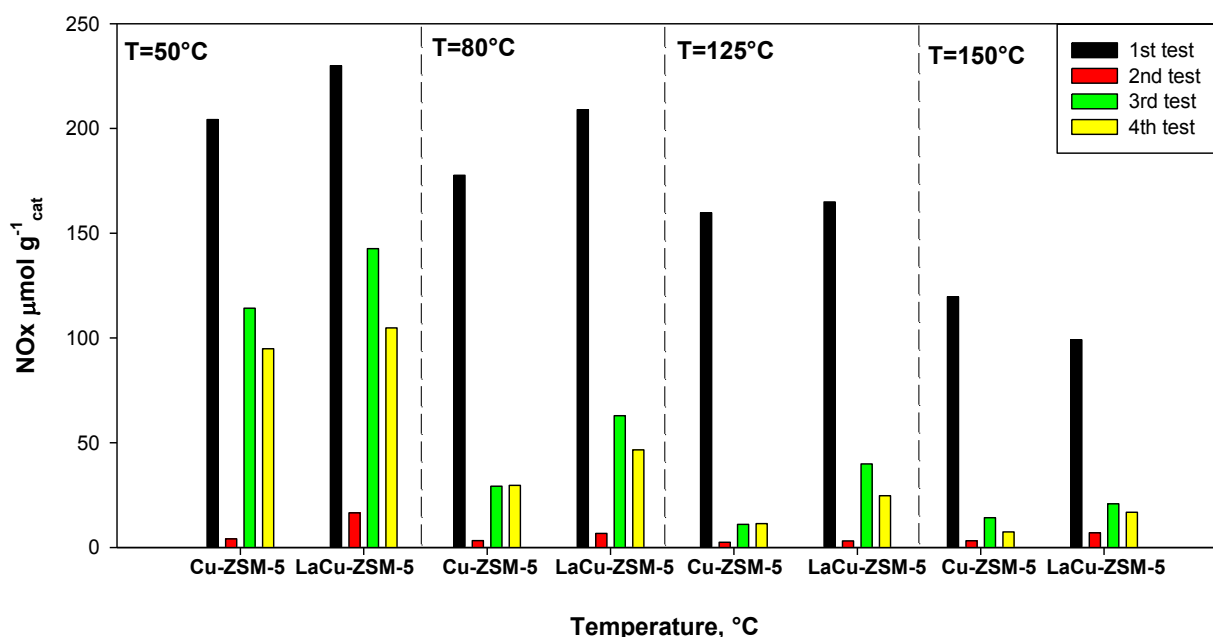


**Fig. 59** – Total amount of NO<sub>x</sub> desorbed during the TPD carried out after NO adsorption on pre-reduced Cu-ZSM5 and LaCu-ZSM5 at each adsorption temperature in the 4 tests

The amount of desorbed NO<sub>x</sub> increases at each temperature if lanthanum is co-exchanged with Cu, confirming the results reported by Palella et al. (2006). This amount noticeably decreases with increasing the temperature, as expected for adsorption phenomena

The loss of NO adsorption capacity in the presence of a wet feed, also reported by Despres et al. (2003), was less intense both in the presence and in the absence of O<sub>2</sub>, confirming that the rare earth cation partially inhibits the NO displacement by H<sub>2</sub>O and/or promotes the nitrates formation. The reduction of NO<sub>x</sub> adsorption by water could be then the main cause of the loss of activity in NO decomposition reported in Palella et al. (2006). Water depressed NO adsorption on Cu-ZSM5 at low temperature. Water almost totally displaces NO pre-adsorbed on copper sites but in the presence of oxygen the oxidation of NO to NO<sub>2</sub>, that partially occurs, promotes the formation of nitrate-like species which are not removed by water as can be seen in the 3<sup>rd</sup> and 4<sup>th</sup> TPD. Lanthanum co-exchange improves the copper adsorption capacity both in the absence and in the presence of water and O<sub>2</sub>. The beneficial effect of La on the catalytic performance of Cu-ZSM5 in NO decomposition is ascribed to the improved NO adsorption.

## 5.1 NO adsorption after adsorption and desorption of water on LaCu-ZSM5

As shown in the previous paragraph, the presence of water in the feed has always a negative effect on the NO adsorption on copper exchanged ZSM5. In order to determine the temperature necessary to water desorption and to verify the reversibility of water effect some tests were carried out as described below.

These tests were performed in seven steps:

1. Catalyst pre-treatment: the catalyst was pre-oxidized (550 °C for 2 h, under 10 vol.% O<sub>2</sub>/He flow);
2. H<sub>2</sub>O saturation: a stream of He (20 l/h) saturated with water at ambient temperature was fed to the quartz reactor for about 30 min at 125 °C;
3. H<sub>2</sub>O removal: water was removed flowing He (20 l/h) increasing temperature (10 °C min<sup>-1</sup>) to a value ranging from 125 to 500 °C keeping the final temperature for a time ranging from 0.5 to 4 h;
4. Oxidation: the catalyst was oxidized again because during the third step it was partially reduced
5. NO saturation: a stream of He/NO was fed to the reactor at 125 °C until catalyst saturation;
6. NO desorption: the catalyst was contacted with pure He flow (30 NI/h) at the adsorption temperature (125 °C) and then a TPD in He flow was performed in order to remove and evaluated the adsorbed NO.
7. NO decomposition activity test: a standard NO decomposition test (T= 450 °C, NO concentration= 800ppm NO, W/F=0.05 gh/NI) was carried out in order to verify the occurrence of any deactivation phenomenon after treatments at different temperatures in the presence of water vapour.

The original catalytic performance was restored after all conditions of phases 1-4 explored thus showing that no permanent deactivation of the zeolite occurred upon water adsorption.

In Fig. 60 NO, N<sub>2</sub>O, NO<sub>2</sub> concentration and temperature profiles during the phases 2-6 of a typical experiments are reported.

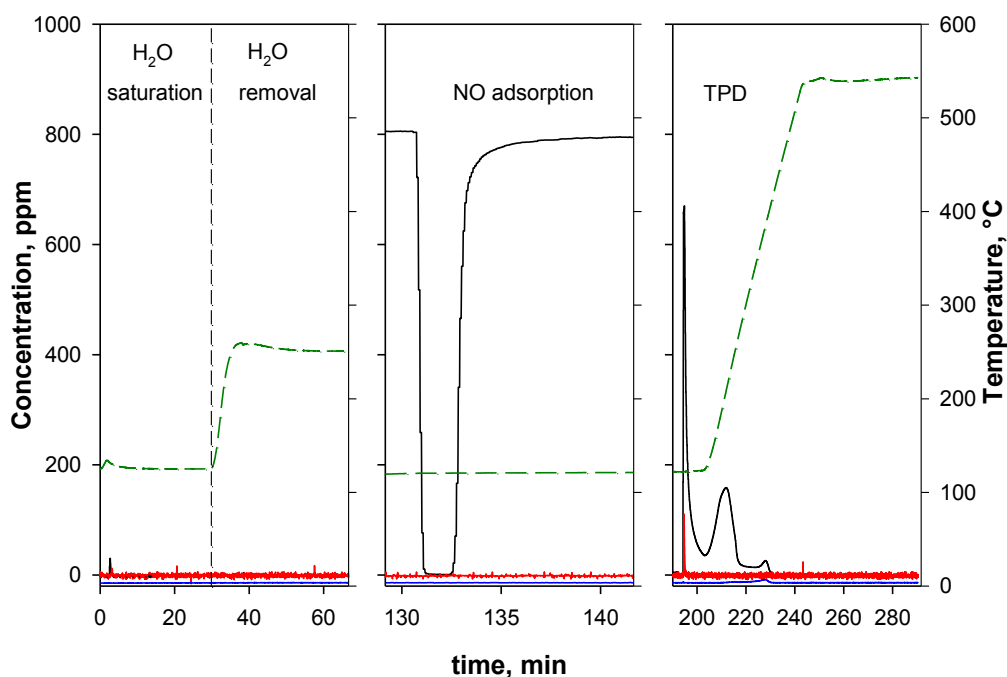


**Fig. 60** – Temperature (---), NO (—), N<sub>2</sub>O (—) and NO<sub>2</sub> (—) concentrations as a function of the time on stream during the phases 2-5 of a typical experiment. Water removal at 250°C for 0.5 h

In the first part of Fig. 60 the temperature profiles during the H<sub>2</sub>O saturation and removal is reported, a weak temperature peak during the saturation caused by the exothermicity of water adsorption on LaCu-ZSM5 is detectable. During the water removal the temperature was raised up to a given value (i.e. 250 °C in the experiment reported in figure 60) and the catalyst purged with He for a fixed time (i.e. 0.5 h in the experiment reported in figure 60). Then the catalyst was cooled down back to 125 °C under 10 vol.% O<sub>2</sub>/He flow in order to re-oxidize the sample (self-reduction occurring above 400 °C). In the middle part of the figure the temperature was constant (125 °C) and a 800ppm NO/He mixture was fed to the reactor (phase 5). At this temperature the LaCu-ZSM5 reactivity was negligible and only NO adsorption on the catalyst surface occurred. In the third part of the figure a TPD was carried out by increasing the temperature at 10 °C/min.

The amount of NO adsorbed (NO<sub>ads</sub>) on the catalyst at the end of the adsorption phase was evaluated by subtracting from the overall NO uptake (NO<sub>uptake</sub>) that of NO necessary to fill the dead volumes of the experimental set-up (NO<sub>hold-up</sub>) evaluated in separate blank tests, as follows:

$$NO_{ads} = NO_{uptake} - NO_{hold-up}$$

Similarly, the amount of NO<sub>x</sub> desorbed (NO<sub>x,des</sub>) from the catalyst at the end of the TPD phase was evaluated by the emission of NO, N<sub>2</sub>O and NO<sub>2</sub> (N<sub>2</sub> is negligible), calculated by the integration of the corresponding TPD profile, as follows:

$$NO_{x,des} = NO_{des} + 2N_2O_{des} + NO_{2des} - NO_{hold-up}$$

In all experiments, the error on mass balance ( $\text{NO}_{\text{ads}}$  vs.  $\text{NO}_{\text{x\_des}}$ ) was within  $\pm 4\%$ .

The original adsorption capacity (under dry condition) of the LaCu-ZSM5 zeolite is  $115 \mu\text{mol/g}_{\text{cat}}$  at  $125^\circ\text{C}$ .

In Fig. 61 the recovered adsorption capacity (the ratio between the desorbed  $\text{NO}_{\text{x}}$  amount during the TPD after water saturation and removal and that desorbed from the catalyst not treated with water) was reported as a function of the removal temperature for two different removal times. This parameter provides a measure of the amount of water still present on the catalyst after the thermal treatment hindering the NO adsorption.

The experimental results at a removal time equal to 0.5 h (time-length of  $\text{H}_2\text{O}$  removal) show that the amount of  $\text{NO}_{\text{x}}$  detected during TPD for different temperatures of desorption of water reaches a plateau at about  $300^\circ\text{C}$ , corresponding to a recovered adsorption capacity of about 0.8. This could be due to an irreversible modification of the catalyst at temperature higher than  $300^\circ\text{C}$ , which however is in contradiction to the restored activity verified after each test, or can indicate a harder diffusion of water molecules from zeolite micro-pores when the concentration is quite suggesting the occurrence of a diffusive regime control in this region. In order to verify this hypothesis tests were performed with a removal time equal to 4 h.

As reported in Fig. 62, longer removal times allow to improve the water removal efficiency at temperature above  $300^\circ\text{C}$ , confirming that water diffusion through zeolite pores could control water release within this temperature range. This hypothesis was verified repeating out experiments at different duration times of phase 3 ( $\text{H}_2\text{O}$  removal). As it was shown in Fig. 63 the adsorption capacity can be completely restored at  $400^\circ\text{C}$  (within the experimental error) with a water removal time of 4 h.

By concluding, under the operative conditions here adopted not only water completely desorbs from the catalyst surface but also did not irreversibly modify the catalyst structure.

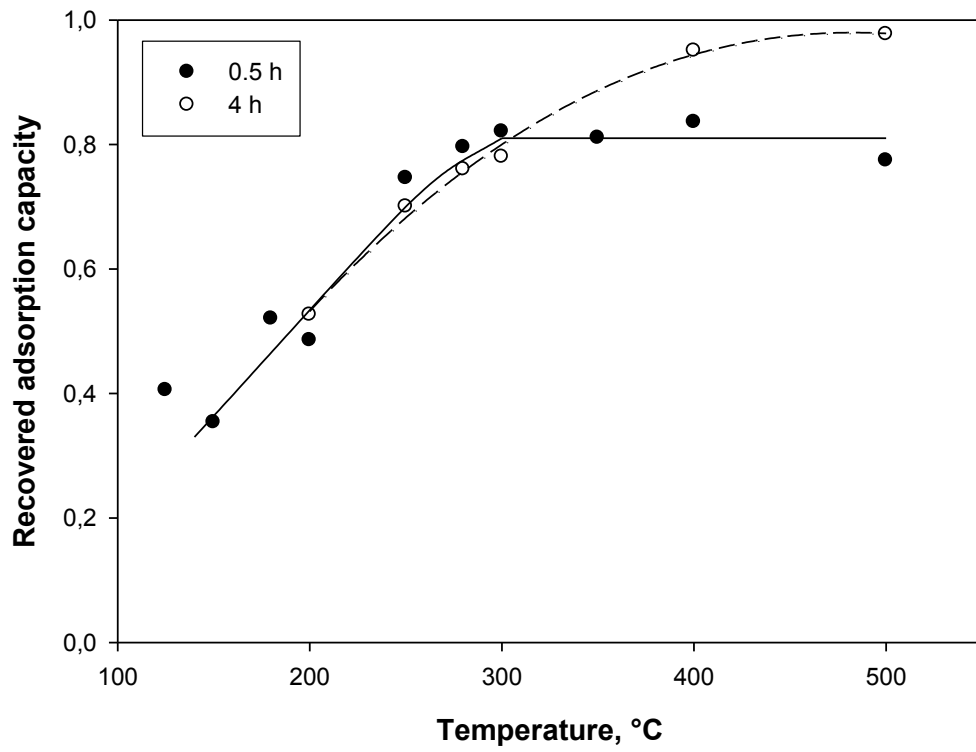


Fig. 61 - Trend of recovered adsorption capacity with the temperature

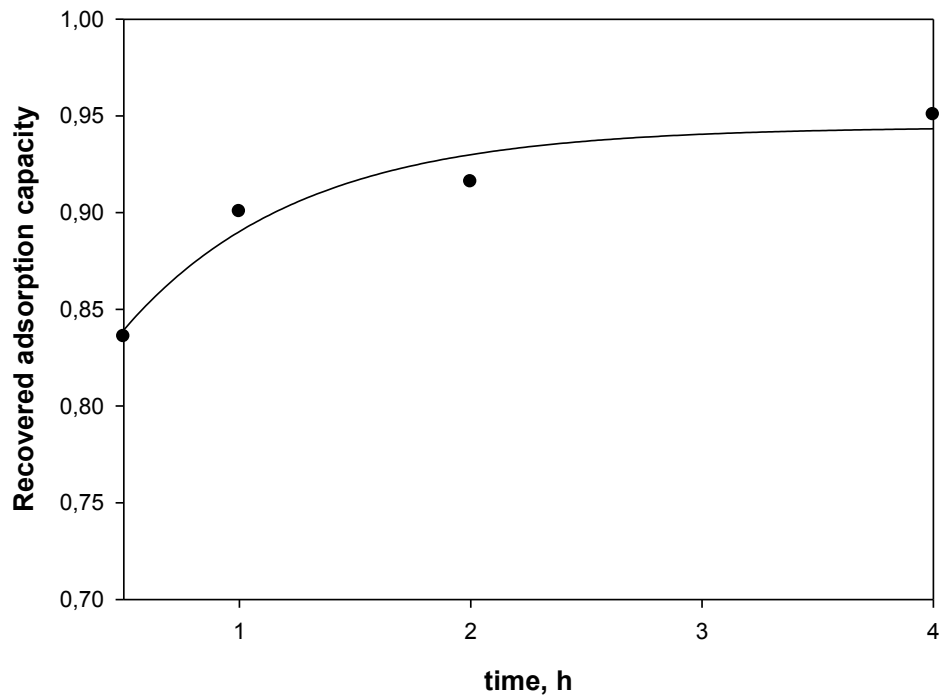


Fig. 62 - Trend of recovered adsorption capacity with the time at 400°C

## 5.2 IR investigation on water effect on NO adsorption

An in-situ FTIR study was performed to define the nature of the adsorbed species and the water effect on the formation of nitrates species. These species, their formation and development on copper site have been considered a key step (Sadykov et al. 1998, Li and Guan 2009, Solans-Monfort 2000) in all DeNO<sub>x</sub> processes (i.e. SCR, direct decomposition). The FTIR analyses were carried out using the apparatus system described in paragraph 3.2.2.1.

The effect of water adsorption on the formation of these NO<sub>x</sub> species on copper sites was rarely investigated. Hadjiivanov et al. (1996) found that once formed nitrates were only slightly affected by water introduction in the feed.

The adsorption test has been carried out in four steps:

- Catalyst pre-treatment: the sample was pre-oxidized in situ (10% O<sub>2</sub>/He flowing mixture (100 ml/min) at 550 °C for 2h) and then cooled down to 50 °C.
- NO adsorption: a stream of NO/He mixture (800 ppm) was fed to the cell at 50 °C for 90 min collecting spectra every 5-10 min.
- H<sub>2</sub>O adsorption: water vapor was continuously added to the feed for additional 70 min collecting several spectra.
- H<sub>2</sub>O removal: water vapor was removed and only He has been fed to the cell.

All spectra collected during NO or H<sub>2</sub>O adsorption (spectral resolution 4 cm<sup>-1</sup> and 50 scan) were rationed against the corresponding background spectra collected on the NO-free sample at the corresponding temperature.

The aim of the first two steps of this experiment was the identification of the different bands produced after adsorption of NO and their evolution with time on stream. The result of NO adsorption was reported below in Fig. 63.

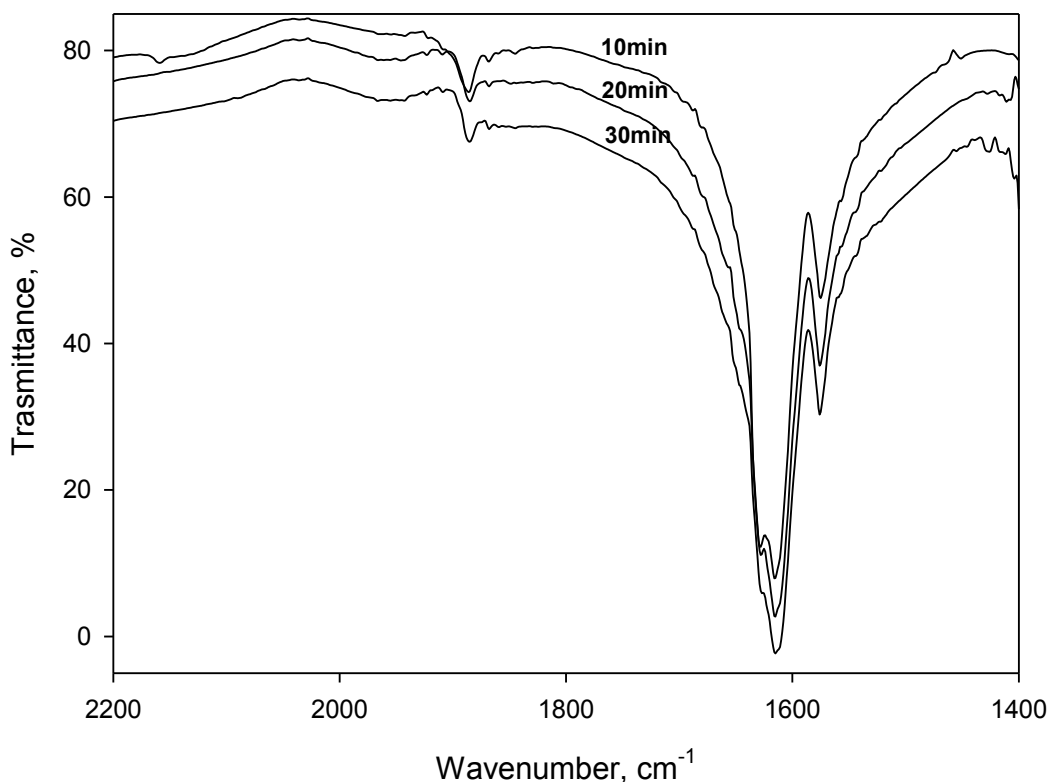


**Fig. 63** - FTIR spectra of NO adsorbed on LaCu-ZSM5 from 800ppm NO/He mixture at 50 °C and different exposure times

The main bands present in the region of NO adsorption were:

- a band at 1573  $\text{cm}^{-1}$ ;
- a band at 1615  $\text{cm}^{-1}$ ;
- a band at 1629  $\text{cm}^{-1}$ ;
- a small peak at 1813  $\text{cm}^{-1}$ ;
- a small signal at 1887  $\text{cm}^{-1}$ .

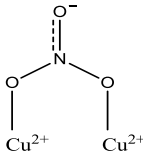
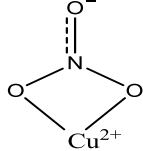
By comparing these experimental bands with the data reported in literature, it is possible assign for each band to the corresponding adsorbed species.

The peaks at 1813 and 1887  $\text{cm}^{-1}$  are both assigned to copper mono-nitrosyl species, the first specie, present only at low NO concentration, disappears after few minutes. The band at 1573  $\text{cm}^{-1}$  is attributed to the formation of chelating nitrates on  $\text{Cu}^{2+}$  whereas the double band at 1626  $\text{cm}^{-1}$  is assigned to bridged nitrates (Konduru and Chuang, 1999). The attribution of the band at 1615  $\text{cm}^{-1}$ , increasing with time on stream, is difficult. In the same paper Konduru and Chuang do not unambiguously assigned this band simply speaking of an overlapped band at lower frequency.

The assignments of the different bands are summarized in table 8.

**Tab. 8** – Frequencies and assignment of the nitrosyl bands

**Frequency (cm<sup>-1</sup>) after NO  
adsorption**

1887	$\text{Cu}^{2+} \text{O}^- (\text{NO})$	MONO-NITROSYL
1813	$\text{Cu}^+(\text{NO})$	MONO-NITROSYL
1626		BRIDGED NITRATE
1573		CHELATING NITRATE

The length-time of NO adsorption was 90 min, after this step water vapour was added to the feed for additional 70 min collecting several spectra. Then the water was removed. The results of the complete experiment are reported in the following graph.

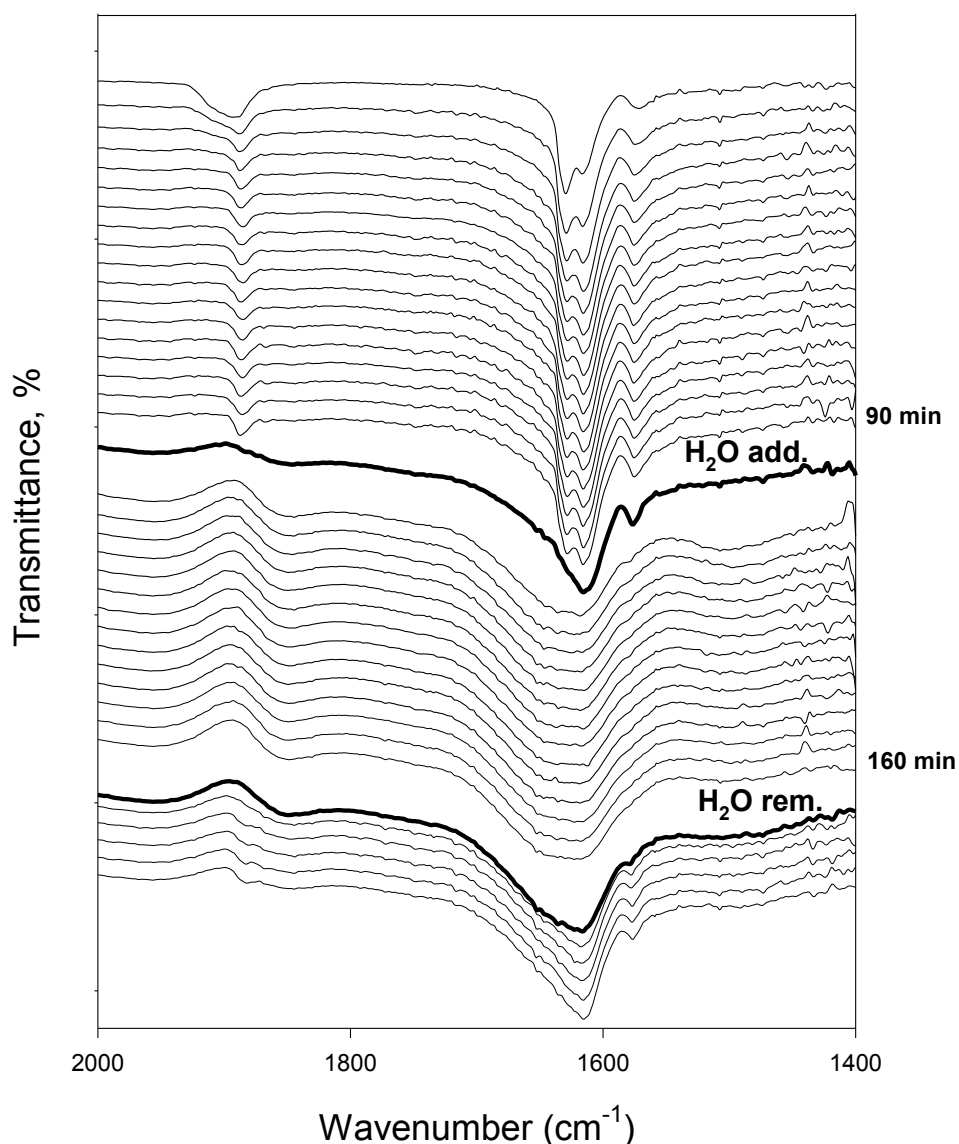


**Fig. 64** - FTIR spectra of NO adsorbed on LaCu-ZSM5 from 800ppm NO/He mixture. At time=90 min 2%vol. H<sub>2</sub>O was added to the mixture, at time=160 min H<sub>2</sub>O was removed from the mixture

Fig. 64 showed that the exposure of LaCu-ZSM5 to a NO/He dry mixture results in a almost immediate formation of mono-nitrosyl and nitrates (both bridged ( $1626\text{ cm}^{-1}$ ) and chelating ( $1573\text{ cm}^{-1}$ )) species. The introduction of water (90min) in the gas mixture causes the immediate and complete disappearance of mono-nytrosil ( $1887\text{ cm}^{-1}$ ) and chelating nitrates ( $1573\text{ cm}^{-1}$ ) showing that these species are displaced by water. At the same time water addition caused the formation a single asymmetric band centered at  $1620\text{ cm}^{-1}$ . This peak broadens upon water exposure. Water removal from the mixture, after overall 160 minutes restored the band at  $1573\text{ cm}^{-1}$  and roughly the shape of the band at  $1620\text{ cm}^{-1}$  which appeared as that observed just after the first minutes of water addition.

On the basis of these results it is possible to suppose that water irreversibly displaces  $\text{Cu}^{2+}\text{O}(\text{NO})$  mono-nitrosyl species whereas water removal restores copper sites adsorbing chelating nitrates, which then should be involves in an adsorption equilibrium with water ad-species as proposed by Sierraalta et al (2005).

In order to understand the nature of the asymmetric band peaked at  $1620\text{ cm}^{-1}$  an additional experiment was carried out. This experiment was performed at the same temperature of the previous adsorption feeding NO to the cell but only water vapour (spectra reported in Fig.65).

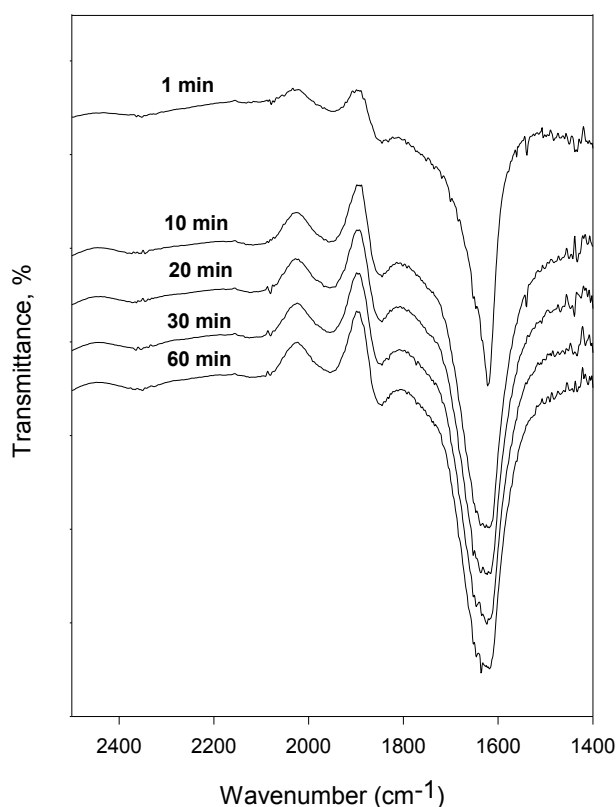


**Fig. 65** - FTIR spectra of  $\text{H}_2\text{O}$  adsorbed on LaCu-ZSM5 mixture 2%vol.  $\text{H}_2\text{O}$  at different exposure times

Fig. 65 showed that the exposure of LaCu-ZSM5 to a water vapour stream results in the appearance of a sharper band peaked at  $1620\text{ cm}^{-1}$ , this band was the typical signal associated to water adsorption in agreement with Hadjiivanov et al. (1996). This frequency is very close to that of nitrate species ( $1626\text{ cm}^{-1}$ ) and suggest a partial overlapping of nitrates and water bands when NO and  $\text{H}_2\text{O}$  are both present in the feed.

Nevertheless, a signal overlapping that attributed to nitrates at lower frequency increasing with time was observed also before water addition, as evidenced in Fig. 66b representing the first 30 min of the complete experiment reported in Fig. 64.

In order to confirm that this band is associable to water in Fig. 66a the hydroxyl region of the same spectra shown in the region 1700-1500  $\text{cm}^{-1}$  in Fig. 66b is reported. It must be pointed out that no spectral ratio was done in Fig. 66a.

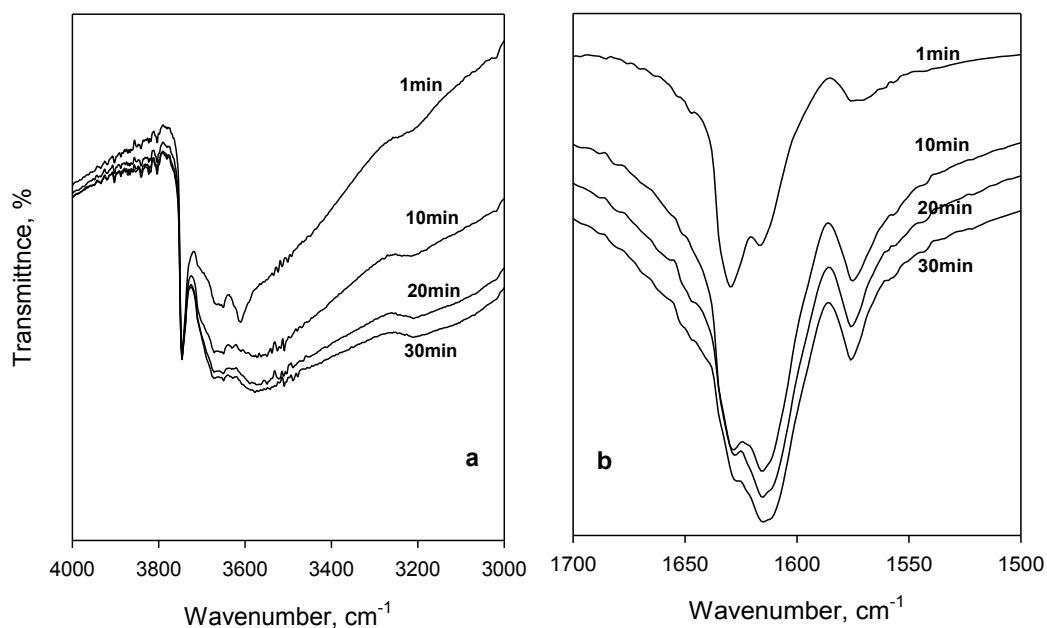


**Fig. 66** - FTIR spectra of LaCu-ZSM5 under 800 ppm NO/He mixture at different exposure times in 400-300  $\text{cm}^{-1}$  region (a) and 1700-1500  $\text{cm}^{-1}$  region (b). Only spectra shown in (b) were ratioed against the corresponding NO-free zeolite spectrum

In the spectrum of LaCu-ZSM5, previously treated at 550°C in  $\text{O}_2/\text{He}$  mixture (spectrum taken at 1 min), the typical OH bands assigned to terminal silanol and site defects (3745  $\text{cm}^{-1}$ ), non-framework aluminium (3665  $\text{cm}^{-1}$ ) and zeolite bridging hydroxyl (3610  $\text{cm}^{-1}$ ) are easily detectable. The broadening of the band at 3665  $\text{cm}^{-1}$  and the disappearance of that at 3610  $\text{cm}^{-1}$  under NO/He mixture with time on stream indicated a progressive hydration of the sample shown by the spectrum dominance of hydrogen bonding (Valyon et al. 1993, Hadjiivanov 1998).

Actually, the formation of  $\text{H}_2\text{O}$  on H-ZSM5 upon NO adsorption in the presence of oxygen by a reaction with the hydroxyls responsible for the band at 3610  $\text{cm}^{-1}$  was proposed by Hadjiivanov et al (1998). Although  $\text{O}_2$  is absent in the NO/He mixture the reaction pathway proposed by Hadjiivanov et al. (1998), the first step, being NO oxidation to  $\text{NO}_2$ , can occur anyhow since  $\text{NO}_2$  is present as impurity in the NO/He mixture and/or through NO oxidation onto the pre-oxidized catalyst surface.

Once verified that the overlapping band at 1615  $\text{cm}^{-1}$  is ascribed to the adsorbed water, another experiment was performed in order to determine the relative thermal stability of NO and  $\text{H}_2\text{O}$  ad-species.

After adsorbing NO 30min on pre-oxidized LaCu-ZSM5 sample (first spectrum, Fig. 67), water vapour was added to the gaseous mixture for 40 minutes (second and third spectra in Fig. 67). Then water was removed and, after 110min, also NO.

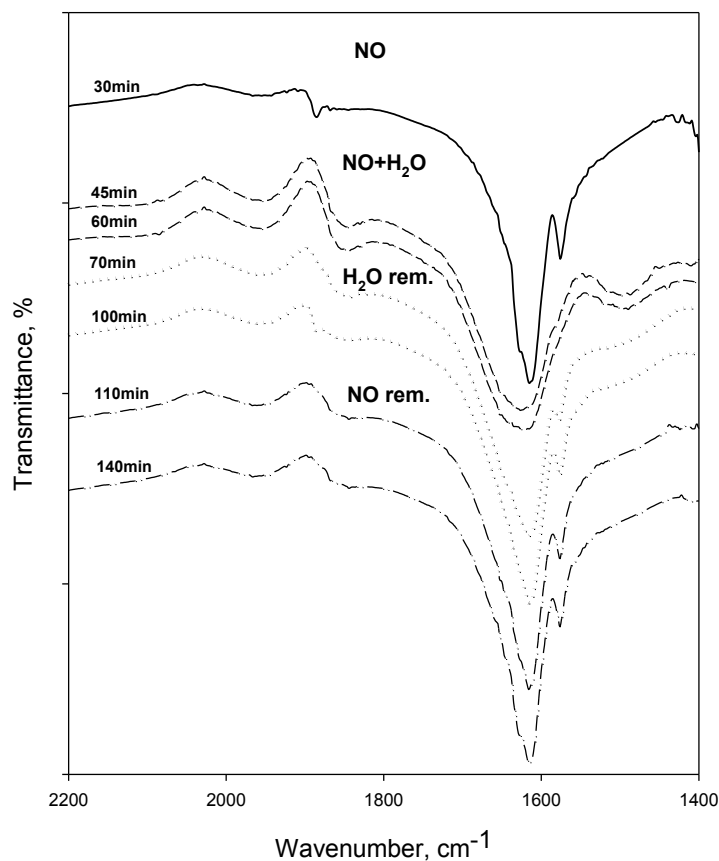


**Fig. 67** - FTIR spectra of LaCu-ZSM5 under 800 ppm NO/He mixture (NO), after water addition after 30min (NO+H<sub>2</sub>O), after water removal after 60 min (H<sub>2</sub>O rem.) and after NO removal (NO rem.) after 100 min

In Fig. 68 it was possible to observe that the mono-nytrosil band (1887 cm<sup>-1</sup>), during water adsorption and after water removal, was not present. On the contrary the band of bridged nitrates (1573 cm<sup>-1</sup>) disappeared upon water addition, but it appears again. This means that the presence of water in the feed causes chelating nitrate reversible disappearance and linear specie irreversible disappearance.

As already described, after 30 min water removal the band of chelating nitrates (1629 cm<sup>-1</sup>) was well detectable again. This can mean that the band of chelating nitrates was unchanged but hidden by the broad water deformation band or that water reversibly replaced chelating nitrates sites but its removal released these sites which could adsorb NO again supporting the thesis of Sierraalta et al. (2005) about the dynamic equilibrium between water and NO.

After the adsorption at 50 °C reported in Fig. 67, the IR cell was heated up to 430 °C and spectra were collected during the heating (Fig. 68). All spectra were ratiomed against the corresponding background spectra collected on the NO-free sample at the corresponding temperature.

A careful analysis of the spectra shows that the broad signal observed was the result of the partial overlap of the bands at 1629 and 1615  $\text{cm}^{-1}$ . In Fig. 68 it was possible to observe that the band at 1615  $\text{cm}^{-1}$  was completely absent at 430 °C, while the nitrates band (1629  $\text{cm}^{-1}$ ) was still present at the same temperature. The zeolite dehydration was confirmed by the analysis of OH spectral region reported in Fig. 68a. Nitrates should be responsible of the catalyst activity, even in the presence of water.

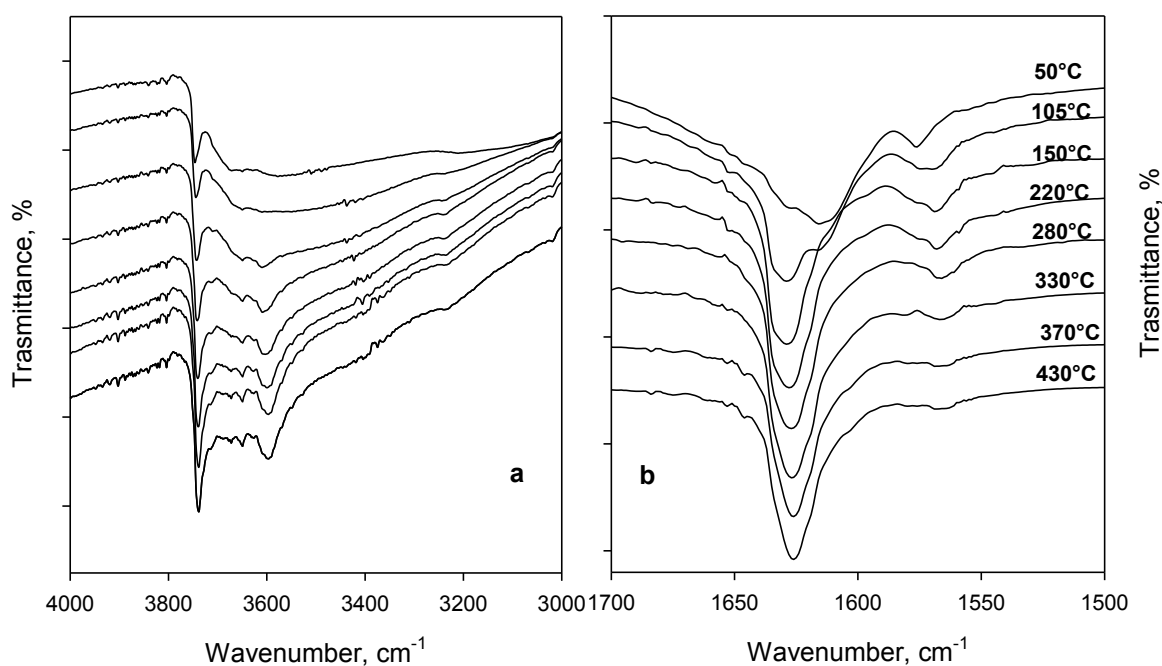


**Fig. 68** - FTIR spectra of LaCu-ZSM5 at different temperature under Ar flow after NO and H<sub>2</sub>O adsorption at 50 °C and subsequent removal in 3800-3500  $\text{cm}^{-1}$  region (a) and 1700-1500  $\text{cm}^{-1}$  region (b)

In order to better understand the result of the previous experiment, water vapor adsorption at 50 °C in the absence of NO was also investigated on the pre-oxidized LaCu-ZSM5 (Fig. 69). After water adsorption, the IR cell was heated up to 220 °C.

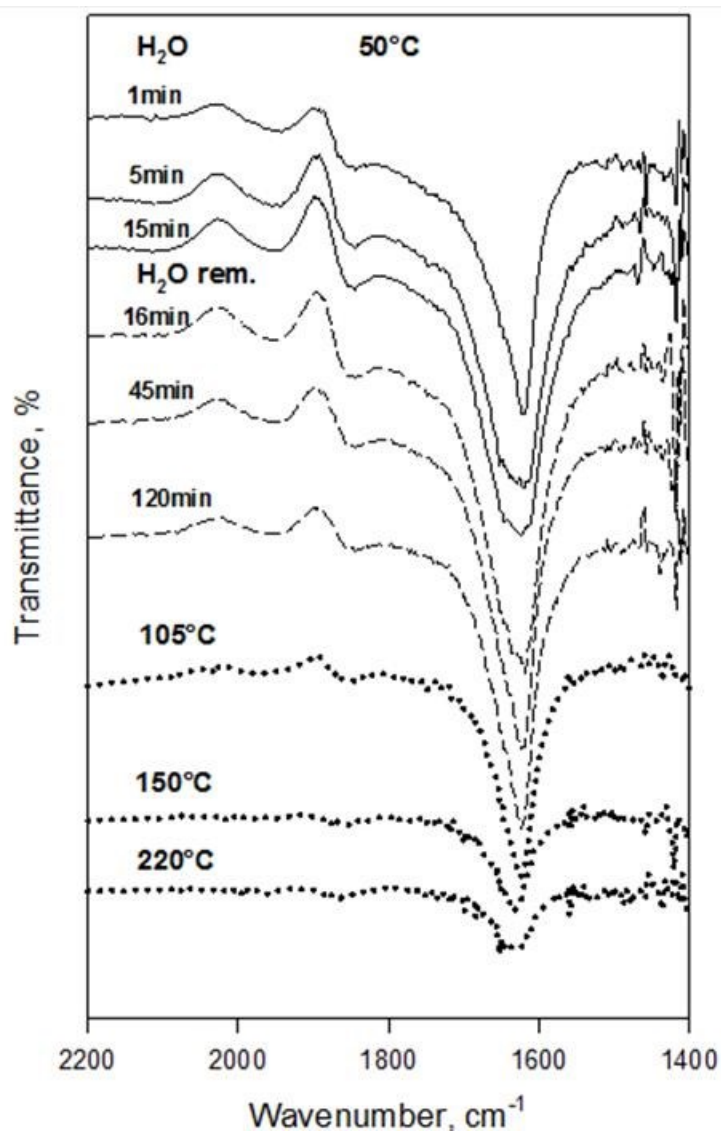


**Fig. 69** - FTIR spectra of LaCu-ZSM5 under 2% H<sub>2</sub>O/He mixture for 15min (H<sub>2</sub>O) at 50 °C, after water removal for 95 min (H<sub>2</sub>O rem.) at 50 °C and at increasing temperature

In Fig. 69 it was possible to observe only one band, that decreased when the temperature increased. In particular this band, associated with water adsorption, almost disappeared at 220 °C. The band detected at 220 °C after the adsorption of water was only noticeably smaller than that observed after the adsorption of both NO and H<sub>2</sub>O. This last experiment confirmed that water was removed at lower temperature than chelating nitrates and that the band almost present in Fig. 68b represented nitrate species.

## **Conclusions**

Water vapour significantly reduces NO adsorption on both Cu- and LaCu-ZSM5 at low temperature (50-150 °C). The catalyst deactivation in NO decomposition caused by water is probably related to a reduced NO adsorption, because water almost totally displaces NO pre-adsorbed on copper sites. Nevertheless, in the presence of oxygen the oxidation of NO to NO<sub>2</sub>, that partially occurs, promotes the formation of nitrate-like species. These species are the only NO<sub>x</sub> species which can successfully compete with water for copper adsorption sites.

The total recovery of the original NO adsorption capacity of the dry zeolite after water thermal removal demonstrates the reversibility of water deactivation. Lanthanum co-exchange improves the copper adsorption capacity both in the absence and in the presence of water and O<sub>2</sub>. The beneficial effect of La on the catalytic performance of Cu-ZSM5 in NO decomposition is ascribed to the improved NO adsorption due to an improved nitrates formation (probably due to higher NO oxidation rate to NO<sub>2</sub>). It is proven that nitrates are more thermally stable being still present when water was completely removed.

## **Chapter 6**

### **NO decomposition<sup>4</sup>**

---

<sup>4</sup> Parts of this chapter appear in G. Landi, L. Lisi, R. Pirone, M. Tortorelli G. Russo, *Applied Catalysis A: General* 464–465 (2013) 61–67

## 6.1 NO<sub>x</sub> adsorption/decomposition

The adsorption/decomposition tests were carried out on structured catalyst, prepared according to Lisi et al. (2009), with LaCu-ZSM5 as active phase and in a specially designed stainless steel reactor. The plant and the reactor used for the NO adsorption experiments are described in paragraph 3.2.1 and 3.2.1.2 respectively.

As reported before, the ultimate aim is to carry out a cyclic process adsorbing NO on the zeolite at quite low temperature, heating up the catalyst to decompose the adsorbed NO into N<sub>2</sub> and O<sub>2</sub> and cooling down back to the adsorption temperature to repeat a new cycle. Nevertheless, in order to verify the system operation and the mass balance a single run was preliminary performed followed by a TPD just after the decomposition step.

Once verified the system feasibility a cyclic operation was carried out to test repeatability and catalyst stability.

### 6.1.1. Single adsorption/decomposition tests

The experimental tests were carried out on the catalyst (2 monoliths, 1.6g zeolite) preliminary oxidized 2h at 550°C according to a cyclic procedure consisting in four stages:

- adsorption: a flowing mixture containing NO (800 ppm) and, in some cases, O<sub>2</sub> (2.5vol.%) was fed to the pre-oxidized catalyst at 50°C; catalyst saturation was considered completed when the NO concentration in the gas phase exiting the reactor raised to a value of 10 ppm, after a transient period in which no NO<sub>x</sub> was detected by the analyzer.
- decomposition: the reactor was heated up to 480 °C at constant heating rate (10 °C/min) under static conditions and kept at this temperature for a fixed period of time (isothermal decomposition time)
- purging: the reactor was rapidly cooled down back to 50°C and evacuated re-opening valves under pure He flow (isothermal desorption).
- TPD: the catalyst was heated at 10 °C/min up to 500 °C analyzing the gaseous species. This test was performed to check the mass balance.

Preliminary experiments using a thermocouple placed inside the reactor and a pressure transducer placed at the outlet of the reactor were made in order to evaluate the pressure increase during each step of the test (adsorption/decomposition and subsequent TPD); this trend was reported in the following figure.

As expected, the pressure profile strictly follows the temperature profile suggesting that the pressure increase is basically related to the temperature increase, the increase of number of moles due to NO desorption being negligible.

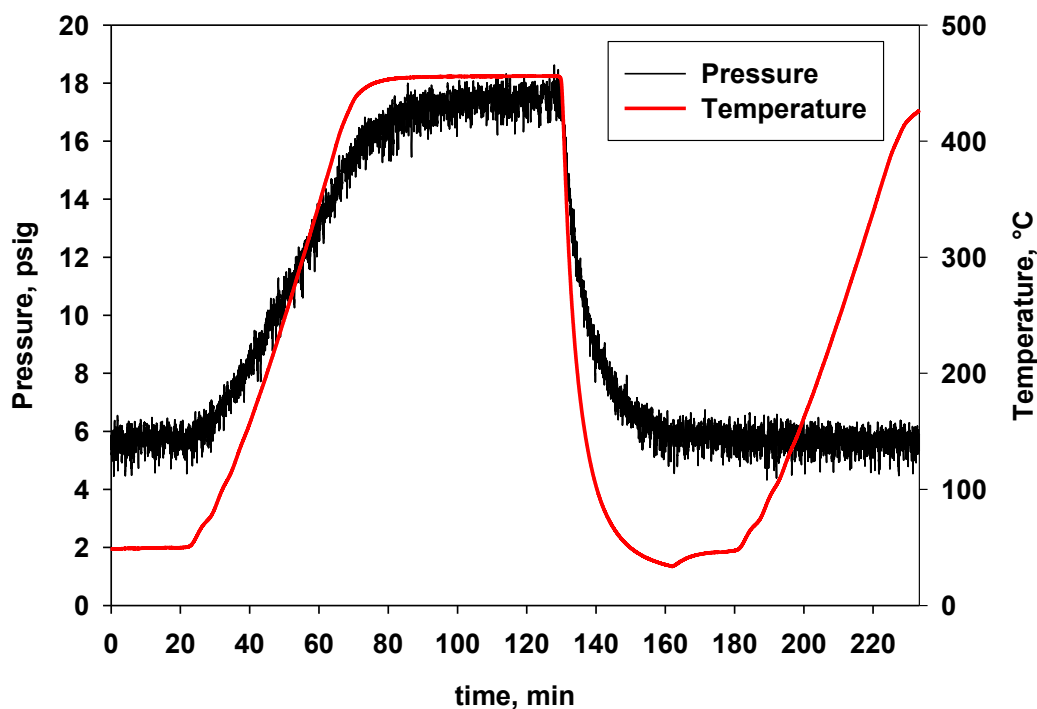
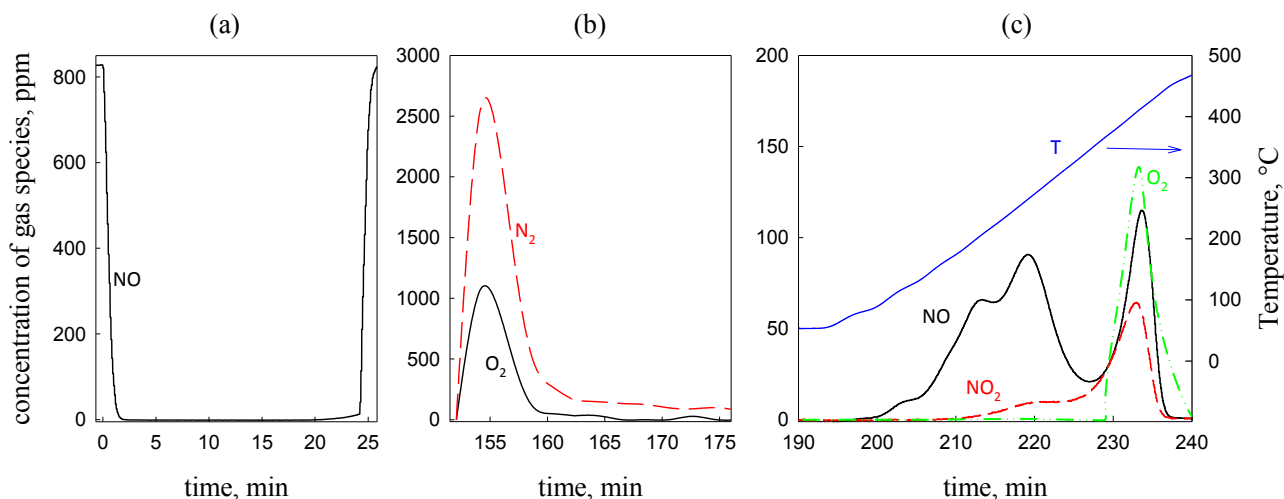


Fig. 70 - Concentration profiles of pressure and temperature as function of time

In Fig. 70 it was possible to observe that during the first 20 minutes pressure and temperature profiles were constants because the reactor was open and a flow-gas was fed to the reactor; after 20 minutes the reactor was isolated and heated and the pressure increased. During the decomposition phase (70-130 minutes) the temperature and pressure profiles were constants; after that the reactor was cooled and, as a consequence, the pressure profile decreased. At 180 minutes the temperature profile increased because the reactor was heated, but the pressure was constant as the reactor was opened and a helium flow passed through the reactor.

The results of a complete experiment were represented in Fig. 71, where the outlet gas phase composition was reported as a function of time during the three phases of the experiment: adsorption, purging and TPD.



**Fig. 71** - Concentration profiles as functions of elapsing time of: (a) NO during the adsorption phase; (b) N<sub>2</sub> (—) and O<sub>2</sub> (—) during the purging phase; (c) NO (—), NO<sub>2</sub> (—) and O<sub>2</sub> (---) during the TPD analysis

The adsorption step (Fig. 71a) confirmed the capacity of the zeolite of adsorbing a significant amount of NO. At 50 °C and 700 h<sup>-1</sup> space time, the time needed to saturate the zeolitic monoliths was about 24 min, for an overall uptake of NO evaluated as 64.5 μmol/g. No N<sub>2</sub>O emission took place in good agreement with the oxidized state of copper (Lisi et al., 2012). After heating the reactor under static atmosphere (constant volume and closed system), the proper decomposition phase was carried out for 1h at 480°C (at this temperature the pressure inside the reactor reaches about 2.5 bar, as expected mainly by the increase of temperature, the increase of number of gas phase molecules being quite negligible in the conditions here explored) and was followed by the rapid reactor cooling back to 50 °C. The decomposition temperature was chosen according to the results reported by Lisi et al. (2009) showing that the maximum NO conversion was obtained at 480°C for Cu-ZSM5 structured catalyst as opposed to powder sample providing the best performance at 450°C. After valves opening, the reactor was flushed with helium and the analysis of the exiting gases was carried out. Only N<sub>2</sub> and O<sub>2</sub> were detected in significant amounts (Fig. 71b) and zero NO emission were observed. This would mean that i) NO was completely converted into N<sub>2</sub> and O<sub>2</sub> and/or ii) unconverted NO was held by the zeolite.

Fig. 71c showed that unconverted NO was adsorbed on the zeolite and was desorbed in the TPD according to three broad peaks in the low-medium temperature region (centred at 115, 205 and 270 °C respectively) and one sharp peak at higher temperature (centred at 410 °C). The desorption of NO<sub>2</sub> occurred almost in phase with the two highest temperature (270 and 410 °C) peaks of NO at lower extent, while O<sub>2</sub> exhibits a single peak simultaneously to NO in the high temperature region.

This TPD profile was in good agreement with previous recent studies of our group: low-medium temperature desorption peaks were related to NO adsorbed on isolated  $\text{Cu}^+$  and  $\text{Cu}^{+2}$  species, while high temperature desorption peaks were the results of the decomposition of nitrate-like species ( $\text{NO}_3^-$ ) (Lisi et al., 2012). Nevertheless, it must be noticed the total absence of weakly adsorbed NO, which was detected in significant amounts at 25 °C before heating the reactor in TPD experiments on pre-reduced powder catalyst.

It was shown (Lisi et al., 2012) that the adsorption of this kind of NO was partially reduced for a pre-oxidized powder catalyst and almost totally depressed in the presence of oxygen. In addition, it was demonstrated that by increasing the adsorption temperature the amount of weakly adsorbed NO decreases. Thus, the disappearance of physisorbed NO can be related to i) adsorbing conditions favouring more stable species (high adsorption temperature, presence of the oxygen in the gas phase (produced by the decomposition of NO)) and ii) relatively small amounts of unreacted NO, not enough to saturate all the copper sites. Whatever the reason, this implies that no emission of unreacted NO takes place after the decomposition phase at the adsorption temperature. Furthermore, the absence of  $\text{N}_2\text{O}$  emission also in this step suggested that copper should be sufficiently oxidized by  $\text{O}_2$  produced by the decomposition reaction.

Single cycle experiments were carried out at 480 °C for different decomposition time lengths in order to determine the decomposition time-length necessary to reach a complete NO conversion. In Fig. 72 the conversions of NO at the 480 °C as function of decomposition time length was shown. It is possible to observe that the conversion is not zero at the decomposition time equal to zero because the reaction starts already during the heating ramp to reach the set temperature.

The NO conversion to  $\text{N}_2$  was calculated with the following expression:

$$x = \frac{2 \cdot n_{\text{N}_2\text{dec}}}{n_{\text{NOads}}} \cdot 100$$

In this expression  $n_{\text{N}_2\text{dec}}$  represented the  $\text{N}_2$  micromoles produced during the decomposition phase, while  $n_{\text{NOads}}$  were the micromoles of NO adsorbed during the adsorption phase.

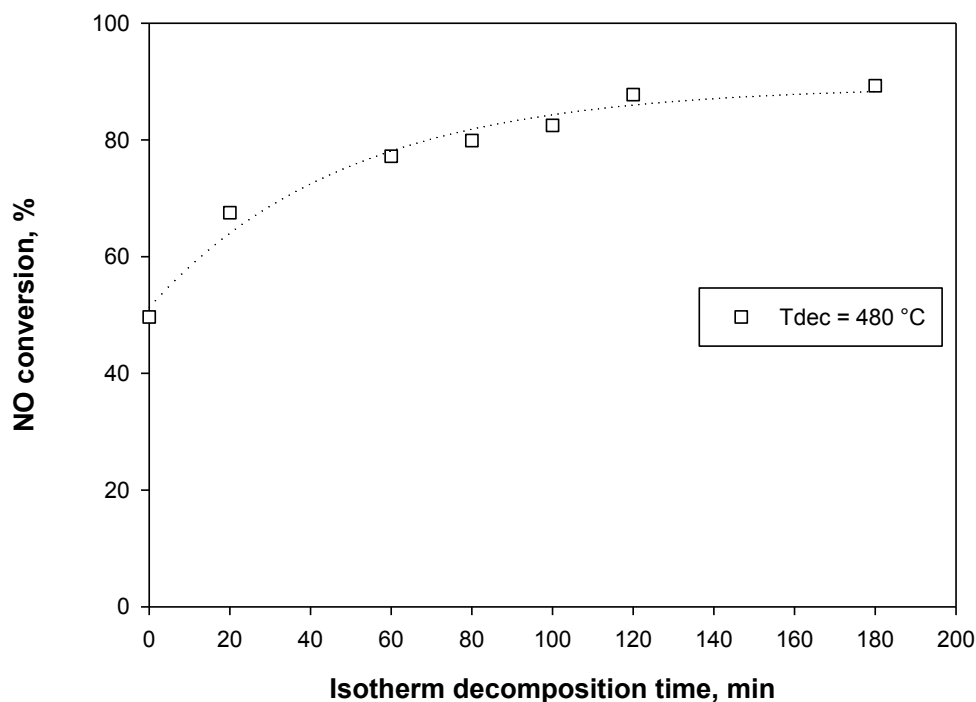


Fig. 72 - Concentration profiles of NO as function of isothermal decomposition time at 480 °C

A decomposition time of about 120 min is necessary to approach the total conversion. Nevertheless, for practical reasons in the following experiments the time length was limited to 1h.

### 6.1.2. Multi-cycle tests

After the single adsorption/decomposition tests, several tests were performed following the procedure reported below.

The catalyst (2 monoliths, 1.6g zeolite) was preliminary oxidized (2h at 550°C) only before the first cycle. After the oxidation, the procedure was the same already described in the previous paragraph except for the TPD. After the purging phase the catalyst was ready for another NO adsorption phase and the cyclic procedure was repeated again many times.

Therefore, it must be pointed out that in the multi cycle tests neither TPD nor pre-oxidation were carried out between a cycle and the following one. A TPD was carried out only after the last cycle of a complete sequence.

The cyclic adsorption/decomposition tests were carried out with 1h decomposition time and a decomposition temperature of 480 °C. The adsorption temperature was always 50 °C feeding about 800 ppm of NO in He ( $Q_{tot} = 5$  l/h).

The catalyst was oxidized at 550 °C for 2h before the first cycle only. In Fig. 73, the NO concentration profile during the adsorption phase was shown for 9 consecutive cycles.

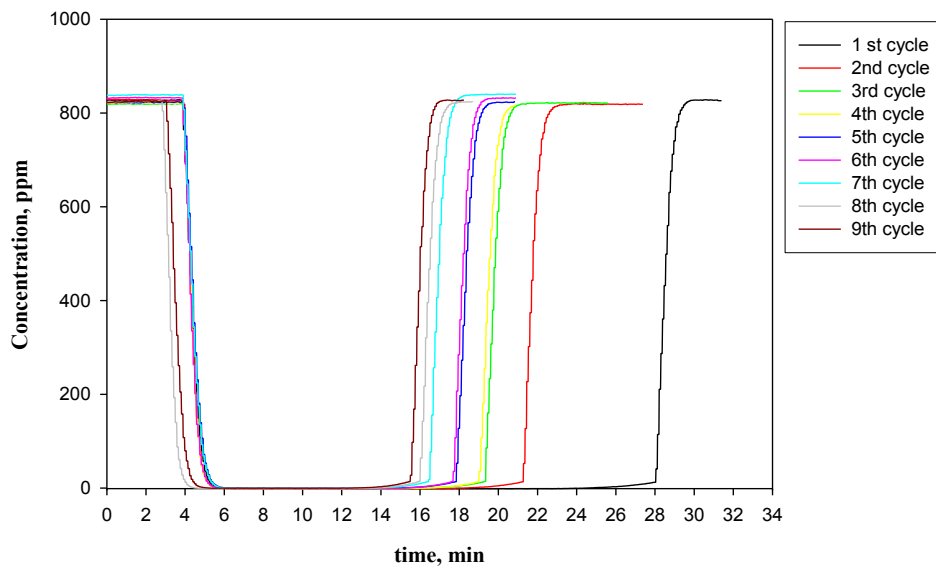


**Fig. 73** - NO concentration profiles during the adsorption phase for each cycle

In Fig. 74 the amount of NO adsorbed during the adsorption phase for each cycle was reported as evaluated from the integration of curves reported in Fig. 73.

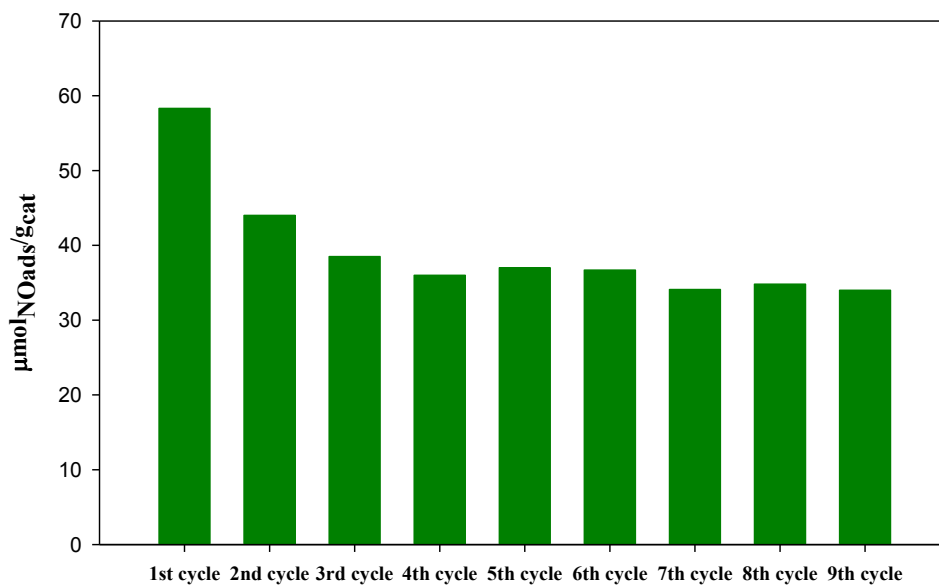


**Fig. 74** - Amount of NO adsorbed for each cycle

In Fig. 74 it is possible to observe that the time length and the NO adsorbed during the adsorption phase are maxima in the first cycle and then progressively decreased with cycles approaching a constant value after about 3 cycles suggesting that the catalyst reached a steady-state condition related to a similar starting situation at the end of each cycle.

The amount of N<sub>2</sub> and O<sub>2</sub> produced during the NO decomposition in each cycle was reported in Table 9. The N<sub>2</sub> production was quite constant for each cycle suggesting that the zeolite

decomposed always the same amount of NO preserving its activity. Except for the first cycle, also O<sub>2</sub> production showed rather constant value.

**Tab. 9** – NO adsorbed, N<sub>2</sub> and O<sub>2</sub> produced for each cycle

Cycle	NO <sub>ads</sub> ( $\mu\text{mol/g}$ )	N <sub>2</sub> <sub>prod</sub> ( $\mu\text{mol/g}$ )	O <sub>2</sub> <sub>prod</sub> ( $\mu\text{mol/g}$ )
1	58.3	20.4	7.2
2	44.0	17.6	15.4
3	38.5	17.9	16.8
4	36.0	17.8	17.9
5	37.0	18.4	18.0
6	36.7	18.4	18.1
7	34.1	17.6	17.4
8	34.8	17.1	16.7
9	34.0	17.5	16.7

In table 9 the NO<sub>x</sub> desorbed during purging phase were not shown because their amount was negligible in all cycles compared to the desired products (NO<sub>des</sub>  $\approx$  0.1  $\mu\text{mol/g}_{\text{cat}}$  , NO<sub>2des</sub>  $\approx$  0.4  $\mu\text{mol/g}_{\text{cat}}$  and N<sub>2</sub>O<sub>des</sub> = 0  $\mu\text{mol/g}_{\text{cat}}$ ).

NO conversion to N<sub>2</sub> for each cycle was reported in Fig. 75. The NO conversion to N<sub>2</sub> was defined as the ratio between the N<sub>2</sub> outlet micromoles (multiplied by 2), during the purging phase, and the NO adsorbed during the adsorption phase of the corresponding cycle. In other words the conversion was evaluated on the basis of NO adsorbed per each cycle, which, excluding the first one, could not correspond to the total amount of NO adsorbed on the zeolite due to the re-adsorption of unreacted NO cooling down again the sample to 50°C limiting the subsequent adsorption.

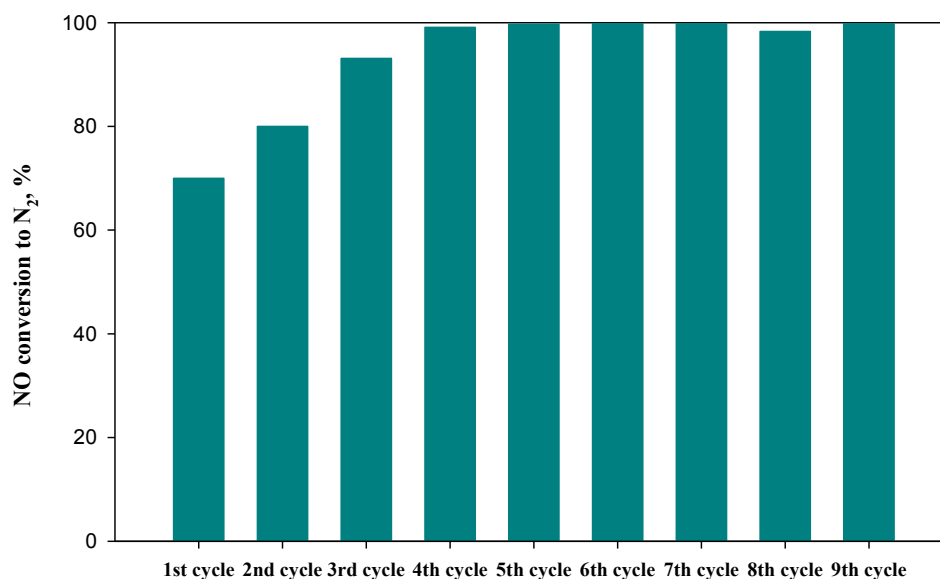


**Fig. 75** - N<sub>2</sub> conversion for each cycle

The NO conversion to N<sub>2</sub> increased up to a value of about 100% and the N<sub>2</sub>/O<sub>2</sub> ratio approached a value closer to the expected stoichiometric one showing that all NO adsorbed after the third cycle was totally converted into N<sub>2</sub> and O<sub>2</sub>. In other words, after the third cycle a NO amount equal to that adsorbed during the adsorption step of the corresponding cycle is converted to N<sub>2</sub> and O<sub>2</sub>.

Actually, the unreacted NO<sub>x</sub> re-adsorbed on the catalyst limit the amount of NO adsorbed after the first cycle and a steady-state condition was reached only after few cycles. The insufficient decomposition time (1 h) caused a gradual accumulation of adsorbed NO<sub>x</sub> on the zeolite during the first 3 cycles.

In the following cycles the incomplete NO decomposition causes a partial regeneration of the catalyst releasing a fraction of sites which were ready for a new adsorption of an amount of NO equal to that previously converted; for this reason the conversion is unitary after the third cycle.

Nevertheless, although the amount of adsorbed NO<sub>x</sub> involved a not complete regeneration of the zeolite after each cycle the very important result is that zero NO<sub>x</sub> emissions during all the tests were detected.

After the 9th cycle a TPD analysis was made (shown in Fig. 76). From the result of this analysis it was possible to calculate the residual NO<sub>x</sub> still adsorbed on the catalyst and calculate the mass balance. The TPD profile carried out after a large number of cycles was qualitatively very similar to the TPD carried out after only one cycle (Fig. 71c) confirming that the conditions for the adsorption of unreacted NO were always the same after every cycle.

From the quantitative point of view, the amount of NO<sub>x</sub> desorbed in the TPD test carried out after the ninth cycle was 38 μmol g<sup>-1</sup>, a value higher than that desorbed in the TPD carried out after one single run, suggesting that prior reaching a steady-state (after the third cycle) the system carried on accumulating NO<sub>x</sub> species on the surface. The same phenomenon also occurred for O<sub>2</sub> which contributes to nitrate formation during the first cycles leading to a N<sub>2</sub>/O<sub>2</sub> ratio much higher than 1 after the first cycle but that approaches the stoichiometric one in the following cycles. On the other hand, formation of nitrates, in particular bridged nitrates, was also observed just from the first beginning of exposure of Cu-ZSM5 to NO by FTIR analysis (Lisi et al, 2012).

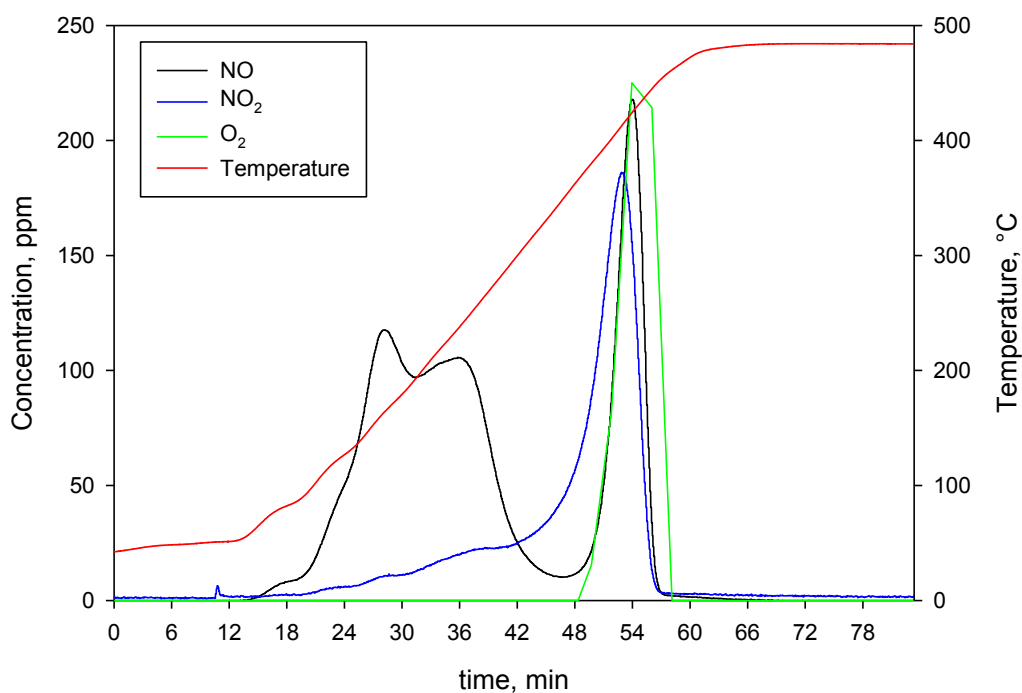


**Fig. 76** - TPD after the 9th cycle

Finally, it was possible to check the total nitrogen mass balance for all the cycles as reported below:

$$NO_{xads} = NO_{xTPD} + 2N_2$$

In this expression NO<sub>xads</sub> represented the sum of the NO adsorbed in the nine cycles, NO<sub>xTPD</sub> was the amount of NO desorbed during the TPD after the last cycle and N<sub>2</sub> indicated the sum of the N<sub>2</sub> in the nine cycles. The mass balance was closed with an error of 8.46 %.

### 6.1.3. Multi cycles tests in the presence of oxygen

Another important aspect investigated was the influence of the presence of oxygen in the feed stream.

After these single decomposition tests 4 multi cycles tests in the presence of O<sub>2</sub> in the feed were performed.

The multi cycles tests in the presence of O<sub>2</sub> (2.5%) were carried according to the same procedure reported for the tests in the absence of oxygen. In Fig. 77, the NO concentration profiles during the adsorption phase for the four cycles were shown.

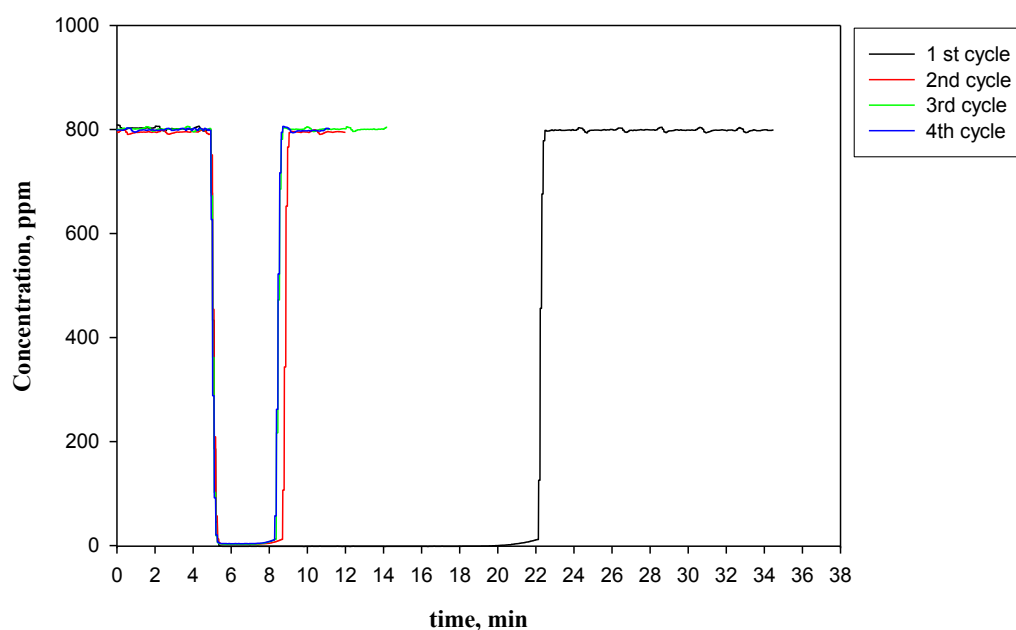
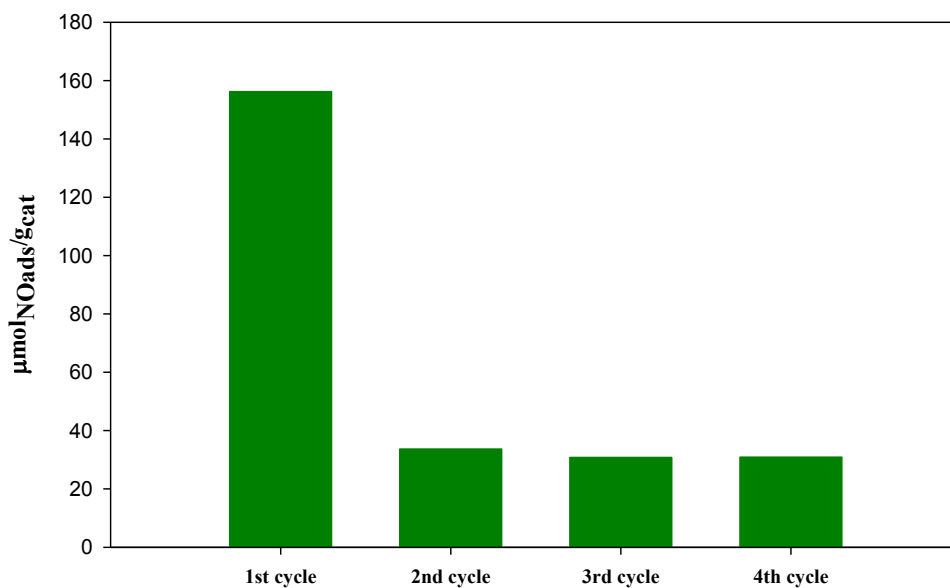


Fig. 77 - NO concentration profiles during the adsorption phase for each cycle

From Fig. 77 it was possible to calculate, integrating the area described by each curve, the amount of NO adsorbed for each cycle. These values, divided by the catalyst amount, were reported in Fig. 78.



**Fig. 78** - Amount of NO adsorbed per each cycles in the presence of 2.5 % O<sub>2</sub>

A comparison between the micromoles of NO adsorbed per catalyst weight obtained in the presence and in the absence of oxygen was shown in Fig. 79.

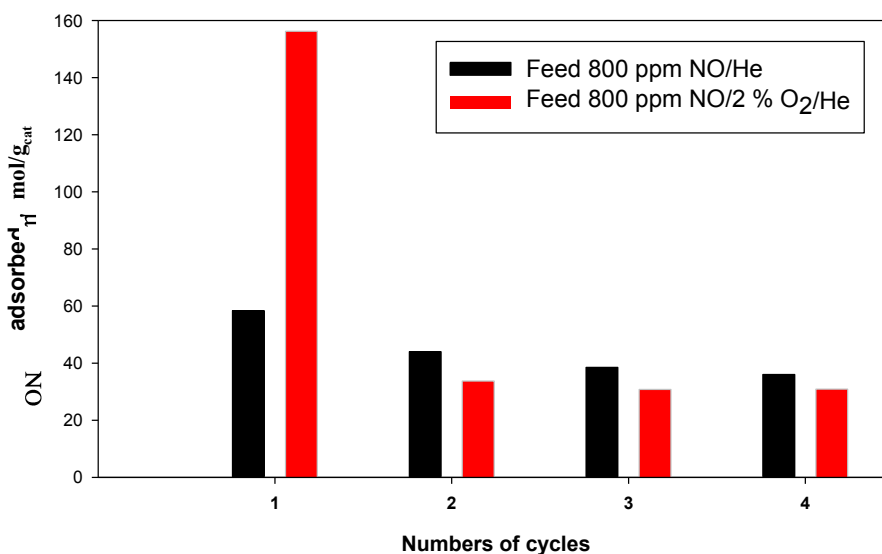


**Fig. 79** - Micromoles of NO adsorbed per gram of catalyst for the two performed set of run

It was possible to observe (in Fig. 79) that in the presence of oxygen, the amount of NO adsorbed in the first cycle was roughly doubled, in agreement with previous findings on Cu-ZSM5 powders (Lisi et al., 2012). Nevertheless, starting from the second cycle, the amount of NO adsorbed was stabilized around values very similar to those obtained in the absence of O<sub>2</sub>.

In table 10 the amount of NO adsorbed and that of N<sub>2</sub> produced in the presence of oxygen were reported. O<sub>2</sub> concentration was not reported due to the high value of oxygen in the feed which did not allow a good determination of the amount produced by NO decomposition.

**Tab. 10** – Amount of NO adsorbed and N<sub>2</sub> produced for each cycle

Cycle	NO <sub>ads</sub> ( $\mu\text{mol/g}$ )	N <sub>2</sub> <sub>prod</sub> ( $\mu\text{mol/g}$ )
1	156.2	22.4
2	33.7	14
3	30.8	15.9
4	30.9	15.8

Using the values of Table 10 it was possible to determine the conversion of N<sub>2</sub> for each cycle (Fig. 80).

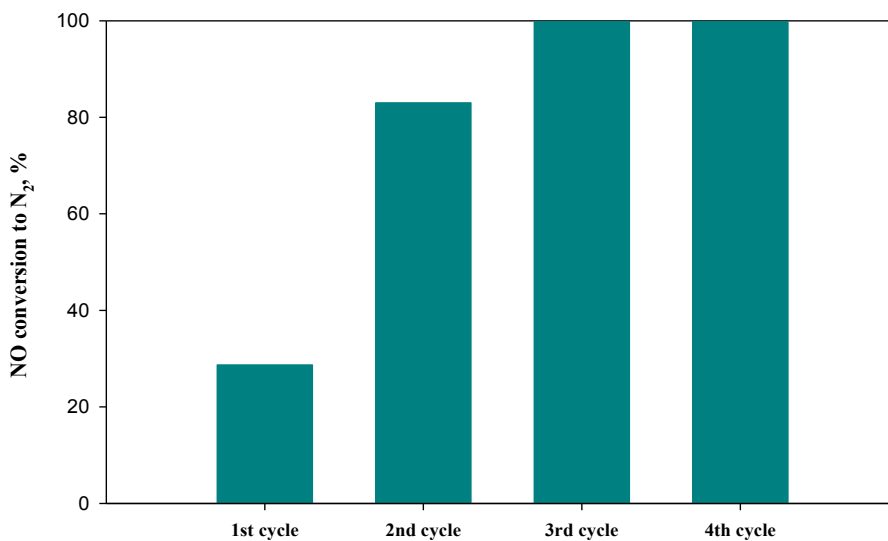


**Fig. 80** - N<sub>2</sub> conversion for each cycle

The low conversion of the first cycle, observed in Fig. 80, suggested that the accumulation of adsorbed NO on the zeolite was even larger than in the absence of O<sub>2</sub> in the feed. In the same figure it was possible to observe that after the second cycle the total NO conversion was reached.

By comparing the results reported in tables 9 and 10 it was possible to observe that after the first cycle the amount of NO adsorbed was almost the same value than that observed in the absence of O<sub>2</sub> and, at the same time, the total NO conversion was approached.

It was important to observe that the amount of stored  $\text{NO}_x$ , equal to the  $\text{NO}_x$  adsorbed in the first cycle, was higher in presence of  $\text{O}_2$  in the feed than during  $\text{O}_2$ -free adsorption tests. This implied that during the decomposition tests a larger  $\text{NO}_x$  amount was released in the same volume and, thus, a higher  $\text{NO}_x$  partial pressure was present inside the reactor. So, the increased  $\text{NO}_x$  and  $\text{O}_2$  partial pressures produce two opposite effects on the reaction rate (apparent reaction orders are 2 and -0.5 with respect to  $\text{NO}$  and  $\text{O}_2$  (Pirone et al., 2001)), apparently counterbalancing each other.

A comparison between the  $\text{NO}$  conversion to  $\text{N}_2$  obtained in the presence and in the absence of oxygen was shown in Fig. 81. The complete conversion was obtained for both cases within three cycles.

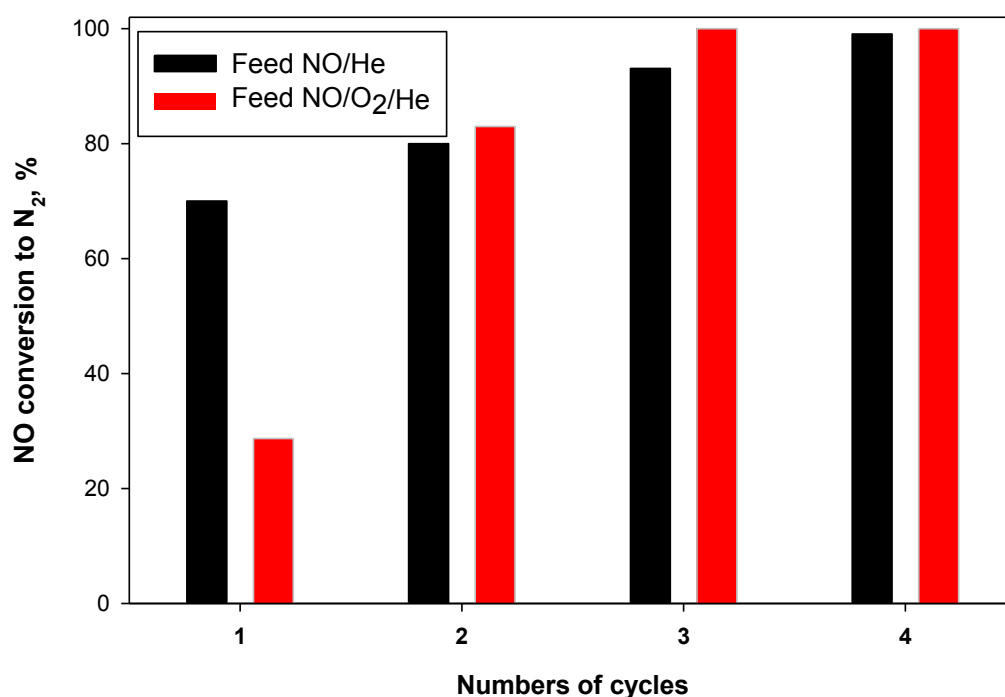
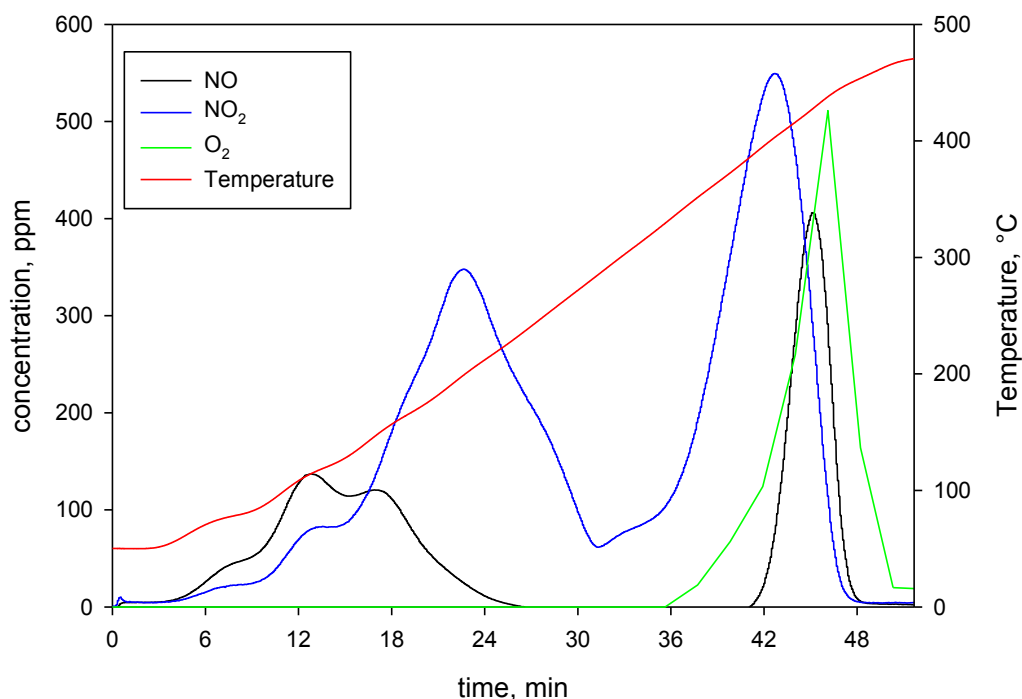


Fig. 81 -  $\text{NO}$  conversion to  $\text{N}_2$  for each cycle

After the fourth cycle a TPD analysis was performed (in Fig. 82).



**Fig. 82** - TPD after the 4th cycle

In Fig. 82 it was possible to observe that a large amount of  $\text{NO}_2$  was desorbed from the catalyst surface during the TPD phase. This phenomenon indicates that part of nitric oxide was oxidized to nitrogen dioxide by the oxygen present in the feed during the adsorption phase. The high temperature bands of  $\text{NO}$  and  $\text{NO}_2$  were related to nitrates decomposition.

Starting from the TPD analysis it was possible to calculate the  $\text{NO}$  and  $\text{NO}_2$  amount corresponding to the two peaks at high temperature.

The results were  $17 \mu\text{mol}$  and  $55 \mu\text{mol}$  respectively. In correspondence of these two peaks, there was a peak corresponding to  $34 \mu\text{mol}$  of  $\text{O}_2$  (reported in Fig. 82).

The total nitrogen mass balance for all the cycles was:

$$NO_{xads} = NO_{xTPD} + 2N_2$$

and was closed with an error of 5.8 %.

## 6.2 Preliminary FTIR test of NO adsorption/decomposition

A FTIR test was carried out under conditions very close to those taking place in the steel reactor and, although the contact time was not directly comparable, the spectroscopic experiments were qualitatively similar of the experiments described above. The aim of this test was to study the nature of the adsorbed species and their evolution at high temperatures.

A LaCu-ZSM5 self-supported disk ( $\phi=13$  mm) was placed into a high-temperature and high pressure cell equipped described in 3.2.2.2.

The experimental IR test was carried out on the catalyst preliminary oxidized 2h at 550°C according to a cyclic procedure consisting in four steps:

- adsorption: a flowing mixture containing NO (800 ppm) was fed to the pre-oxidized catalyst at 50°C; catalyst saturation was considered completed when there was no change between the spectrum recorded and the previous one. Then the cell was closed.
- decomposition: the cell was heated up to the desired temperature at constant heating rate (7 °C/min) under static conditions and kept at this temperature for 20 minutes.
- cooling: the cell was cooled down back to 50°C (in static condition) and evacuated re-opening valves under pure He flow (isothermal desorption).

All spectra were ratiored against the corresponding background spectra collected on the NO-free sample at the corresponding temperature.

At 50 °C the sample was contacted with 800ppm NO/He/Ar mixture for 95min collecting spectra every 10 min (see Fig. 85).

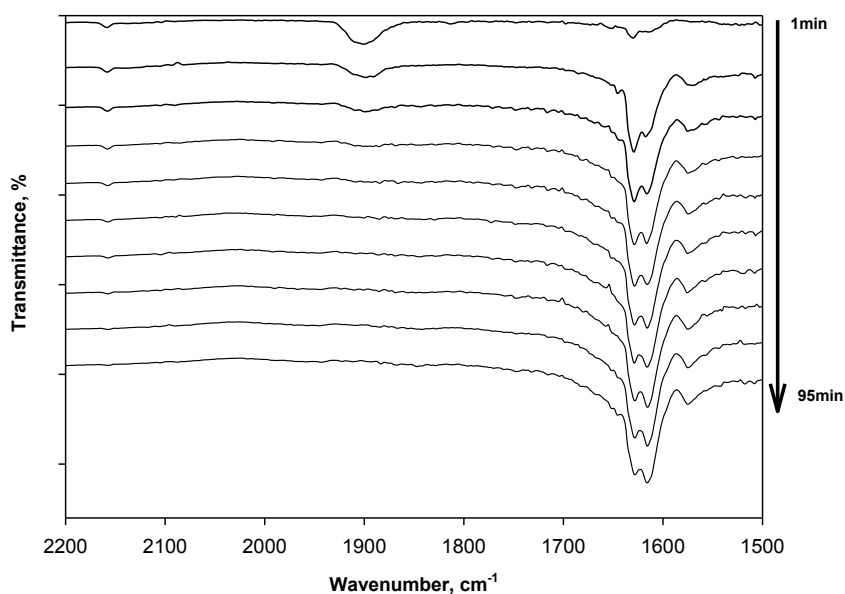


**Fig. 83** - FTIR spectra of NO adsorption on pre-oxidized LaCu-ZSM5 at 50°C recorded at different contact times

In Fig. 83 it was possible to observe the rapid formation of mono-nitrosyl  $\text{Cu}^{2+}\text{O}^-\text{NO}$  at about  $1900\text{ cm}^{-1}$  together with the incipient formation of chelating and bridged nitrates at  $1630$  and  $1571\text{ cm}^{-1}$  respectively. The band at  $1615\text{ cm}^{-1}$  has been previously ascribed to water. Mono-nitrosyls evolved towards nitrates with time on stream and after about 20 min a stable situation was achieved.

The cell was then closed using two two-ways valves and the temperature slowly (about  $7\text{ }^\circ\text{C min}^{-1}$ ) increased up to  $450\text{ }^\circ\text{C}$  collecting spectra at different temperatures. The evolution of the adsorbed species, during this phase, was reported in Fig. 84.

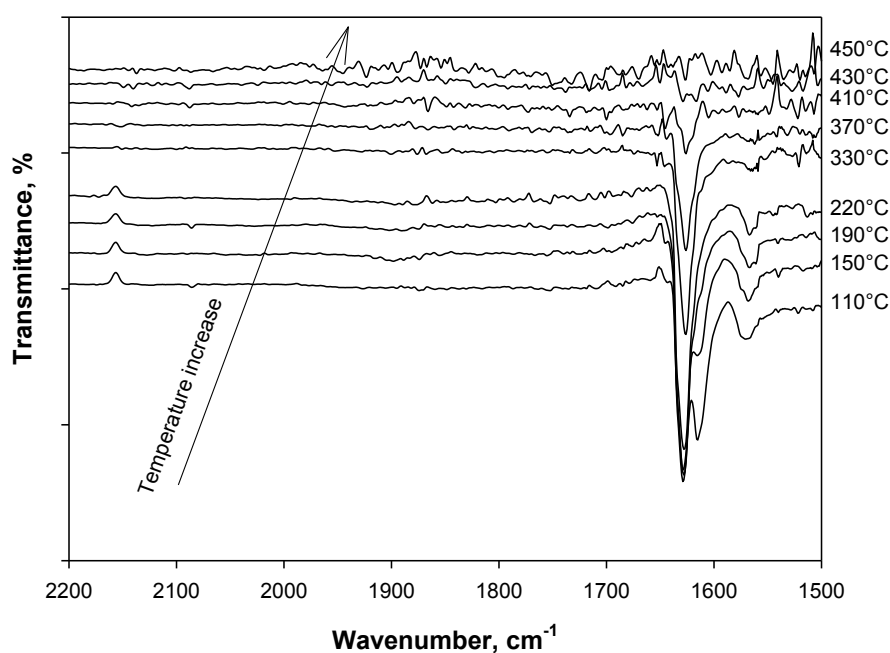


**Fig. 84** - FTIR spectra of NO during the heating phase from  $110$  to  $450\text{ }^\circ\text{C}$

As it can be seen, between  $330$  and  $370\text{ }^\circ\text{C}$  the bands of adsorbed nitrates started to disappear suggesting their desorption from the zeolite or their conversion into  $\text{N}_2$  and  $\text{O}_2$ . At  $450\text{ }^\circ\text{C}$  no bands were detectable in the spectrum. The sample was kept at  $450\text{ }^\circ\text{C}$  for 20 minutes collecting spectra every 5 min, observing no modification of the FTIR spectra (Fig. 85).

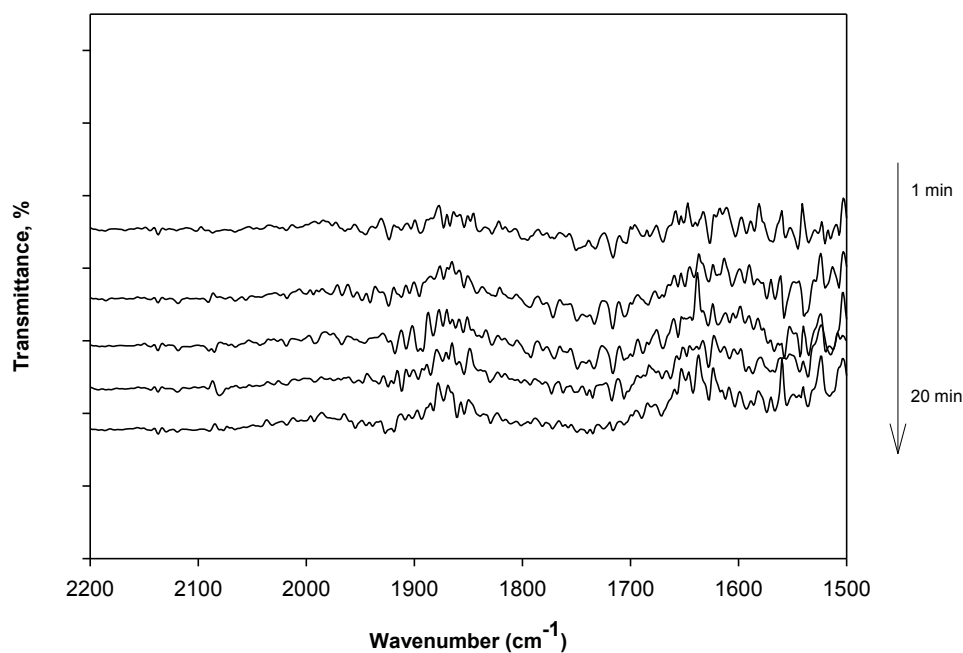


**Fig. 85** - FTIR spectra recorded during the decomposition phase at 450 °C

Then, the cell was cooled down again to 50 °C collecting spectra at different temperatures. In this stage, the bands of nitrates and a weak band of mono-nitrosyl reappear at about 190 °C suggesting that unreacted NO is re-adsorbed as hypothesized before (see Fig. 86).

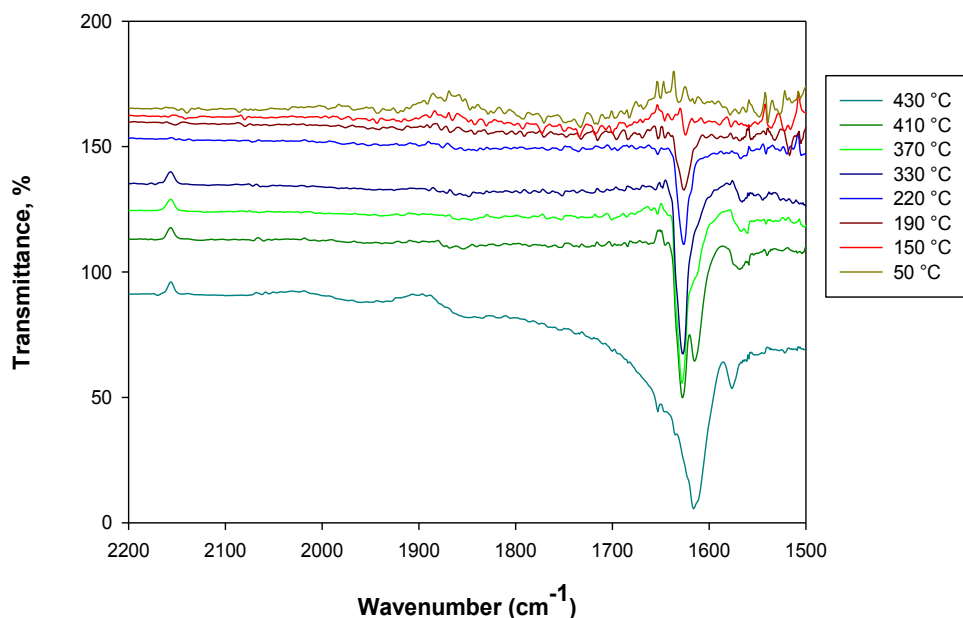


**Fig. 86** - FTIR spectra of NO adsorbed during the cooling phase from 450 to 50°C

As the temperature reached 50 °C, the spectra were collected every 10 min for 40min (see Fig. 87), observing no modification of the spectra.

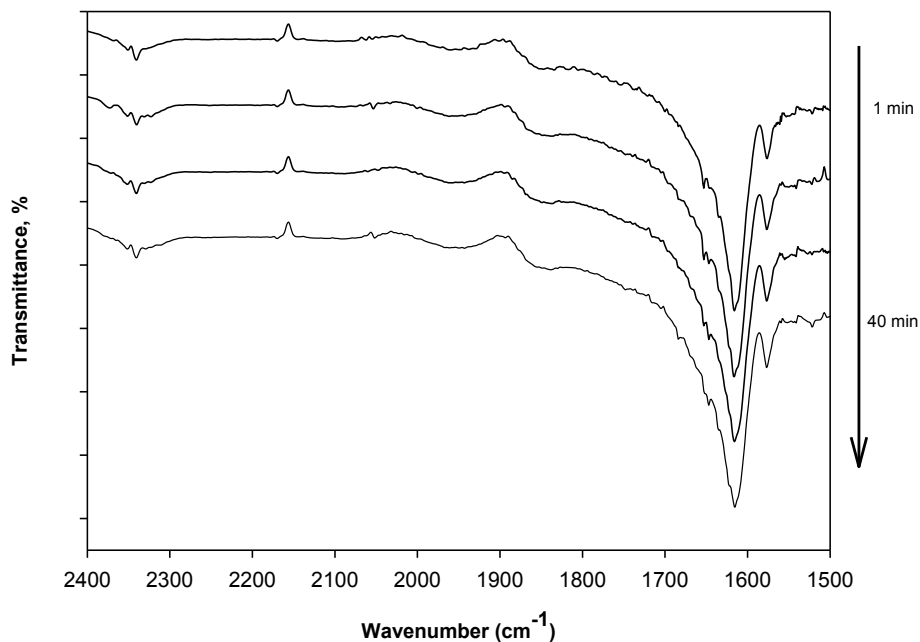


**Fig. 87** - FTIR spectra at 50°C, after the cooling phase, for 40min

The results confirmed the hypothesis of re-adsorption of unreacted NO during the cooling down step after the decomposition reaction which limits the subsequent NO adsorption but on the other hand avoids any NO emission and also confirmed the nature of the adsorbed species that was mostly nitrate-like.

## Conclusions

In conclusion, NO could be effectively adsorbed on LaCu-ZSM5 monolith at 50 °C until catalyst saturation; the adsorption proceeds through a complete removal of NO<sub>x</sub> from the gas phase. It was proven that NO could be converted at 480 °C into N<sub>2</sub> and O<sub>2</sub> which were the only products exiting the reactor after cooling down the system back to the adsorption temperature; the unconverted NO was re-adsorbed during the cooling phase. It was possible to carry out several subsequent cycles of adsorption/decomposition (even in the presence of O<sub>2</sub>) without catalyst pretreatment between a cycle and the following. After few cycles, the amount of NO adsorbed and subsequently decomposed for each cycle levels to a constant value, independently of the O<sub>2</sub> co-feeding. The catalyst stability to the sequence of adsorption/desorption cycles was verified.

This technique can be effectively used to remove nitrogen oxides from flue gases with to reactor operating simultaneously and out of phase properly tuning the times necessary for each step .

## **CONCLUSIONS**

## General conclusions

The main objective of this thesis has been the proposal of an innovative system for the abatement of nitrogen oxides, consisting in a cyclic process of adsorption/decomposition of NO on a LaCu-ZSM5 based monolith. This new system has been investigated in order to overcome one of the most hindering limits to the application of the direct decomposition of NO related to the slow reaction kinetics entailing the use of impractical catalyst volumes under a continuous flow operation. The novel technique is based on the good properties of the Cu-exchanged ZSM5 both as adsorbent and as catalyst for NO decomposition.

Part of the thesis has been also devoted to the effect of water vapour on the adsorption of NO on the zeolite which can represent a further limitation to the application of this process.

The key results of this work can be summarized as follows.

Regarding NO adsorption:

- Our copper-exchanged ZSM5 contains copper pairs  $\text{Cu}^{2+}\text{-O-Cu}^{2+}$ . When interacting with NO these  $\text{Cu}^{2+}$  ions disproportionate to  $\text{Cu}^+$  and  $\text{Cu}^{3+}$ . Both cations can form dinitrosyl complexes;
- At  $T=50\text{-}150^\circ\text{C}$  NO forms on copper sites, in addition to mono-nitrosyl, nitrate species;
- The presence of water vapour inhibits NO adsorption on copper sites displacing mostly mono-nitrosyls;
- Nitrates are definitely more stable and successfully compete with water which cannot displace these species;
- Both zeolite co-exchange with lanthanum and the presence of  $\text{O}_2$  in the gas feed contribute to enhance NO adsorption also in the presence of water due to the promoting effect on the formation of nitrates;
- Adsorbed water is thermally less stable than nitrates and at  $T=250\text{-}300^\circ\text{C}$  can be removed from the zeolite, nitrates being unaffected.

Regarding the feasibility of the adsorption/decomposition process:

- The LaCu-ZSM5 monolith can effectively adsorb NO from flue gas providing zero NO emissions up to saturation of the zeolite at  $T=50^\circ\text{C}$ ;
- The decomposition of adsorbed NO can be carried out increasing the temperature to  $480^\circ\text{C}$  under batch conditions converting a fraction of adsorbed NO depending on the reaction time;

- After cooling down the system back to the adsorption temperature  $N_2$  and  $O_2$  produced can exit the reactor and the regenerated zeolite is ready for a new cycle;
- The unreacted fraction of NO is re-adsorbed on the zeolite during the cooling step thus avoiding any polluting emission;
- Both adsorption and decomposition performance is preserved also in the presence of  $O_2$  in the gas stream;
- Repeatability of cycles and stability of the catalyst has been verified.

The innovative system proposed could in theory allow an operation with two reactors working out of phase, one adsorbing and another decomposing NO, ensuring zero nitrogen oxides emissions. Of course, this implies that proper operation times, reactors volumes and all the other parameters necessary to obtain the right synchronism are correctly tuned. Nevertheless, the development of the complete system is not the objective of this thesis.

## **APPENDIX A – Infra Red spectroscopy of probe molecules on solid catalysts**

The infrared spectroscopy is a technique based on the determination of the interaction between an IR radiation and a sample. Both the frequencies at which the sample adsorbs and the related intensities can be measured with this technique. Infrared spectroscopy represents one of the most important tools for characterization of the surface chemistry of heterogeneous catalysts.

The adsorption of probe molecules is often used to characterize metal centers. Indeed, when a molecule is adsorbed on a surface important change occurs influencing the vibrational motion of its atoms changing the frequency value of some specific motions (Barò, 1990). In addition, the number of vibrational modes changes and the original symmetry of the gaseous probe molecule lowers. As a consequence, the spectrum of an adsorbed probe molecule provides a lot of information on the metallic centers involved in the interaction.

Generally, CO and NO are used for the samples characterization. These two probes are complementary when studying copper-containing catalysts because CO is preferentially adsorbed on  $\text{Cu}^+$  sites, while NO on  $\text{Cu}^{2+}$  ions (Fu et al. 1991 and Hadjiivanov et al. 1999). Some authors, such as Praliaud et al. (1998), believe that only CO can be adsorbed on  $\text{Cu}^+$ . On this point there is a general disagreement, for example Soria et al. (2000) and Hadjiivanov and Knözinger (2000) are not in agreement with Praliaud et al..

Another very important application in IR investigation is the use of isotopically labelled molecules; these molecules are useful to prove the existence of a definite atom in a surface species, but can also answer the question about the nature of atoms to which this atom is bonded and about the number of these bonds (Hadjiivanov et al., 2009). There are also cases where the utilization of labelled molecules is motivated simply by the fact that they are registered in a more convenient spectral region (in a region where the noise level is low).

Isotopic mixtures are used to determine the structure of polyligand species. The spectra obtained with NO adsorption were quite complex, for this reason in this thesis a literature approach (Mihaylov et al., 2011) it is used to facilitate the understanding of the spectra.

When in the spectrum there are two bands characterizing two different linear complexes of metal ions, the adsorption of isotopic mixture would lead only to a shift of these bands to lower frequencies and four bands will be observed in the IR spectrum (see Fig. 88, panel A).

In the cases when polyligand species are formed, adsorption of isotopic mixtures will result in appearance of six bands in the IR spectrum: two bands [ $\nu_s(\text{NO})$  and  $\nu_{as}(\text{NO})$ ] due to dinitrosyls with two NO ligands, two bands [ $\nu_s(^{15}\text{NO})$  and  $\nu_{as}(^{15}\text{NO})$ ] of the dinitrosyls with two  $^{15}\text{NO}$  ligands and two bands [ $\nu(\text{NO})$  and  $\nu(^{15}\text{NO})$ ] characterizing mixed-ligand species  $\text{Me}(\text{NO})(^{15}\text{NO})$ .

The NO stretching mode of the mixed-ligand species should be located between the symmetric and antisymmetric modes of the  $\text{Me}(\text{NO})_2$  and the isotopic  $^{15}\text{NO}$  stretching mode of the mixed-ligand species – between the symmetric and antisymmetric modes of the  $\text{Me}(^{15}\text{NO})_2$  (see Fig. 88, panel B).

With equimolar (1:1)  $\text{NO}+^{15}\text{NO}$  mixtures the molar ratio of the  $\text{Me}(\text{NO})_2:\text{Me}(\text{NO})(^{15}\text{NO}):\text{Me}(^{15}\text{NO})_2$  species should be 1:2:1.

Therefore, the bands due to mixed-ligand species should be the most intense ones (they will have a twice as high intensity as that for the other bands).

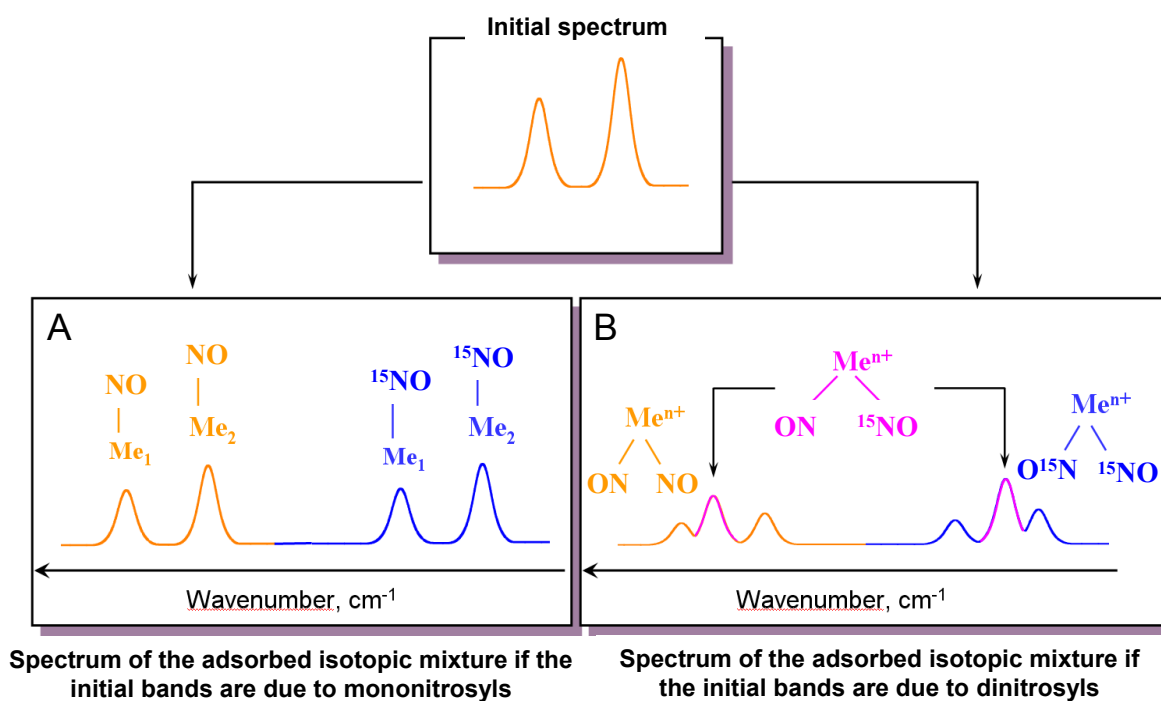


**Fig. 88** - Determine the structure of dinitrosyls by using  $\text{NO} + ^{15}\text{NO}$  isotopic mixture

Because the spectra of adsorbed isotopic mixtures are complex and many bands overlap, for better understanding a comparison of the real spectrum and the so-called “simulated mononitrosyl” spectrum is used.

The simulated spectrum represents the sum of the spectra of  $\text{NO}$  and  $^{15}\text{NO}$  divided by two.

The steps to get the simulated spectrum are the following: (i) take the spectrum recorded after adsorption of NO, (ii) calculate the spectrum of  $^{15}\text{NO}$  by shifting of the real NO spectrum along X-axis by the isotopic shift factor [ $\nu(\text{NO})/\nu(^{15}\text{NO}) = 1.018$ ] and (iii) sum the two spectra and divide it by two.

If all of the bands observed in the real spectrum correspond to N-O vibrations of mononitrosyl species, the simulated spectrum should coincide with the spectrum registered after adsorption of the isotopic mixture (Fig. 88, panel A). If they do not coincide, there are some polynitrosyl complexes formed (Fig. 88, panel B).

The bands that are of lower intensity in the real spectrum correspond to dinitrosyls with equal ligands [ $\text{Me}(\text{NO})_2$  and  $\text{Me}(^{15}\text{NO})_2$ ] and the new bands in the real spectrum correspond to the mixed-ligand species [ $\text{Me}(\text{NO})(^{15}\text{NO})$ ].

## References:

- Ansell G.P., Diwell A.F., Golunski S.E., Hayes J.W., Rajaram R.R., Truex T.J., Walker A.P., Mechanism of the lean NO<sub>x</sub> reaction over Cu/ZSM-5, *Applied Catalysis B, Environmental* 2 (1993) 81
- Barò A. M., Spectroscopic characterization of heterogeneous catalyst – Volume 57, Part B pag. 145, J. L. G. Fierro Editor (1990) – *Studies in Surface Science and Catalysis*
- Bell A. T., Experimental and theoretical studies of NO decomposition and reduction over metal-exchanged ZSM-5, *Catalysis Today* 38 (1997) 151
- Braterman P.S., *Metal Carbonyl Spectra*, Academic Press, London, 1975
- Campa M.C., Indovina V., Minelli G., Moretti G., Pettiti I., Porta P., Riccio A., The catalytic activity of Cu-ZSM-5 and Cu-Y zeolites in NO decomposition–Dependence on copper concentration, *Catalysis Letters* 23 (1994) 141
- Centi G., Perathoner S., Nature of active species in copper-based catalysts and their chemistry of transformation of nitrogen oxides, *Applied Catalysis A-General*, 132 (1995) 179
- Dědeček J., Sobalík Z., Tvarůžková Z., Kaucký D., Wichterlová B., *Coordination of Cu ions in high-silica zeolite matrices. Cu<sup>+</sup> photoluminescence, IR of NO adsorbed on Cu<sup>2+</sup>, and Cu<sup>2+</sup> ESR study*, *J. Phys. Chem.* 99 (1995) 16327
- Despres J., Koebel M., Kröcher O., Elsener M., Wokaun A., *Adsorption and desorption of NO and NO<sub>2</sub> on Cu-ZSM-5*, *Microporous and Mesoporous Materials* 58 (2003) 175
- Drenchev, N., Georgiev, P.A., Hadjiivanov, K., *FTIR study of <sup>12</sup>C<sup>16</sup>O and <sup>13</sup>C<sup>18</sup>O coadsorption on Cu-ZSM-5*, *Journal of Molecular Catalysis A: Chemical* 341 (2011) 7
- Eränen, K., Kumar, N., Lindfors, L.-E., *Enhancement of the catalytic activity of Cu-ZSM-5 for nitric oxide decomposition by introduction of copper during the zeolite synthesis*, *Applied Catalysis B, Environmental* 4 (1994) 213
- Fanson, P.T., Stradt, M.W., Lauterbach, J., Delgass, W.N., *The effect of Si/Al ratio and copper exchange level on isothermal kinetic rate oscillations for N<sub>2</sub>O decomposition over Cu-ZSM-5: A transient FTIR study*, *Appl. Catal. B* 38 (2002) 331
- Fu Y., Tian Y., Lin P., A low-temperature IR spectroscopic study of selective adsorption of NO and CO on CuO/γ-Al<sub>2</sub>O<sub>3</sub>, *J. Catal.* 132 (1991) 85
- Garin F., *Mechanism of NO<sub>x</sub> decomposition*, *Applied Catalysis A: General* 222 (2001) 183
- Giordanino F., Vennestrøm P.N.R., Lundegaard L.F., Stappen F.N., Mossin S., Beato P., Bordiga S., Lamberti C., *Characterization of Cu-exchanged SSZ-13: a comparative FTIR, UV-Vis, and EPR study with Cu-ZSM-5 and Cu-β with similar Si/Al and Cu/Al ratios*, *Dalton Transaction* 42 (2013) 12741

Gómez-García M.A., Pitchon V., Kiennemann A., *Pollution by nitrogen oxides: an approach to NO<sub>x</sub> abatement by using sorbing catalytic materials*, Environment International 31 (2005) 445

Góra-Marek K. and Datka J., *IR studies of coadsorption of CO and NO on Co<sup>2+</sup> and Cu<sup>+</sup> sites in zeolites*, Vibrational Spectroscopy 57 (2011) 148

Green T. E., Hinshelwood C.N., *CCXXIV-The catalytic decomposition of nitric oxide at the surface of platinum*, J. Chem. Soc. (1926) 1709

Hadjiivanov K., Klissurski D., Ramis G., Busca G., *Fourier transform IR study of NO<sub>x</sub> adsorption on a CuZSM-5 DeNO<sub>x</sub> catalyst*, Applied Catalysis B: Environmental 7 (1996) 251

Hadjiivanov K., *IR study of CO and NO<sub>x</sub> sorption on Ag-ZSM-5, Microporous and Mesoporous Materials*, 24 (1-3) (1998) 41

Hadjiivanov K., Saussey J., Freysz J.-L., Lavalley J.-C., *FTIR Study of NO + O<sub>2</sub> Co-adsorption on H-ZSM-5: Re-assignment of the 2133 cm<sup>-1</sup> Band to NO<sup>+</sup> Species*, Catalysis Letters 52 (1998) 103

Hadjiivanov K. and Dimitrov L., *IR spectroscopy study of CO and NO<sub>x</sub> adsorption on a Cu/Zr-HMS catalyst*, Microporous Mesoporous Matererials 27 (1999) 47

Hadjiivanov K. and Knözinger H., *FTIR Study of Low-Temperature CO Adsorption on Cu-ZSM-5: Evidence of the Formation of Cu<sup>2+</sup>(CO)<sub>2</sub> Species*, Journal of Catalysis 191 (2000) 480

Hadjiivanov K., *Identification of neutral and charged NxOy surface species by IR spectroscopy*, Catal. Rev. Sci. Eng., 42 (2000) 71

Hadjiivanov, *Application of isotopically labelled IR probe molecules for characterization of porous materials*, Chapter 10 - Ordered Porous Solids: Recent Advances and Prospects (2009) Elsevier (2009)

Heck R. M., *Catalytic abatement of nitrogen oxides—stationary applications*, Catalysis Today, 53 (1999) 519

Hong, W.J., Iwamoto S., Inoue M., *Direct Decomposition of NO on Ba Catalysts Supported on Ce–Fe Mixed Oxides*, Catalysis Letters 135 (2010) 190

Imanaka N. and Masui T., *Advances in direct NO<sub>x</sub> decomposition catalysts*, Applied Catalysis A: General 431-432 (2012) 1-8

Iwamoto M., Yokoo S., Sakai K., Kagawa S., *Catalytic decomposition of nitric oxide over copper(II)-exchanged, Y-type zeolites*, Journal of the Chemical Society, Faraday Transactions 1 77 (1981) 1629

Iwamoto M., Furukawa H., Mine Y., Uemura F., Mikuriya S. and Kagawa S., *Copper(II) ion-exchanged ZSM-5 zeolites as highly active catalysts for direct and continuous decomposition of nitrogen monoxide*, Journal of the Chemical Society, Chemical Communications 16 (1986)1272

Iwamoto M., Yahiro H., Mine Y., Kagawa S., *Excessively Copper Ion-exchanged ZSM-5 Zeolites as Highly Active Catalysts for Direct Decomposition of Nitrogen Monoxide*, Chemistry Letters 2 (1989) 213

Iwamoto M., Yahiro H., Torikai Y., Yoshioka T., Mizuno N., *Novel Preparation Method of Highly Copper Ion-exchanged ZSM-5 Zeolites and Their Catalytic Activities for NO Decomposition*, Chemistry Letters 11 (1990) 1967

Iwamoto M., Yahiro H., Tanda K., Mizuno N., Mine Y., Kagawa S., *Removal of nitrogen monoxide through a novel catalytic process. 1. Decomposition on excessively copper-ion-exchanged ZSM-5 zeolites*, Journal of Physical Chemistry 95(9) (1991) 3727

Iwamoto M. and Hamada H., *Removal of nitrogen monoxide from exhaust gases through novel catalytic processes*, Catalysis Today, 10 (1991) 57

Iwamoto M. and Hamada H., *Removal of nitrogen monoxide from exhaust gases through novel catalytic processes*, Journal of Catalysis 10 (1991) 57

Iwamoto M. and Yahiro H., *Novel catalytic decomposition and reduction of NO*, Catalysis Today 22 (1994) 5

Iwamoto M., Wang J., Sperati K.M., Sajiki T., Misono M., *Migration of copper ions in Cu-MFI without destruction of zeolite lattice or dealumination upon hydrothermal treatment at 923K*, Chemistry Letters (1997) 1281

Jang H.-J., Hall W. K., and d'Itri J. L., *Redox Behavior of CuZSM-5 Catalysts: FTIR Investigations of Reactions of Adsorbed NO and CO*, J. Phys. Chem. 100 (1996) 9416

Kharas K.C.C., Robota H.J. and Liu D.J., *Deactivation in Cu-ZSM-5 lean-burn catalysts*, Applied Catalysis B: Environmental 2 (1993) 225

Konduru M. and Chuang S.S.C., *Investigation of Adsorbate Reactivity during NO Decomposition over Different Levels of Copper Ion-Exchanged ZSM-5 Using in Situ IR Technique*, J. Phys. Chem. B 103 (1999) 5802

Konduru M.V., Chuang S.S.C., *Dynamics of NO and N<sub>2</sub>O Decomposition over Cu-ZSM-5 under Transient Reducing and Oxidizing Conditions*, Journal of Catalysis 196 (2000) 271

Kucherov A.V., Hubbard C.P. and Shelef M., *Rearrangement of Cationic Sites in CuH-ZSM-5 and Reactivity Loss upon High-Temperature Calcination and Steam Aging*, Journal of Catalysis 157 (1995) 603

Kucherov V., Hubbard C.P., Kucherova T.N. and Shelef M., *Influence of La<sup>3+</sup>, Ce<sup>4+</sup>, Ga<sup>3+</sup>, and Ba<sup>2+</sup> Ions on Rearrangement of Cationic Sites in CuH-ZSM-5 Zeolite and Reactivity Loss upon High-Temperature Treatments*, Kinet. Catal. 4 (1997) 556

Li Y. and Hall K., *Stoichiometric catalytic decomposition of nitric oxide over copper-exchanged zeolite (CuZSM-5) catalysts*, Journal of Physical Chemistry 94 (1990) 6145

Li Y., Armor J.N., *Temperature-programmed desorption of nitric oxide over Cu-ZSM-5*, Applied Catalysis 76 (1991) L1

Li Y., Hall W. K., *Catalytic decomposition of nitric oxide over Cu-zeolites*, Journal of Catalysis 129 (1) (1991), 202

Li Y., Armor J. N., *Catalytic decomposition of nitrous oxide on metal exchanged zeolites*, Appl. Catal. B: Environ. 1 (1992) L21

Li L., Guan N., *HC-SCR reaction pathways on ion exchanged ZSM-5 catalysts*, Microporous Mesoporous Materials 117 (2009) 450

Lisi L., Pirone R., Russo G., Stanzione V., *Cu-ZSM5 based monolith reactors for NO decomposition*, Chemical Engineering Journal 154 (2009) 341

Lisi L., Pirone R., Russo G., Santamaria N., Stanzione V., *Nitrates and nitrous oxide formation during the interaction of nitrogen oxides with Cu-ZSM-5 at low temperature*, Applied Catalysis A: General 413–414 (2012) 117

Liu G. and Gao P., *A review of NO<sub>x</sub> storage/reduction catalysts: mechanism, materials and degradation studies*, Catalysis Science and Technology 1 (2011) 552

Mihaylov M., Lagunov O., Ivanova E., Hadjiivanov K., *Determination of Polycarbonyl Species on Nickel-containing Catalysts by Adsorption of CO Isotopic Mixtures*, Topic in Catalysis 54 (2011) 308

Mihaylov M., Lagunov O., Ivanova E., Hadjiivanov K., *Nature of the Polycarbonyl Species on Ru/ZrO<sub>2</sub>: Re-assignment of Some Carbonyl Bands*, The Journal of Physical Chemistry C 115 (2011) 13860

Mirica L.M., Ottenwaelder X., Daniel T., Stack P., *Structure and Spectroscopy of Copper–Dioxygen Complexes*, Chemical Reviews 104 (2004) 1013

Olsson L., Sjövall H., Blint R.J., *Detailed kinetic modeling of NO<sub>x</sub> adsorption and NO oxidation over Cu-ZSM-5*, Applied Catalysis B: Environmental 87 (3-4) (2009) 200

Parella B. I., Lisi L., Pirone R., Russo G., Notaro M., *Enhancement of Hydrothermal Stability of Cu-ZSM5 Catalyst for NO Decomposition*, Kinetics and Catalysis, 47 (2006) 728

Paze C., Zecchina A., Spera S., Cosma A., Merlo E., Spano G., Girotti G., *Comparative IR and 1H-MAS NMR study of adsorption of CD<sub>3</sub>CN on zeolite H-β: evidence of the presence of two families of bridged Bronsted sites*, Physical Chemistry Chemical Physics 1 (1999) 2627

Penkova A., K. Hadjiivanov, M. Mihaylov, M. Daturi, J. Saussey, J.-C. Lavalley, *FTIR spectroscopic study of low temperature NO adsorption and NO + O<sub>2</sub> coadsorption on H-ZSM-5*, *Langmuir* 20 (2004) 5425

Pham N., Xing G., Miller C.J., Waite T.D., *Fenton-like copper redox chemistry revisited: Hydrogen peroxide and superoxide mediation of copper-catalyzed oxidant production*, *Journal of Catalysis* 301 (2013) 54

Pierloot K., Zhao H., Vancoillie S., *Copper Corroles: the Question of Noninnocence*, *Inorganic Chemistry* 49 (2010) 10316

Pirone R., Garufi E., Ciambelli P., Moretti G., Russo G., *Transient behavior of Cu-overexchanged ZSM-5 catalyst in NO decomposition*, *Catalysis Letters* 43 (1997) 255

Pirone R., Ciambelli P., Palella B., Russo G., *A kinetic study of NO decomposition on Cu-ZSM5*, *Studies in Surface Science and Catalysis* 140 (2001) 377

Praliaud H., Mikhailenko S., Chajar Z, Primet M., *Surface and bulk properties of Cu-ZSM-5 and Cu/Al<sub>2</sub>O<sub>3</sub> solids during redox treatments. Correlation with the selective reduction of nitric oxide by hydrocarbons*, *Applied Catalysis B: Environmental* 16 (4) (1998) 359

Quincoces C.E., Kikot A., Balsadella E.I., Gloria Gonzalez M., *Effect of Hydrothermal Treatment on Cu-ZSM-5 Catalyst in the Selective Reduction of NO*, *Industrial and Engineering Chemistry Research* 38 (1999) 4236

Radojevic M., *Reduction of nitrogen oxides in flue gases*, *Environmental Pollution* 102 (1998) 685

Roy S., Hegde M.S., Madras G., *Catalysis for NO<sub>x</sub> abatement*, *Applied Energy* 86 (2009) 2283

Sadykov V.A., Beloshapkin S.A., Paukshtis E.A., Alikina G.M., Kochubei I., Degtyarev S.P., Bulgakov N.N., Veniaminov S.A., Netyaga V., Bunina R.V., Kharlanov A.N., Lunina E.V., Lunin Matyshak V.V., Rozovskii A.Y., *Hydrocarbon specificity in the selective catalytic reduction of NO(x) over Cu-ZSM-5 and Co-ZSM-5 catalysts*, *Reaction Kinetics and Catalysis Letters* 64 (1998) 185

Schay Z., Guzzi L., *Decomposition of NO over Cu-ZSM-5 Zeolites: A Transient Kinetic Study*, *Catal. Today* 17 (1993) 175

Schay Z., Knözinger H., Guzzi L., Pál-Borbély G., *On the mechanism of NO decomposition on Cu-ZSM-5 catalysts*, *Appl. Catal. B: Environ.* 18 (1998) 263

Sepúlveda-Escribano A., Márquez-Alvarez C., Rodríguez-Ramos I., Guerrero-Ruiz A., Fierro J.L.G., *Decomposition of NO on Cu-loaded zeolites*, *Catalysis Today* 17 (1-2) (1993) 167

Seyedejn-Azad F., Zhang D., *Kinetic Studies of the Direct Decomposition of Nitric Oxide*, *Iranian Journal of Chemical Engineering* 2 (2005) 82

Sierraalta A., Bermudez A., Rosa-Brussin M., *Density functional study of the interaction of Cu<sup>+</sup> ion-exchanged zeolites with H<sub>2</sub>O and SO<sub>2</sub> molecules*, Journal of Molecular Catalysis A: Chemical 228 (2005) 203

Skalska K., Miller J. S., Ledakowicz S., *Kinetics of nitric oxide oxidation*, Chemical Papers 64 (2010) 269

Skalska K., Miller J. S., Ledakowicz S., *Trends in NO<sub>x</sub> abatement: A review*, Science of the Total Environment 408 (2010) 3976

Solans-Monfort X., Branchadell V., Sodupe M., *Theoretical Study of the Structure of ZCu(NO<sub>2</sub>)(NO). A Proposed Intermediate in the NO<sub>x</sub> Decomposition by Cu-ZSM-5*, The Journal of Physical Chemistry A 104 (2000) 3225

Soria J., Martinez-Arias A., Martinez-Chaparro A., Conesa J.C., Schay Z., *Influence of the Preparation Method, Outgassing Treatment, and Adsorption of NO and/or O<sub>2</sub> on the Cu<sup>2+</sup> Species in Cu-ZSM-5: An EPR Study*, Journal of Catalysis 190 (2) (2000) 352

Spoto G., A. Zecchina, S. Bordiga, G. Ricchiardi, G. Martra, G. Leofanti, G. Petrini, *Cu(I)-ZSM-5 zeolites prepared by reaction of H-ZSM-5 with gaseous CuCl: Spectroscopic characterization and reactivity towards carbon monoxide and nitric oxide*, Appl. Catal. B 3 (1994) 151

Torre-Abreu C., Ribeiro M.F., Henriques C., Ribeiro F.R., Delahay G., *Deactivation of CuMFI catalysts under NO selective catalytic reduction by propene: influence of zeolite form, Si/Al ratio and copper content*, Catalysis Letters 43 (1-2) (1997) 31

Valyon J., Hall W. K., *Studies of the surface species formed from nitric oxide on copper zeolites*, Journal of Physical Chemistry 97 (6) (1993) 1204

Valyon J., Hall W. K., *On the preparation and properties of CuZSM-5 catalysts for NO decomposition*, Catalysis Letters 19 (2-3) (1993) 109

Yadav G.D., Nair J.J. *Sulfated zirconia and its modified versions as promising catalysts for industrial processes*, Microporous Mesoporous Mater (1999) 33

Yahiro H. and Iwamoto M., *Copper ion-exchanged zeolite catalysts in deNO<sub>x</sub> reaction*, Applied Catalysis A 222 (2001) 163

Yan J.Y., Lei G.D., Sachtler W.M., Kung, H.H., *Deactivation of Cu/ZSM-5 Catalysts for Lean NO<sub>x</sub> Reduction: Characterization of Changes of Cu State and Zeolite Support*, Journal of Catalysis 161 (1996) 43

Yu J. J., Cheng J., Ma C. Y., Wang H. L., Li L. D., Hao Z. P., Xu Z. P., *NO<sub>x</sub> decomposition, storage and reduction over novel mixed oxide catalysts derived from hydrotalcite-like compounds*, Journal of Colloid and Interface Science 333 (2009) 423

- Zecchina A., Arean C. O., *Diatomic molecular probes for mid-IR studies of zeolites*, Chemical Society Reviews 25 (1996) 187
- Zeldovich J., *Oxidation of nitrogen in combustion and explosion*, Comptes Rendus de l'Académie des Sciences USSR 51 (1946) 217
- Zhang, Y. and Flytzani-Stephanopoulos M., J.N. Armor (Ed.), Environmental Catalysis, Symposium Series 552, Vol.2, American Chemical Society (1994), p. 7
- Zhang W.X., Yahiro H., Mizuno N., Izumi J., Iwamoto M., *Removal of nitrogen monoxide on copper ion-exchanged zeolites by pressure swing adsorption*, Langumir 9 (1993) 2337
- Zhang Y., Flytzani-Stephanopoulos M., *Hydrothermal Stability of Cerium Modified Cu-ZSM-5 Catalyst for Nitric Oxide Decomposition*, Journal of Catalysis 164 (1996) 131
- Zhu Y., Wang D., Yuan F., Zhang G., Fu H., *Direct NO decomposition over  $La_{2-x}Ba_xNiO_4$  catalysts containing  $BaCO_3$  phase*, Applied Catalysis B: Environmental 82 (2008) 255
- Ziolek M., Sobczak I., Nowak I., Daturi M., Lavalley J.C., *Effect of hydrogen sulphide on nitric oxide adsorption and decomposition on Cu-containing molecular sieves*, Applied Catalysis B: Environmental 28 (2000) 197.